NTNU

Norwegian University of
Science and Technology

HF Formation Upon Addition of Different Industrial Aluminas to Cryolitic Baths

Camilla Sommerseth

Chemical Engineering and Biotechnology
Submission date: June 2011
Supervisor: Christian Rosenkilde, IMTE
Co-supervisor: Karen Sende Osen, SINTEF

Norwegian University of Science and Technology
Department of Materials Science and Engineering

Abstract

The aluminium smelter at Hydro Sunndal has experienced problems with an unexpected increased loss of AlF_3 from the electrolyte when using a certain quality of alumina. One hypothesis considered was that the fluoride loss was a direct result of unusually high HF formation when the quality was added to the cryolitic melt. This work has set out to study the HF formation potential of three different industrial alumina qualities. Alumina A was an alumina quality that worked well in the smelter. Alumina B was the alumina quality where the aforementioned drop in AlF_3 was observed and alumina C, made by the same producer, controversially did not to exhibit the same loss at smelter.

The present work has been divided into two parts: a characterisation section, where the aluminas have been characterised by techniques such as LOI, TGA, DSC and XRD, and an experimental section, where the industrial aluminas were added to a cryolitic melt. The HF formation and the corresponding H_2O concentration were measured *in-situ* using a tunable diode laser during the alumina additions to the cryolitic melt.

Through this work it has been found that both primary and secondary alumina A form less HF than alumina B and C. The LOI, TGA and XRD characterisation has shown that alumina B and C contain a substantial amount of gibbsite, whilst the gibbsite level in alumina A is negligible. A clear correlation between the quantity of moisture found through LOI characterisation and HF formation has been found. It has also been shown that all types of moisture found through LOI testing contribute to HF formation; both physisorbed and chemisorbed types, as well as structural hydroxyl.

From the present work it cannot be explained why alumina B caused a drop in AlF_3 in the electrolyte, whilst alumina C did not. One explanation postulated is that alumina C has better scrubber efficiency than alumina B. Examining this hypothesis has been outside the scope of this master work. If variations in scrubber efficiency for the two aluminas fail to explain the drop in AlF_3, the solution may be found in parameters outwit the alumina quality e.g. weather conditions at the time of production or storage conditions at the calciner.

Preface

This work has been carried out at NTNU, Department of Materials Science and Engineering as part of the course TMT4900, spring 2011. I hereby declare that the work has been carried out by me, Camilla Sommerseth, according to the regulations at NTNU.

Some parts of Chapter 3, Background and Theory, have similarities to the Theory chapter in the report written by myself in the course TMT4500, autumn 2010. However, modifications have been done, sentences rewritten or changed and additions made.

I have received a lot of help when working with my Master project, and I would like to thank the following.

My supervisor Christian Rosenkilde, for all help, good discussions and support! You have a great way of lifting me up when I've been feeling lost.

My co-supervisor, Karen Sende Osen at SINTEF Materials and Chemistry for all help in the laboratory, all good discussions and all guidance. I couldn't have done it without you!

I would also like to thank Astrid Johanne Meyer and Linda Therese Kristiansen at Hydro Porsgrunn for answering my numerous questions and providing me with alumina samples.

Ove Bjorøy at NEO for essential help with the laser.

Ole Kjos for essential help in the laboratory.

Sophie Weber for doing the TGA/DSC tests for me.

Julian Tolchard for help with the XRD laboratory, help with the Rietveld refinement and with general analysis of the data. Stein Rørvik also deserves a thank you here.

Thor Anders Aarhaug for various help regarding equipment and FTIR.

The KMB ROMA research project, especially Arne Petter Ratvik, Thor Anders Aarhaug and Egil Skybakmoen for the great opportunity it was for me to participate at The Minerals, Metals and Materials Society (TMS) conference in San Diego. Also thank you for including me into the project through summer jobs, project work and master work. Last, but not least, thank you for financing my work.

Henrik Gudbrandsen for helping me with instrumentation in the laboratory.

Aidan Rooney for proofreading.

Sigrid and Inga for all the good times!

Finn for supporting, helping and believing in me throughout these five past years at NTNU. You're the best!

Trondheim, 29.06.11.

Camilla Sommerseth

Contents

Symbols

Table 1: List of Symbols.

Symbol	Unit	Explanation
a		Activity
C(t)	ppm	Concentration at time t
d_{hkl}		Spacing between the planes
ΔG^0	J/mol	Gibbs energy
M	g/mol	Molar mass
m	g	Mass
n	mol	Amount of substance
P	atm	Pressure
R	J/(mol·K)	Gas constant
T	K	Temperature
t	s or min	Time
V	L	Volume
$\dot{v}$	L/s	Volume flow into reactor
θ	°	Diffraction angle
λ	m	Wavelength of X-radiation

1 Introduction

The Hall-Héroult process celebrates its 125th anniversary in 2011, as the only competitive way of producing aluminium commercially. In the Hall-Héroult process, aluminium is produced electrochemically from alumina (Al_2O_3) in a cryolitic electrolyte. The liquid aluminium is deposited on the cathode, while oxygen from the alumina consumes the carbon anodes to create CO_2. The overall cell reaction is shown in Reaction 1. [1]

$$\frac{1}{2}Al_2O_3(diss)+\frac{3}{4}C(s)=Al(l)+\frac{3}{4}CO_2 \tag{1}$$

Alumina used in the aluminium industry has three tasks. The most obvious of these is as the raw material for the aluminium production; however, it is also used in the dry scrubber to adsorb fluorides formed in electrolysis cells and as crust material covering the electrolyte from the ambient air. The dry scrubber inhibits the release of fluorides into the atmosphere. It is an installation in the fume treatment system of the plant, where alumina is used to adsorb fluorides from the exhaust gas of the electrolysis cells. [1] HF is formed both from a reaction with air moisture with fluorides gases found above the bath and as a reaction with moisture in the alumina fed to the cell with fluorides in the bath [2]. The air moisture enters the cell via the draught air used to carry the fume gases from the cells towards the dry scrubber. The alumina that is used in the dry scrubber is later used to feed the electrolysis cells. In this way, the alumina creates a closed loop of fluorides, minimizing the fluoride losses from the bath.

It is important that the alumina used by the aluminium industry, manages all three tasks; as raw material in the electrolyte, as crust cover material and as the dry scrubber component [3]. To enable the alumina to adsorb the fluorides, it is important to maintain a high surface area. To obtain a high surface area, the alumina has to be under calcined and this results in certain level of moisture in the alumina. α-alumina has a very low surface area, hence, making it less suitable for dry scrubbing purposes. It is a paradox, then, that the same moisture that helps pick up the fluorides also participates in creating more hydrogen fluoride (HF) in the electrolyte [2]. If HF is lost to the atmosphere, this represents a permanent loss of aluminium fluoride from the electrolyte. A loss of aluminium fluoride may lower the current efficiency of the cell [3].

Emissions of HF used to be a great problem around aluminium smelters prior to the introduction of the dry scrubber in the 1960's. These emissions to the atmosphere have been greatly reduced, however, there are still problems with HF escaping into the pot rooms of the plants when work is carried out on the cells (e.g. anode change or tapping of aluminium). HF in the pot rooms can pose as a respiratory hazard for the pot room staff [4].

In this report, a distinction between HF formation and HF emission has been made. Formation of HF is when the gas is formed in the electrolysis cell in or above the bath. Emission of HF is HF lost to the atmosphere, i.e. to the pot rooms or past the dry scrubber. [5]

In the aluminium industry today, smelters have to rely on more than one alumina supplier. The various alumina refineries have their own techniques, production routes and equipment to produce alumina. They also collect bauxite, the raw material for production of alumina, from different sites around the world. This creates diversity in the quality of smelter grade alumina (SGA) from the various suppliers. It is not uncommon that smelters experience changes in the working conditions of the cells when changing between alumina qualities [6]. Norsk Hydro, Sunndal, has experienced problems with one of the alumina qualities they use when producing aluminium. When using a certain alumina quality, they have experienced a loss in aluminium

fluoride from the cells. The bath chemistry is changed when a drop in AlF_3 occurs and the cryolite ratio (defined later) is affected. This master thesis will explore and isolate the causes of the varied fluoride losses experienced from the electrolyte when using different alumina qualities.

The work presented in this report is in continuation with the work done in the course TMT4500, Materials Technology, by the author autumn 2010 [7]. One hypothesis is that this alumina quality (labelled alumina B in this report) forms more HF than other alumina qualities. Another hypothesis is that alumina B has poorer scrubber capacity than the other aluminas. In this work, three different aluminas have been examined: alumina A, B and C. Alumina A is an alumina quality that works satisfactorily in the electrolysis cells at Hydro Sunndal. Alumina B is a problematic alumina quality that has shown the aforementioned drop in AlF_3. Alumina C is produced at the same alumina refinery as alumina B, but this alumina quality has not shown the characteristic drop in AlF_3.

Three different size fractions of alumina A and B will be examined: -45μm, +150μm and bulk fractions (powder size fractions will be defined later). For alumina C, only the bulk fraction will be examined. Alumina A and B have been separated into different particle sizes by sieving. The -45μm powder fractions contain only particles smaller 45μm in diameter. The +150μm fraction contain only particles larger than 150μm in diameter. The bulk fraction is the mixture of all the size fractions in the alumina, and it is the bulk fraction that is used when producing aluminium. The particle size distribution varies from batch to batch and from refinery to refinery. [8, 9]

Two additional qualities of alumina A have also been added to this work: a hydrate quality (high in gibbsite, low in α-alumina) and a quality that has been calcined at 1200°C for 1.5 hours (low in gibbsite, high in α-alumina).

The problem has been addressed in two parts. Part one is a characterisation section, where the aluminas has been characterised by loss on ignition tests (LOI), thermal gravimetric analysis (TGA), differential scanning calorimetry (DSC) and X-ray diffraction (XRD). The first three tests set out to determine the moisture content in the various aluminas, while XRD was used to determine the various phases present in the aluminas. The second part was addition of the aluminas to a cryolitic melt. A Lasergas II Single Gas Monitor from NEO (Norsk Elektro Optikk AS) was used to continuously log the concentrations of HF and H_2O in the exhaust gas from the furnace, *in situ*.

2 Background and Methodology

The following chapter will present some basics on aluminium and alumina production. Some important concepts on alumina will also be defined. Finally the background for the thesis will be presented.

2.1 The Hall-Héroult Process

Aluminium is produced by the Hall-Héroult process. The Hall-Héroult process was invented in 1886 by Charles Hall and Paul Héroult. Even though the production has been changed and modified significantly since the early days of the aluminium reduction cell, the principles are still the same 125 years later. Figure 1 shows a principle sketch of an electrolysis cell producing aluminium electrochemically according to the Hall-Héroult principles. In modern cells, alumina (Al_2O_3) is fed to the cells by point feeders in small portions. Alumina then dissolves into the bath/electrolyte. Aluminium is produced electrochemically at the cathode, while oxygen from the alumina consumes the carbon anodes creating CO_2(g), as shown in Reaction 1. [1, 3, 10]

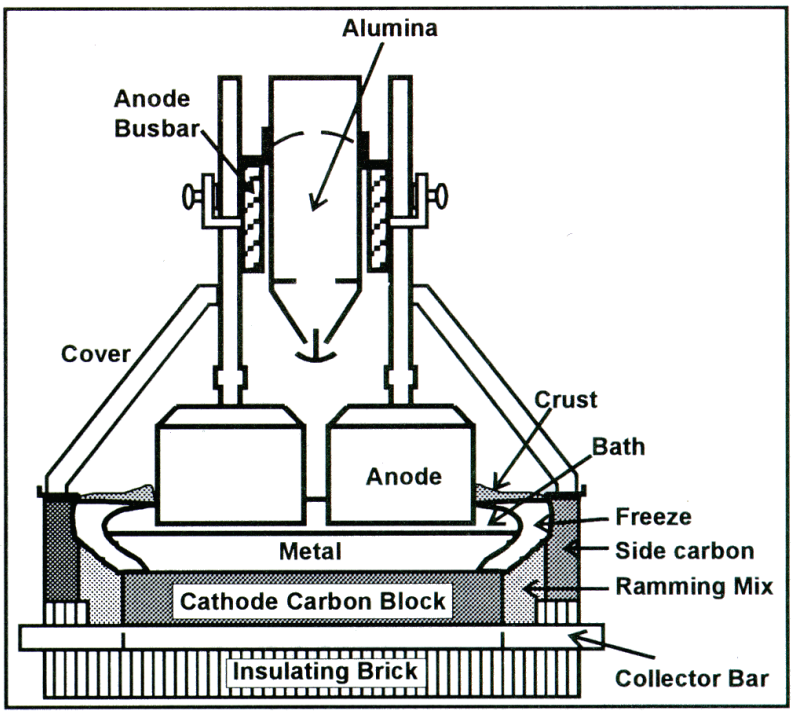

Figure 1: A principle drawing of the Hall-Héroult process [11].

Liquid aluminium is denser than the electrolyte and, hence, settles at the bottom of the bath when it is produced. The top surface of the liquid metal acts as the cathode in the cell. [1, 3]

In an electrolysis hall, the cells are connected in series creating a pot line. High voltage rectifiers are used to maintain the same current on each cell. Modern cells today run on high amperage (up to 500 kA) to improve the productivity, while older cells run on lower amperage. [1, 3]

2.2 The Bayer Process

Alumina is produced from bauxite in the Bayer process. Bauxite is strip-mined and contains about 40-60% alumina on the forms gibbsite ($Al(OH)_3$), boehmite (AlOOH) and diaspore ($Al_2O_3 \cdot H_2O$). Bauxite also contains silica, titania, iron oxides among other small trace elements. In the Bayer process, alumina is extracted from bauxite by washing with sodium hydroxide, NaOH, at high temperature and pressure. This process is called digestion. The alumina is then clarified and a red mud is extracted from the aluminate solution. Fe_2O_3 is the compound giving the red mud its characteristic colour. Gibbsite is then precipitated by seeding and nucleation from the sodium aluminate solution. Calcination is performed to transform alumina trihydrate (gibbsite) to alumina. A fluid bed calciner is used and γ-alumina is produced. Further heating to 1250 °C also creates α-alumina. Depending on the calcination time, a relatively anhydrous alumina quality can be produced. For aluminium production, however, it is desirable to keep some of the moisture present in the alumina. This creates a smelter grade alumina, SGA. The amount of α-alumina should not exceed 30% because as higher amount of α-alumina give a poor crust quality. [1, 12]

Figure 2 shows a principle sketch on how alumina is produced in the Bayer process.

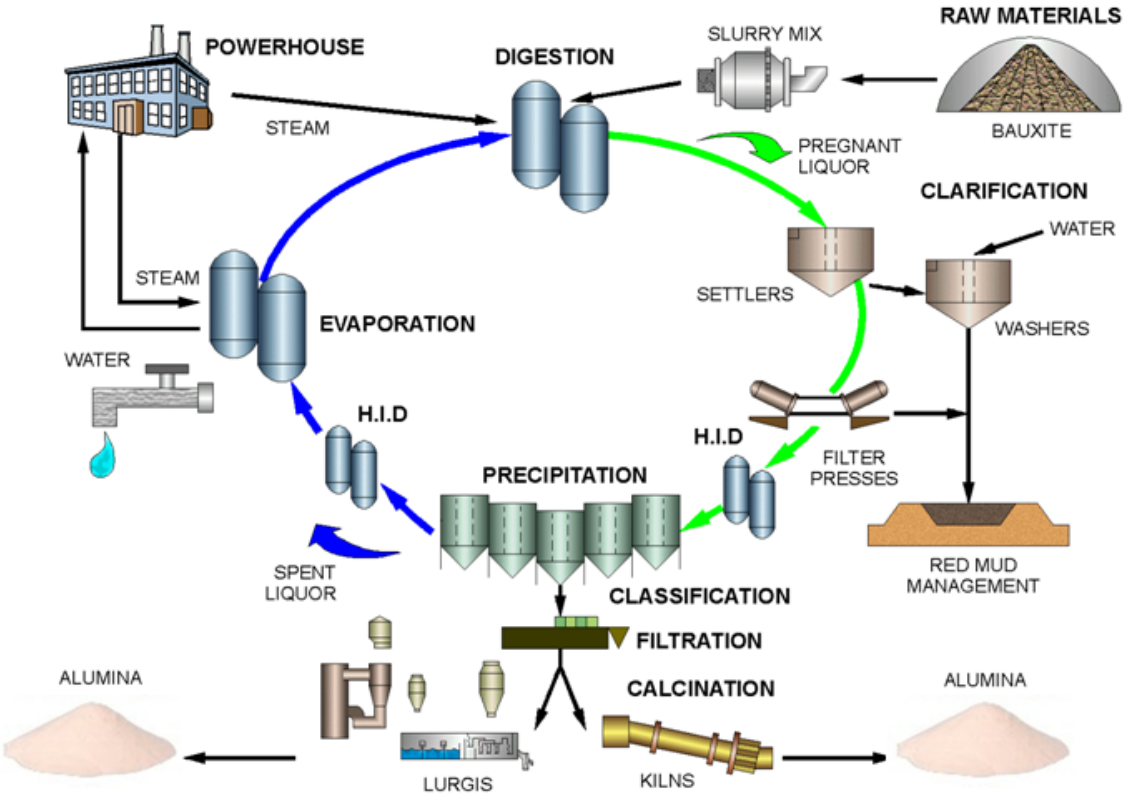

Figure 2: A principle sketch of how alumina is produced in the Bayer process [13].

2.3 Alumina

As previously mentioned, alumina is the raw material for aluminium production. In prebaked cells alumina is fed into the electrolyte in small portions by point feeders. Every 1-2 minutes the cells are fed with 1-2 kg of alumina, creating a nearly continuous feeding of the cells. According

to Reaction 1, the stoichiometric ratio implies that 1.89 kg of Al_2O_3 is required to produce 1 kg of aluminium. Preferably, alumina is fed in small portions to the bath as too large feed portions can create sludge of undissolved matter in the cell. This sludge will settle under the aluminium metal pad, and it is hard to remove. However, it is also important that the concentration of alumina is kept above a critical value, since the anode effect is caused by critically low alumina concentrations in the electrolyte. The anode effect causes lower current efficiency and higher emissions of greenhouse gases and is clearly undesirable. The optimum alumina concentration is around 2-4 wt% in the electrolyte. Alumina is also used to create the solid crust above the electrolyte. This crust is thermally insulating and helps conserve the heat in the cell. The electrolyte is protected from ambient air by the crust. The crust also covers the carbon anodes, protecting them from airburn. The third use of alumina is in the dry scrubber to eliminate fluoride emissions to the atmosphere. [1, 10, 12]

Alumina has several roles to play in aluminium production, and all of these roles put a great demand on the properties of the alumina. These properties include: particle size distribution, attrition index, specific surface area, loss on ignition, gibbsite content, phase distribution, impurity level and density [10].

2.3.1 Impurities in Alumina

The quality of the alumina used in the electrolysis process is important. Alumina with a poor quality can create problems e.g. metal with high impurity levels and lower current efficiency of the cell. Na_2O is the most eminent impurity, of about 0.5-0.6 %. Sodium oxide will react with aluminium fluorides to create cryolite, and this is considered a loss of AlF_3 in the bath. Calcium oxide is another impurity that can be present in the alumina. This compound can react with fluorides in the bath to create CaF_2. Silica, titania, iron oxide, phosphorous and vanadium might also be present as impurities. Phosphorous is one of the worst impurities due to its ability to reduce at the cathode and oxidize at the anode numerous times. As a result, the current efficiency is lowered, since phosphorous constantly "steal" current during the redox reactions. [12]

2.3.2 Primary and Secondary Alumina

Primary alumina is defined as alumina that has not been through the dry scrubber. Its appearance is white. Secondary alumina is defined as alumina that has been used in the dry scrubber to adsorb HF. Secondary alumina is greyer in colour than primary alumina due to carbon impurities. Usually secondary alumina is the quality usually being fed to the cells, unless a very high purity aluminium metal is to be produced [10].

2.3.3 Moisture in Alumina and Loss on Ignition

Alumina has a strong affinity for water due to its polar surface. Moisture adsorbs on alumina in different ways [14]:

- physisorbed water/physical adsorption of water
- chemisorbed water
- incorporated structural hydroxyl water in the crystal lattice

The definition of physically adsorbed water is water that adsorbs to a surface due to relatively weak Lifschitz-van der Waals forces. This means that the water adsorbs on the surface of the molecule due to attractive interaction forces that arise from permanent and/or induced dipoles. These forces are relatively weak. [15]

Chemisorption can be defined as electrons being regrouped in gas molecules and on the surface of a molecule to create covalent chemical bonds. [15]

Structural hydroxyl can be defined as OH-groups being bonded to aluminium atoms in the crystal lattice (e.g. gibbsite ($Al(OH)_3$ and boehmite (AlOOH). [16]

Loss on Ignition (LOI) is a measure on the mass loss of alumina upon heating. This mass loss is due to moisture evaporating from the alumina. LOI is often defined by which temperature range the alumina has been heated. When heating alumina from room temperature to 1000°C, all the three moisture types will evaporate. The total moisture content in the alumina will then evaporate. When heating from 0-110°C all of the physisorbed water and some of the chemisorbed water will evaporate. This loss on ignition is termed LOI(0-110°C). When performing an LOI(110-300°C) test, more chemisorbed water is removed as well as the structural hydroxyl water that is combined with gibbsite. In the transition alumina phases, the strongly bound chemisorbed and structural hydroxyl waters exist. These waters will evaporate at LOI(300-1000°C). [14]

According to Grjotheim and Kvande [12], the value of the LOI plays an important part when it comes to the dissolution of the alumina in the electrolyte. Between 0-1% LOI(300-1000°C), it was observed that the dissolution time of the alumina decreased with increasing LOI. Above 1% LOI(300-1000°C), this trend flattened out.

2.4 The Role of Alumina in the Dry Scrubber

The introduction of the dry scrubber in the 1960's added a new dimension to the alumina specification requirements. The alumina should not only fulfil the requirements to dissolve optimally in the electrolyte, it should also exhibit desirable properties when it comes to collecting fluoride gas and particulates in the dry scrubber. Before the dry scrubber was introduced, the fluoride emissions caused a deficit of fluorides in the electrolyte. The fluorides were emitted to the atmosphere and, hence, lost. Now, the off gas from the cell enters the fume treatment system of the plant and the gas is passed through the dry scrubber. With the dry scrubber technique, the fluorides are picked up by alumina and returned to the bath. More than 99% of all the fluorides formed in the aluminium production is picked up by the dry scrubber. Chemisorption is the mechanism by which the fluoride gas is recovered. [12]

The surface area is important for the alumina powder's capacity of HF removal in the dry scrubber, as well as its HF formation potential. The dry scrubber efficiency is directly related to the surface area available for adsorption of HF. Another important factor for scrubber efficiency is the pore size distribution. Smaller pores will inhibit the collection of HF, and it has been found that γ- ρ- and χ-aluminas have small pores with the consequence that these aluminas have poorer scrubber properties. High surface area within the alumina powders require that the powder has been less calcined at the alumina refinery; which, in turn, will result in relatively high gibbsite content. This high gibbsite content is important for good scrubber efficiency; however, it also contributes to increased HF formation due to the reaction between the structural hydroxyl in the alumina and fluorides in the electrolyte. [17]

2.5 The Electrolyte

Molten cryolite, Na_3AlF_6, has a high solubility of alumina. Cryolite based melts are therefore the main component of the electrolyte in an aluminium producing cell. Various additives are used in the cryolite to decrease the operating temperature and increase the current efficiency. The most common additives are aluminium fluoride, AlF_3, and calcium fluoride, CaF_2, but other additives may also be present in the bath. Baths containing excess aluminium fluoride are acidic and aluminium fluoride is defined as a strong Lewis acid. The acidic environment suppresses dissolution of sodium and produced liquid aluminium in the bath, causing the current efficiency to increase. The voltage across each cell is usually 4V. [1, 3, 10]

The usual temperature of the electrolyte is approximately 955 to 965°C, but it can both higher and lower. The electrolyte is not consumed during electrolysis, but some components evaporate from the bath and hereby enter the ventilation system of the plant. Also some electrolyte is lost through hydrolysis and penetration into the cathode lining. The typical distance between the lower ends of the anodes to the top surface of the liquid aluminium is 4-5cm. The electrolyte composition is vital in keeping the current efficiency as high as possible. [1]

2.5.1 Cryolite Ratio

The definition of the cryolite ratio (CR) is the mole ratio of sodium fluoride over aluminium fluoride. Most industrial aluminium cells operate at a cryolite ratio of about 2.2 for optimal current efficiency. [3]

2.5.2 Current Efficiency

The main factors affecting the current efficiency in industrial cells are [1]:

- AlF_3 content
- LiF content
- MgF_2 and CaF_2 contents
- Al_2O_3 content
- Content of impurities
- Temperature
- Superheat
- Cell design
- Magnetic field compensation

In modern electrolysis cells it is common to operate with excess concentrations of AlF_3 at about 12.7 wt% (CR=2.2). For this project work, the most important factor is aluminium fluoride. Fluoride losses from the melt occur according to Reactions 3 and 2. The main reason for increased current efficiency when operating with excess aluminium fluoride, is reduced metal solubility into the electrolyte, for both aluminium and sodium metals [1].

2.6 HF Formation

Hydrogen fluoride forms 1) due to hydrolysis of air moisture from the air draught carrying the exhaust gases from the cells towards the dry scrubber and 2) due to hydrolysis of moisture in the alumina fed to the cells [5]. The crust on top of the cryolite based melt is hence important in reducing the HF formation due to moisture in the air [18]. HF formation in the vapour phase above the melt and in the bath itself are shown in Reaction 2 and 3, respectively [2]. HF formation in the bath represents a loss of AlF_3. This loss will affect the cryolite ratio, the acidity of the bath and the current efficiency [1]. Figure 3 shows a principle sketch on the formation of HF inside an electrolysis cell [19].

$$NaAlF_4(g)+H_2O(g)=\frac{1}{3}Al_2O_3(diss)+2HF(g)+\frac{1}{3}Na_3AlF_6(g) \tag{2}$$

$$AlF_3(diss)+\frac{3}{2}H_2O(g)=\frac{1}{2}Al_2O_3(diss)+3HF(g) \tag{3}$$

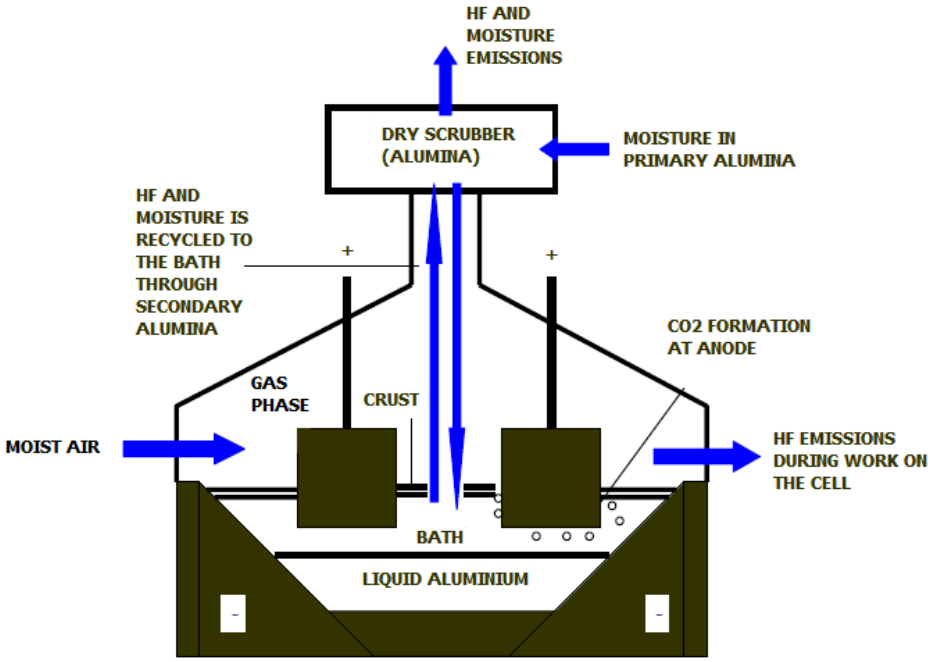

Figure 3: A principle drawing of the HF formation inside an electrolysis cell [19].

The main moisture source for HF formation has been identified as the structural hydroxyl moisture in smelter grade alumina [2, 5, 20]. Hyland et al [2] reported that smelter grade alumina has LOI(300-1000°C) between 0.4 and 0.9. Of this total moisture, only 5-11% is structural hydroxyl moisture. Experiments have shown that increasing structural hydroxyl moisture in the alumina increases the HF formation [2].

2.7 Methodology

2.7.1 NEO Lasergas II Single Gas Monitor

More or less HF is formed when adding different aluminas to a cryolitic melt. It was desirable to use a method that measures how much HF was formed and how fast it was formed. It was chosen to measure the HF formation and the corresponding H_2O concentration by using a tunable diode laser.

The Lasergas II Single Gas Monitor from the Norwegian company NEO Monitors AS has been used for measuring the HF formation and the corresponding moisture concentration in the off gas during addition of alumina to a cryolitic melt. The laser equipment has a short response time. The measuring principle is *in situ* and continuous, based on tuneable diode laser absorption spectroscopy. The measuring gas is led into a measuring cell with path length of 10cm. *"The LaserGas^{TM} utilizes a transmitter/receiver configuration (mounted diametrically opposite each other) to measure the average gas concentration along the line-of-site path [21]."* Each gas has their own distinct absorption lines at specific wavelengths and the measuring principle uses infrared single-line absorption spectroscopy. [21]

2.7.2 X-Ray Diffraction

X-Ray Diffraction (XRD) was used to quantify the phases in the aluminas. Extensive literature exists on the field of XRD, and this section will only give a brief introduction to XRD and its use. Powder XRD is a way of identifying phases, determining lattice parameters and lattice type in a polycrystalline powder sample. An X-ray beam hits the sample and the beam gives rise to a diffraction pattern. The sample is held at various angles in the instrument and the intensities and positions of the diffracted beam are recorded by an X-ray detector. The interplanar spacing, d_{hkl}, of the Miller planes (h k l) determines the position of the diffracted beam, and causing Bragg's law to be valid (Equation 4). [22, 23]

$$\lambda = 2d_{hkl}sin\theta \tag{4}$$

In the equation, λ represents the wavelength of the X-radiation and θ is the diffraction angle. The intensity of the beam is dependent on the position and type of atoms present, as the beam is diffracted more or less due to constructive or destructive interference. The diffractogram that is obtained from peaks at specific angles and with a certain intensity gives rise to a unique diffraction pattern for each crystalline compound. [22, 23]

A D8Focus unit from Bruker has been used to perform the XRD tests on the alumina samples in this work.

2.7.3 Thermal Gravimetric Analysis and Differential Scanning Calorimetry

Thermal Gravimetric Analysis (TGA) is used to measure the mass change of a sample upon heating. Differential Scanning Calorimetry, DSC, measures the change in power supply on the sample against a reference. Both the sample and the reference are kept at the same temperature by using separate power supplies. Change in enthalpy is measured by logging the power supplied

to the reference vs. the power supplied to the sample. Evaporation of water from an alumina sample is an endothermic reaction. [22]

The instrument used when performing both TGA and DSC was a Netzsch QMS403C. This instrument measures both the mass loss and the enthalpy changes of the sample, i.e. performing TGA and DSC, simultaneously.

3 Literature Study

3.1 Previous Work in this Field

This section will give a short summary of the relevant work on the field of HF formation when alumina is added to cryolitic melts.

3.1.1 Addition Order of Alumina to a Cryolitic Bath

Dando et al [6] have added different aluminas with various pre-treatment to a cryolitic bath. They performed electrolysis in their laboratory setup. The HF formation was measured continuously during the experiment. One finding of Dando et at's work was that the addition order did not affect the HF formation.

3.1.2 Moisture in Alumina and HF Formation

A lot has already been written in the Background and Methodology chapter, about the moisture content in the alumina. However, some features from previous research needs to be emphasized.

As mentioned previously, alumina has a high affinity for moisture. Alumina quickly adsorbs or desorbs water according to the ambient humidity. This type of water will mainly evaporate upon heating to 110°C [14]. However, some of the adsorbed water may form irreversibly bound gibbsite, $Al(OH)_3$ [14], and this fraction will evaporate in the temperature range from approximately 220-330°C [10].

In industry, the LOI losses most often referred to are in the range of 300-1000°C. Hyland, Gillespie and Metson [14] argues that this might be due to the fact that it is easier to create reproducible experiments in this temperature range. When doing experiments in the laboratory, the alumina will pick up or lose moisture if care is not taken to preserve the sample in its original atmosphere. This moisture will result in either a mass loss or addition in tests of LOI from room temperature to 300°C. LOI(300-1000°C) is used by the aluminium industry to verify that the calcination step in the Bayer process has fully decomposed the hydrates effectively. [14, 17]

Various scientists [6, 17] have suggested that today's specification sheet for smelter grade alumina, is inadequate. Gibbsite has been shown to be one of the major components causing HF evolution [17]. Also, Hyland et al [2] suggested that structural hydroxyl (gibbsite and boehmite) contribute more to HF formation than physically adsorbed water. They argue that the structural hydroxyl has a longer residence time in the electrolyte, and will dissolve when alumina dissolves. It has been suggested that the physically adsorbed water may flash off before it enters the electrolyte due to the high temperature near the bath [2]. Hence, it is important to have a good way of quantifying the amount of structural hydroxyl, physisorbed water and chemisorbed water. In light of this knowledge it has been suggested that the LOI value reported in the alumina specification sheet is problematic. The mass loss from evaporation of moisture in gibbsite is mixed together with the mass loss from surface adsorbed moisture with today's procedure of reporting LOI. The moisture from gibbsite evaporates from approximately 220-330°C [24]. These findings are supported by Perander et al, by using TGA. They showed that the moisture in gibbsite ($Al(OH)_3$) starts evaporating at around 250°C, creating boehmite [17]. Gibbsite will contribute with mass losses in both the temperature ranges, from RT-300°C and from 300-1000°C. Hence, when wishing to quantify the amount of gibbsite, it has been recommended to redefine the

temperature limits of the LOI measurements. The specification sheets used by industry today have shown a lack in prediction of the important quantities of gibbsite in the various aluminas. Perander et al [17] suggests that by using methods like XRD and TGA it is possible to quantify the gibbsite levels to a much more accurate extent, and this will improve the specification sheets from the alumina supplier.

3.2 Phases in Alumina

Figure 4 shows possible thermal decomposition routes for gibbsite [10, 25].

Gibbsite decomposes into various transition aluminas (χ-, κ-, γ-, γ'-, δ-, θ-, η- and ρ-alumina) until it reaches α-alumina. It should be noted that γ'-alumina has recently been discovered, and there is ongoing debate on its existence. The decomposition not only depends, as shown in the figure, on the size of the gibbsite particles, but also on the residence time in the calciner and on the heating rate. This creates alumina of high diversity. [10]

XRD is a method that can be used to identify the phases present in an alumina sample.

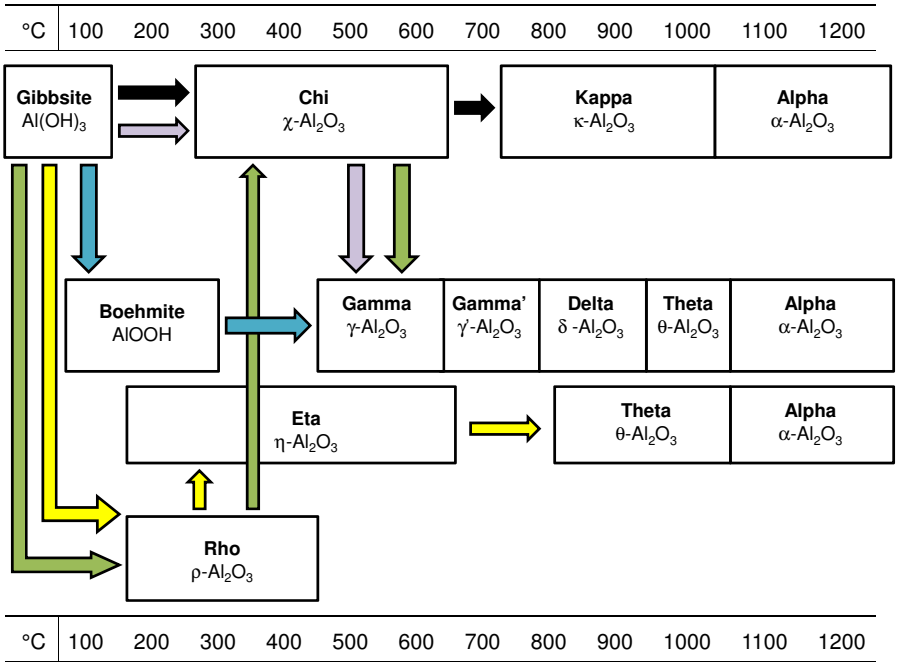

Figure 4: The possible thermal decomposition routes for gibbsite, adapted from [10, 25]. The green arrows show a flash calcination route [26]. The yellow arrows show the flash calcination under vacuum route [25]. The blue arrows show the route for flash calcination of large crystals [27]. The purple arrows show another flash calcination route [27, 28] and the black arrows show flash calcination of small crystals [27] or calcination at low heating rates or in dry air [25].

3.3 Alumina Particle Size Distribution and Fines in the Alumina

Fines in the alumina are formed both during production of smelter grade alumina and during handling of the alumina at the aluminium smelter. These fines may contain either increased levels of α-alumina due to increased retention time in the calciner or increased levels of gibbsite, depending on the calciner technology. In an aluminium smelter, fines are found undesirable. Fines containing higher levels of under calcined phases like boehmite and gibbsite can cause increased dusting, less aluminium output due to less Al_2O_3 present for reduction, increased HF formation and loss of bath (linked to the increased HF formation). [29]

3.4 Thermodynamic Considerations

Equation 5 shows the equilibrium expression for Reaction 3. It has been shown that HF formation in the bath happens according to Reaction 3 due to hydrolysis of bath components.

$$\Delta G^\circ = -RTln\frac{a_{Al_2O_3}^{1/2}P_{HF}^3}{a_{AlF_3}P_{H_2O}^{3/2}} \tag{5}$$

ΔG° equals the standard Gibbs energy. R is the gas constant and T is the temperature in Kelvin. a indicate the activities of the specie and P is the partial pressure of the specie.

Haupin and Kvande have created a mathematical model for calculating the hydrogen fluoride evolution in Hall-Héroult cells by using thermodynamics, kinetics and physical properties of the bath. They have found that HF formation is kinetically limited to approximately 25% of the equilibrium value of H_2O. A real electrolysis cell with all its features and parameters laid basis for their research findings. [5].

Solheim and Sterten [30] have developed a model helping to estimate the activities of NaF, AlF_3 and Al_2O_3 in a cryolitic melt. For details on the model, see the reference [30].

4 Experimental

4.1 Powder Separation

Alumina A and B were sieved at Norsk Hydro Porsgrunn to create three different powder sizes: -45 μm, +150 μm and bulk fractions. The -45 μm fraction only contain particles smaller than 45 μm in diameter, while the +150 μm fraction only contain particles larger than 150 μm in diameter. The aluminas hold different properties depending on the size of the particles. [8, 10]

4.2 Mass Loss upon Heating

4.2.1 Loss on Ignition

In this work, LOI measurements were performed. Mentioned previously, the temperature ranges used by industry are problematic due to the mixing of physisorbed, chemisorbed and structural hydroxyl water. Hence, the temperature ranges were modified to account for this. The temperature ranges used were:

- Room temperature to 160°C
- 160°C to 350°C
- 350°C to 1000°C

A muffle furnace was used when heating the samples. Two parallel samples were run for each alumina quality. 3 ± 0.5 g of alumina powder was put in an unlidded Pt-crucible. The samples were kept at each temperature (160, 350 and 1000°C) for two hours, then taken out of the furnace. A lid was placed on top of the crucible, placed in a desiccator and brought to an analytical balance for weighing. The analytical balance had an accuracy of 4 decimal places (0.0001g). The samples were not placed in a desiccator after being heated for two hours at 1000°C, they were simply placed on a plate made of a refractory material and quickly weighed on the analytical balance.

The mass loss upon heating when performing LOI testing is calculated by using the formulas given in Appendix F.

4.2.2 Thermal Gravimetric Analysis and Differential Scanning Calorimetry

The TGA and DSC testing was performed by PhD candidate Sophie Weber. A Netzsch QMS403C instrument was used to perform the testing. 20-30mg of alumina was weighed out for each test. The alumina powder was placed in a small sample holder of approximately 6mm diameter and 4mm height. The TGA and DSC testing were done simultaneously by the instrument. For the DSC testing, a reference sample holder was used to measure the change in enthalpy. To make the test more similar to the LOI test, it was experimented with using both hold times of two hours at 160, 350 and 1000°C and ramping the temperature directly up to 1000°C for the hydrate sample. For the other samples, the temperature was ramped directly up to 1000°C.

4.3 X-Ray Diffraction

XRD was performed on a D8Focus unit from Bruker using Cu K-alpha X-rays. The 2θ angles were run from 10-80° with a step width of 0.02°. The slit size was 0.2 mm. This procedure is in accordance with Perander's PhD work [10].

4.3.1 Sample Preparation

Some alumina powder was placed in a mortar and moistened with isopropanol. The alumina powder was then crushed using the mortar. A dropper was used to disperse the alumina/isopropanol mixture evenly on a single crystalline silicon sample holder. The alumina and isopropanol mixture was left to dry and then placed in the D8Focus.

4.4 Testing, Troubleshooting and Calibration of the Laser Instrument

When the laser was used in previous experiments [7], the moisture measurements were suspected offset. As work progressed it was suggested that an effort should be made to increase the understanding of the H_2O signal [7]. Extensive work has been put into increasing the H_2O understanding and a procedure on how to test, troubleshoot and calibrate the instrument has been made. The procedure on how to calibrate and troubleshoot the laser instrument can be found in Appendix A. Figure 5 shows the experimental setup used when testing the laser.

4.4.1 Moisture Testing and Verifying

N_2 gas from the NTNU grid was used when performing the moisture concentration testing. The flow of the gas was set by using an El-Flow Select Mass Flow Meter/Controller from Bronkhurst. This flow meter has been labelled A in Figure 5. The N_2 gas was enriched with moisture when entering the three bubble flasks shown in the figure. The temperature of the water bath was known and the H_2O concentration could be calculated by using the relationship between saturation pressure and temperature shown in Appendix B. The moisture enriched gas was diluted by adding dry N_2 gas from flow meter B. The flow was kept constant during the testing.

Flow meter A had been calibrated for N_2 while flow meter B had been calibrated for argon at the factory. Flow meter B was calibrated for N_2 in the laboratory. The calibration curves of flow meter A and B are shown in Appendix C.

The laser measured a large offset compared to the expected moisture concentration. To verify that it was the laser that caused the offset, and hence excluding a system error, an FTIR unit was placed in series with the laser to measure the moisture concentration simultaneously with the laser.

After a service (details in Appendix A) on the instrument performed by Ove Bjorøy at NEO, the offset in the moisture measurements of the laser was minimized. Various known concentrations of H_2O was added to the system and a relationship between the real and the measured value of H_2O was found. A new calibration constant for the laser was found by using this method.

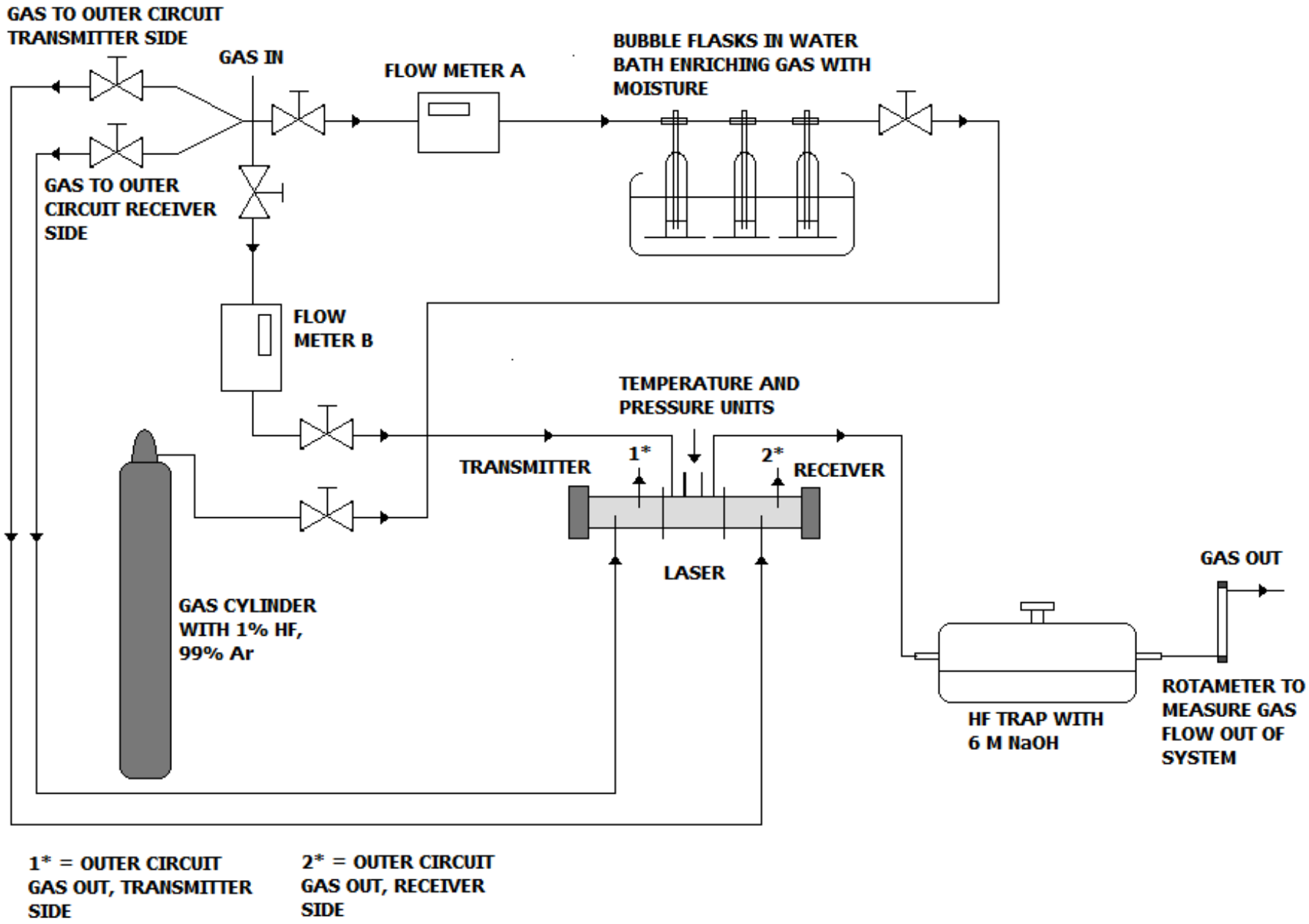

Figure 5: Experimental setup when testing and troubleshooting laser for verifying H_2O and HF concentrations.

4.4.2 HF Testing and Verifying

The laser was verified in terms of HF concentration by adding a calibration gas of 1% HF, 99% Ar to the laser, as shown in Figure 5.

4.5 Alumina Additions to a Cryolitic Melt

The laboratory measurements where different industrial aluminas were added to a cryolitic melt, were performed in continuation with the laboratory work performed by the author autumn 2010 [7]. A lot of method development was performed in the previous work to create a basis for the experiments in this thesis.

4.5.1 Laboratory Experimental Setup

A sketch of the experimental setup is shown in Figure 6. 1/16" PFA tubes were used to transport the gas. Nitrogen gas from the grid at NTNU was used during the experiments. The outer circuits of the laser were flushed with dry N_2 gas to remove any moisture from the transmitter and receiver compartments. Flow meters (A and B) were used to determine the gas flow of N_2 into the furnace, and nitrogen gas was constantly purged through the furnace. The nitrogen gas also acted as a carrier gas for the HF formed. The main nitrogen gas flow into the furnace was from the bottom of the furnace, as shown in Figure 6. A small gas flow entered the furnace through the feeder tube to keep this tube free from any condensation from the bath to keep the passage clear for alumina additions.

It should be pointed out that the lengths of the PFA tubes in between elements in Figure 6 are not in order of magnitude of the laboratory setup. It is emphasized that Figure 6 is only a schematic diagram.

During additions of alumina the only moisture source for hydrogen formation was moisture in the alumina fed to the cell. The gas leaving the furnace was led into the laser for analysis and was then led into an HF trap containing 6M NaOH to neutralize the hydrogen fluoride into sodium fluoride. A rotameter was placed after the HF trap to measure gas flow out of the system. The remaining gas left the system through the ventilation system in the lab. The u-tube was added to the laboratory equipment for safety. If the tube leading the gas out of the furnace would have become blocked, the gas would be forced into the u-tube. The u-tube contained glycerol and the level of this oil would change significantly due to the overpressure caused inside the furnace.

Figure 7 shows the experimental setup inside the furnace. The Pythagoras tube (h=72cm, $Ø_{outer}$=9.6cm) was covered by a nickel foil. The radiation shields were also made of nickel. The support system of the radiation shields, the thermocouple, gas and feeder tubes (h=7.4cm, $Ø_{outer}$=1.2cm) were all made of alsint. A platinum crucible was used to contain the cryolitic melt. The platinum crucible (h=6cm, $ø_{top}$=5.8cm, $ø_{bottom}$=3.2cm) was then placed inside a lidded nickel crucible (h=7.4, ø=7cm) as shown in Figure 8. The lid had holes for the three necessary components only: thermocouple, gas and feeder tube. The purpose of the lid was to keep the crucible system as closed as possible.

The feeder system used is shown in Figure 8a. This feeder system is in accordance with the proposed improvement of the feeder systems in earlier works [7]. The Y shape of the tube increased the control with the alumina feed, and made it possible to flush the feeder tube with gas to keep it open from condensate of the bath. Between every feeding of the bath, the silicon

tube and the glass container had to be changed. A clamp squeezed the silicon tube, and this clamp was unscrewed to release the alumina into the bath.

It should be noted that no electrolysis was performed during the experiments.

4.5.2 Experimental Procedure

NaF and AlF_3 were weighed out on an analytical balance and mixed thoroughly in the Pt-crucible. The Pt-crucible was placed in the Ni-crucible and then placed in the furnace. The furnace was sealed. Dry nitrogen gas was purged through both the furnace and the outer circuits of the laser.

The furnace was preheated over night at 200°C to remove any surface moisture in the NaF-AlF_3 mixture, as well as the alsint pieces. A computer program made sure that the temperature of the furnace was raised to 1000°C at 6 am on the morning of the experiment. A thermocouple was used to make sure that the cryolitic melt held 1000°C. A temperature of 1000° created a superheat of the melt equal to 19.5°C (the liquidus temperature of the melt is 980.5°C [31]). When the NaF-AlF_3 mixture had melted and a stable HF concentration baseline had been reached, alumina powder was weighed out and added to the melt through the feeder system and the feeder tube. The HF and H_2O concentrations were logged by a computer. New additions of alumina were made when a new stable baseline of HF had been reached. A procedure was found, that both the first and the last addition of alumina should be calcined alumina A, to check the reproducibility of the experiment.

As part of the procedure, the gas tube leading the gas out of the system was changed every time the feeder container had to be changed (in between every feeding of the cell). The gas out tube was changed to prevent it getting blocked by condensation from the bath.

The gas flows through flow meter A and B are summarized in Table 2. These gas flows were kept constant to allow for reproducibility.

Table 2: Gas flows.

Flow meter	Gas flow NmL/min
A	78.8 NmL/min
B	20.0 NmL/min

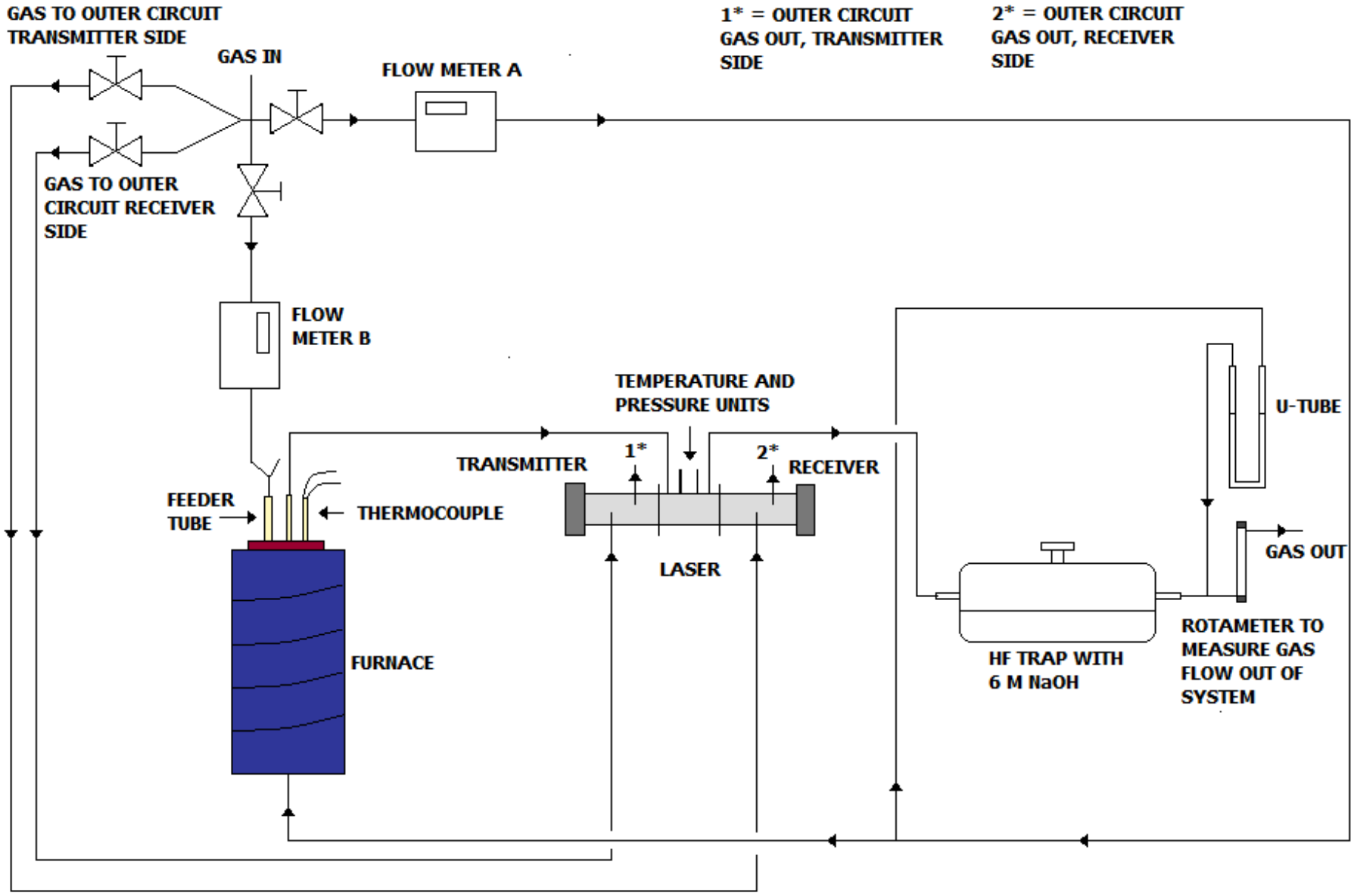

Figure 6: Sketch of the laboratory setup when performing experiments with alumina additions to a cryolitic melt.

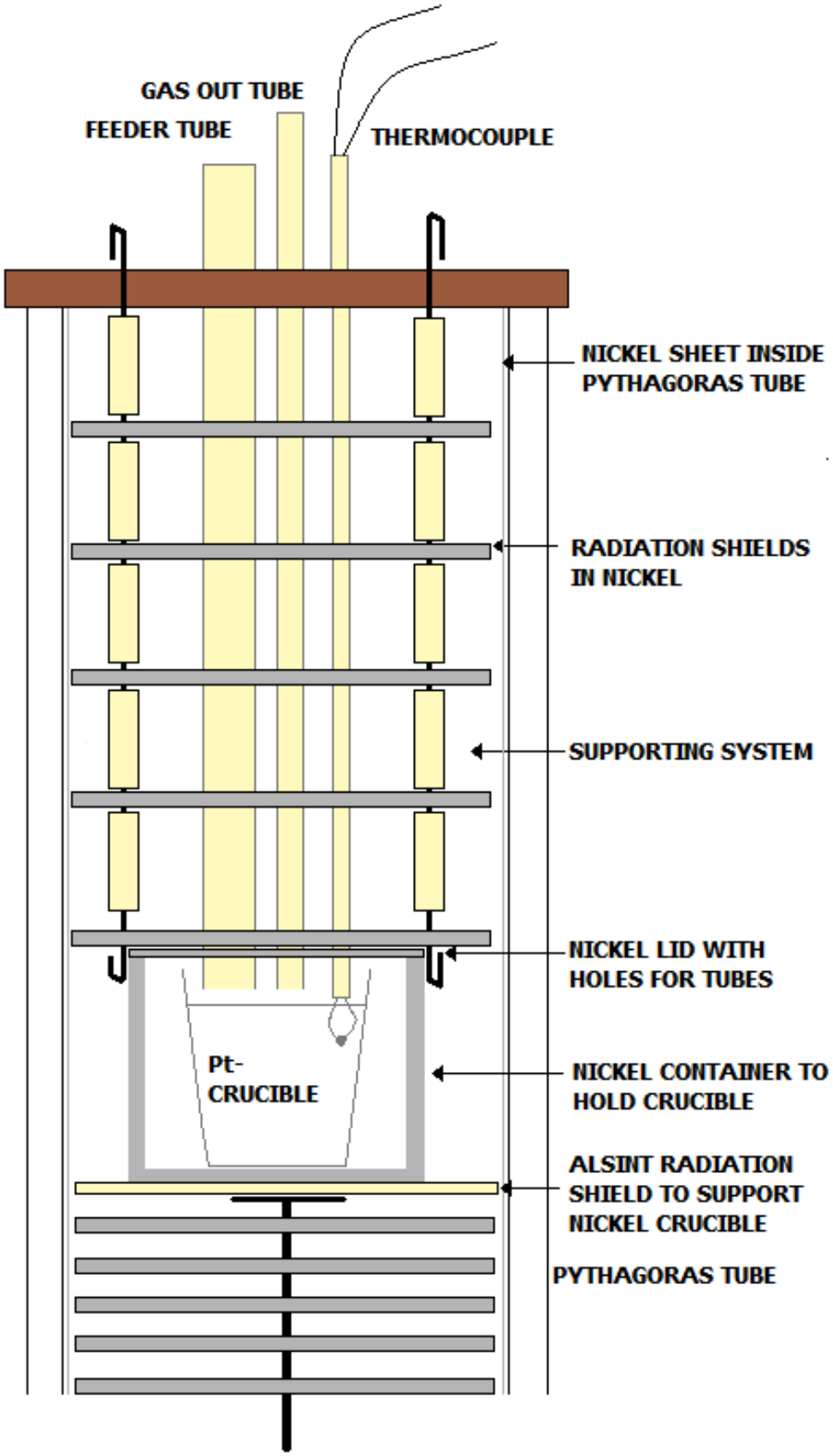

Figure 7: Sketch of the experimental setup inside the furnace.

(a) Feeder system (b) Crucible without lid (c) Crucible with lid

Figure 8: Photos of the feeder system, the Ni-crucible with the Pt-crucible inside without and with the lid.

4.5.3 Chemicals

Aluminium fluoride was sublimed at 1090°C under vacuum to remove oxides. The aluminium fluoride was kept as a solid in a desiccator before it was crushed in a mortar immediately before it was used in the experiment. The NaF was dried in an incubator at 160°C before use.

Alumina A, B and C are industrial alumina qualities used at Hydro Sunndal. Primary alumina was obtained by taking samples from alumina that had not yet entered the dry scrubber, while samples of secondary alumina was acquired by taking feeder samples from the feeder system on different cells in the pot room at Hydro Sunndal. Alumina A, B and C (both primary and secondary) were kept in plastic containers. Various pre-treatment regimes were used before addition to the melt, as part of the experimental procedure. The experimental cryolite melt had a cryolite ratio of 2.2, and contained NaF and AlF_3 only when the experiments started. However, earlier work has shown that a comparable melt with no alumina added did containe 0.63% alumina. The fact that alumina was found present is an indication that oxygen from moisture present in AlF_3 and NaF reacts to form some Al_2O_3.

Table 3 shows the properties of the chemicals used in the experiments.

Table 3: Conditions of supplied reagents.

Bath component	Producer	Pre-treatment	Amount [g]
AlF_3	Noralf/Norzink	Sublimated	71.42
NaF	Fluka Analytical	No pre-treatment	78.59
NaF	AlfaAesar	No pre-treatment	78.59
Al_2O_3 A	Confidential	Sieved into particle size fractions	0.15
Al_2O_3 A	Confidential	Calcined at 1200°C	0.15
Al_2O_3 B	Confidential	Sieved into particle size fractions	0.15
Al_2O_3 C	Confidential	Sieved into particle size fractions	0.15
Sum (excl. Al_2O_3 add.)			150

5 Results

5.1 Characterisation of the Industrial Aluminas

Several tests have been carried out to characterise the industrial aluminas. TGA, DSC and XRD have only been carried out on primary alumina. LOI has been carried out on both the primary and secondary alumina.

5.1.1 Loss on Ignition - Primary Alumina

All LOI results are reported to the nearest 0.01%. This is in accordance with the norm when reporting LOI in alumina specification sheets as well as internally in Hydro.

The average results for two samples are given with standard deviation. Standard deviation can be used when comparing two or more distributions [32]. Standard deviation gives an impression on the variation between the two samples.

Appendix F shows how to calculate the mass losses of the different temperature ranges and the LOI results for the two parallels of each test creating the foundation for the results given in Table 4. Table 4 shows the average numbers of the two parallels from the LOI measurements.

Table 4: Averaged LOI measurements performed on the primary alumina qualities, with drying at 160°C. *denotes single result due to spilling of the parallel sample at 1000°C.

Quality	LOI(RT-160°C) Avg ± stdv %	LOI(160-350°C) Avg ± stdv %	LOI(350-1000°C) Avg ± stdv %
A, hydrate	0.19 ± 0.02	28.89 ± 0.02	5.72 ± 0.02
A, calcined	0.50 ± 0.05	0.15 ± 0.00	0.08 ± 0.09
A, bulk	1.14 ± 0.03	0.44 ± 0.00	0.64*
A, +150 μm	1.06 ± 0.02	0.59 ± 0.03	0.93 ± 0.04
A, -45μm	1.47 ± 0.03	0.59 ± 0.03	0.79 ± 0.08
B, bulk	1.51 ± 0.03	0.68 ± 0.04	1.08 ± 0.15
B, +150 μm	1.78 ± 0.02	1.11 ± 0.10	1.08 ± 0.07
B, -45 μm	1.47 ± 0.04	1.76 ± 0.00	1.29 ± 0.04
C, bulk	1.59 ± 0.01	1.07 ± 0.02	0.88 ± 0.04

Table 5 shows average results of the LOI measurements on samples of alumina A that had been kept in a desiccator filled with water for three days at room temperature. Samples with a high amount of physisorbed water were created this way. The LOI testing was performed on samples that had been taken straight out of the desiccator without being stored in ambient conditions, thereby retaining their properties.

Table 5: Averaged LOI measurements performed on bulk fraction alumina A, humidified for three days at STP.

Quality	LOI(RT-160°C) Avg ± stdv %	LOI(160-350°C) Avg ± stdv %	LOI(350-1000°C) Avg ± stdv %
A, bulk	13.69 ± 0.17	0.62 ± 0.10	0.80 ± 0.14

5.1.2 Loss on Ignition - Secondary Alumina

Table 6 shows the results when performing LOI testing on the secondary aluminas. Note that one of the bulk fraction alumina B crucibles tipped over and some powder was spilled before it was weighed at 350°C. It was weighed at 350°C to get a value for LOI(350-1000°C) regardless of this spillage.

Table 6: Averaged LOI measurements performed on the secondary aluminas, with drying at 160°C. *denotes single result due to spilling of the parallel sample at 350°C.

Quality	LOI(RT-160°C) Avg ± stdv %	LOI(160-350°C) Avg ± stdv %	LOI(350-1000°C) Avg ± stdv %
A, bulk	2.18 ± 0.01	0.88 ± 0.02	1.93 ± 0.10
A, +150 μm	1.87 ± 0.02	0.89 ± 0.02	1.60 ± 0.04
A, -45μm	1.49 ± 0.01	0.87 ± 0.05	5.01 ± 0.01
B, bulk	2.23 ± 0.02	1.33*	2.31 ± 0.20
B, +150 μm	1.83 ± 0.04	1.05 ± 0.02	2.17 ± 0.10
B, -45 μm	1.38 ± 0.02	1.77 ± 0.03	5.69 ± 0.06
C, bulk	1.98 ± 0.02	1.26 ± 0.02	2.28 ± 0.27

5.1.3 Thermal Gravimetric Analysis and Differential Scanning Calorimetry

The results from the TGA and DSC analysis for the hydrate sample (high in gibbsite) of alumina A are shown in Figure 9. For this alumina quality the scan was run for both with and without dwell times at 160°C, 350°C and 1000°C for two hours. Figure 9 shows the comparison between the results of the TGA and DSC analysis with and without dwell times.

The results from the TGA and DSC analysis for the calcined alumina A are shown in Figure 10.

The results from the TGA and DSC analysis for the three different size fractions of alumina A are shown in Figures 11, 12 and 13. A comparison of the changes in mass for the three fractions is shown in Figure 14.

Figures 15, 16 and 17 show the results from the TGA and DSC analysis that was performed on the bulk, -45μm and +150μm fractions for alumina B. Figure 18 shows a comparison of the mass losses for the three fractions of alumina B.

Figure 19 shows the results from the TGA and DSC analysis that was performed on the bulk fraction.

Table 7 shows a summary of the mass change when performing TGA.

Table 7: Summary of the TGA results.

Quality	Δmass % RT-160°C	Δmass % 160-350°C	Δmass % 350-1000°C	Total Δmass % RT-1000°C
A, hydrate	0	27.20	7.62	34.81
A, hydrate dwell	0	27.87	6.82	34.67
A, calcined	0.30	0.10	0.16	0.56
A, bulk	0.80	0.29	0.53	1.62
A, +150 μm	1.74	0.52	0.67	2.93
A, -45 μm	1.27	0.45	0.49	2.20
B, bulk	1.44	0.90	0.74	3.09
B, +150 μm	1.62	0.94	0.89	3.45
B, -45 μm	1.24	1.70	0.82	3.76
C, bulk	1.29	1.04	0.73	3.05

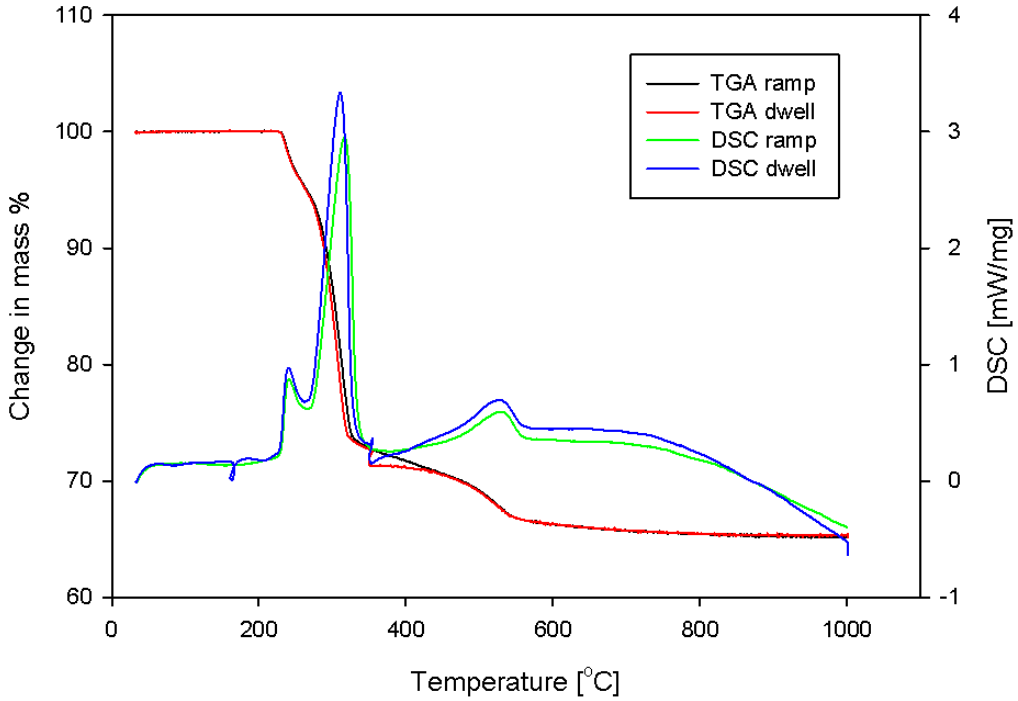

Figure 9: Comparison of the results from the TGA and DSC analysis for the hydrate samples of alumina A with and without dwell times of two hours at 160°C, 350°C and 1000°C. The graph shows a significant drop in mass from 220-320°C, this drop in mass can be identified as evaporation of moisture in gibbsite.

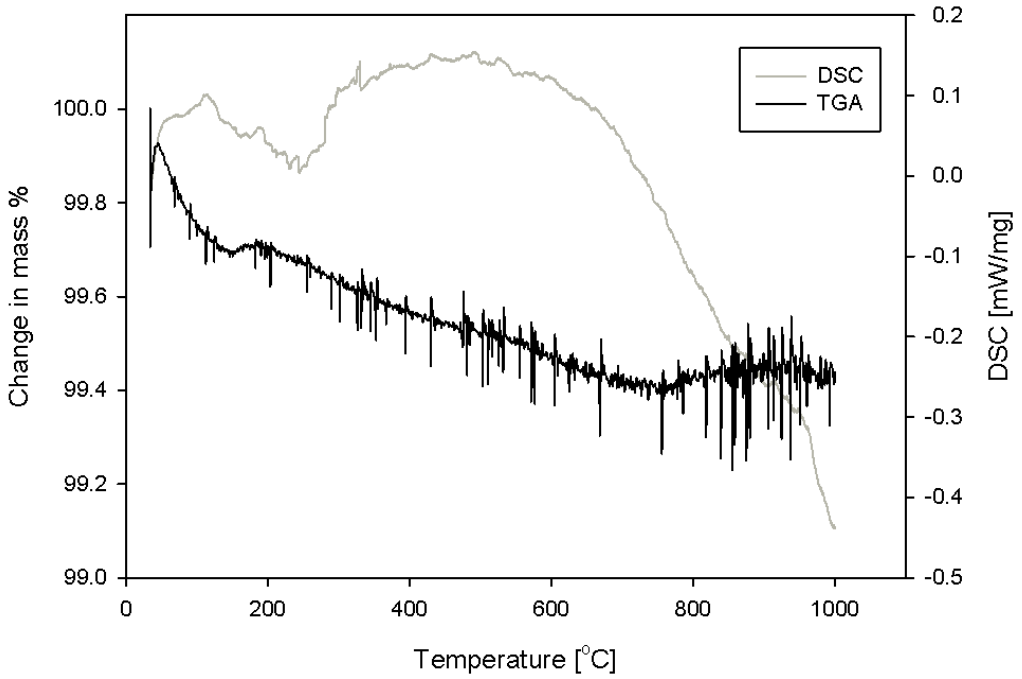

Figure 10: TGA and DSC analysis for the calcined sample of alumina A. Only a small change in mass is observed, indicating that the sample mainly consist of dry α-alumina.

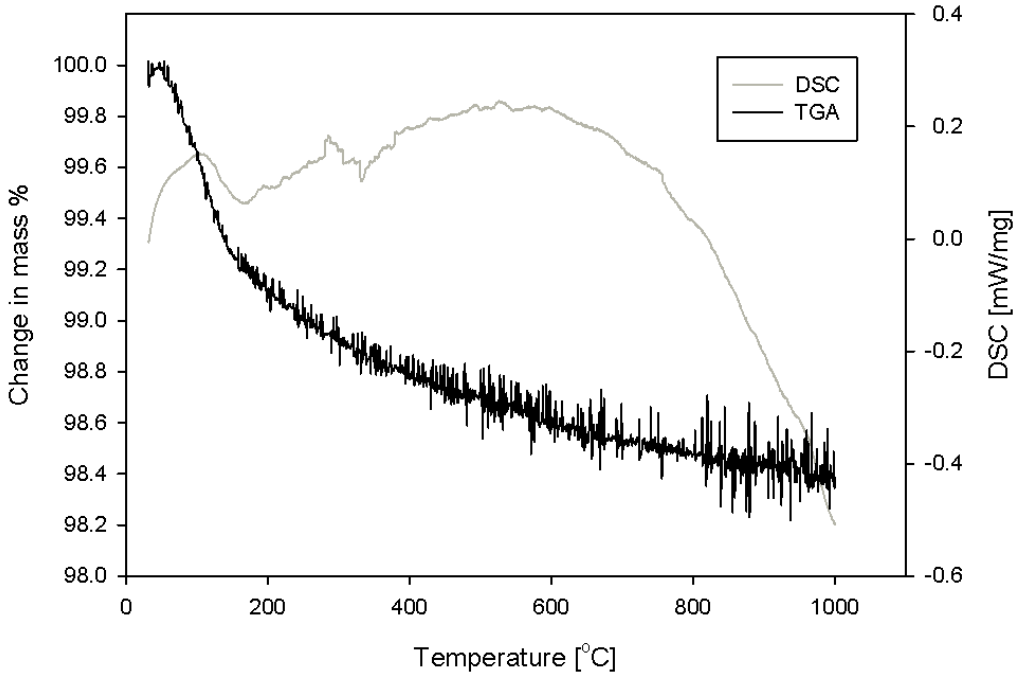

Figure 11: TGA and DSC analysis for alumina A, bulk fraction.

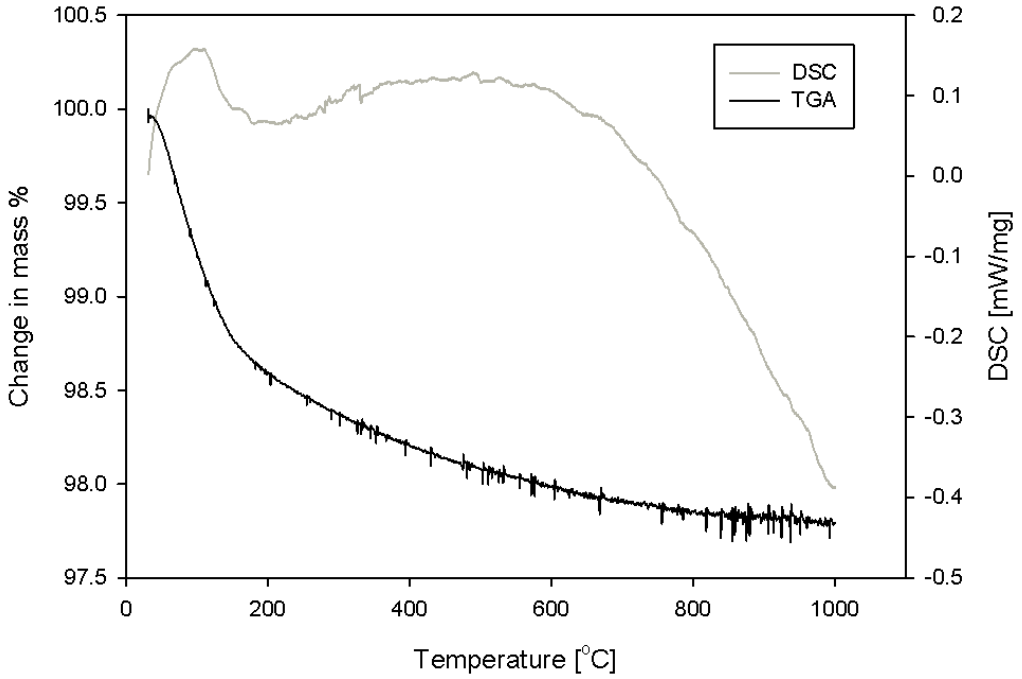

Figure 12: TGA and DSC analysis for alumina A, -45μm fraction.

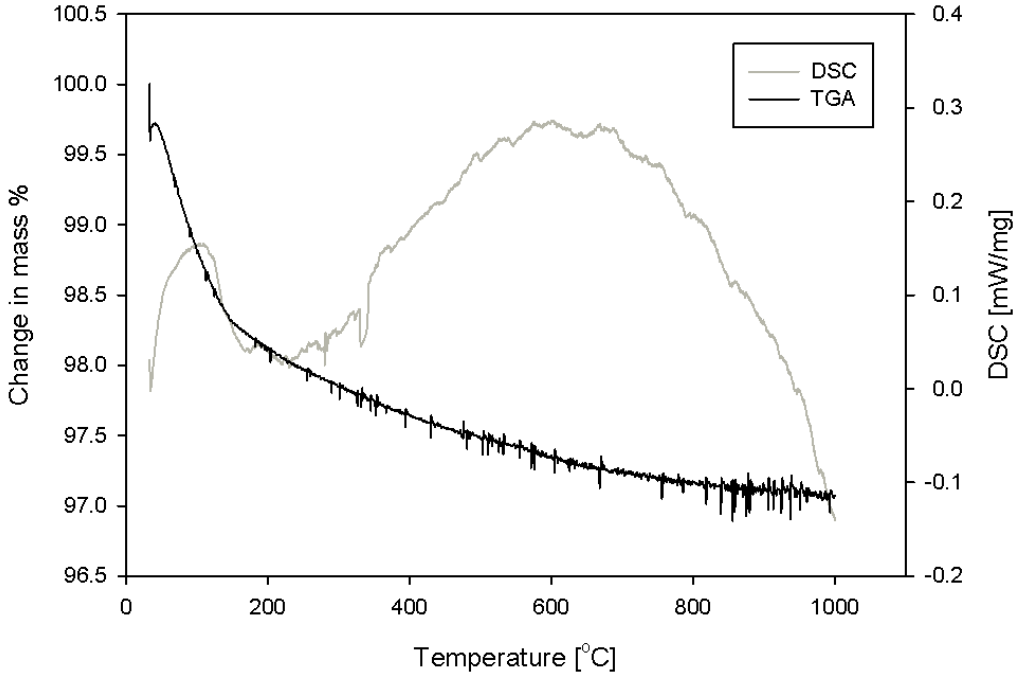

Figure 13: TGA and DSC analysis for alumina A, +150μm fraction.

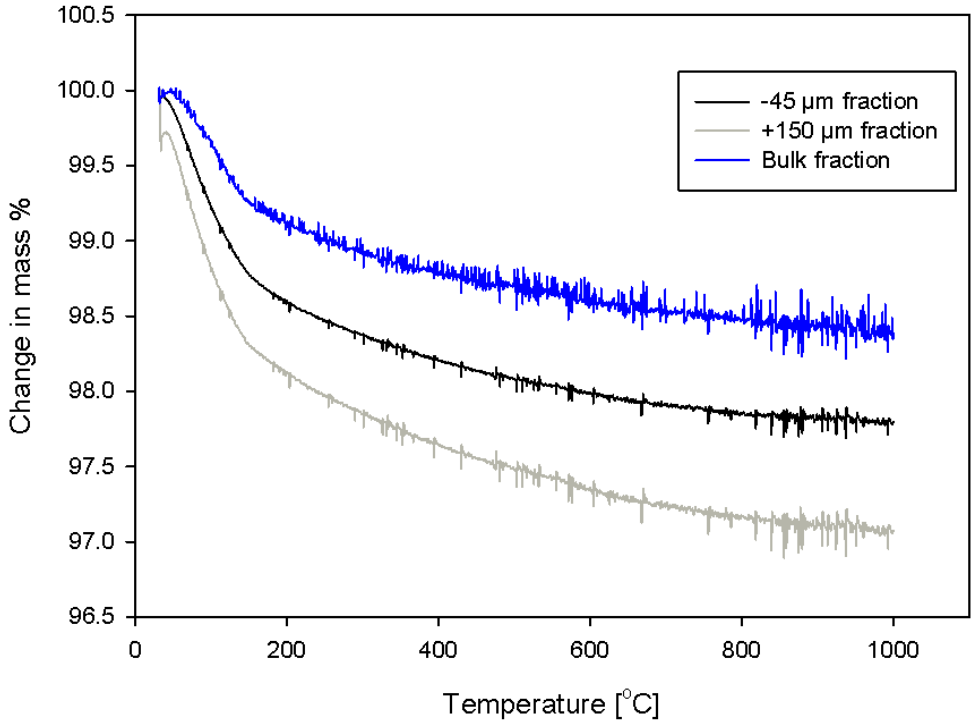

Figure 14: A comparison of the changes in mass for the three size fractions of alumina A. The graphs show that alumina A mainly consist of physisorbed moisture.

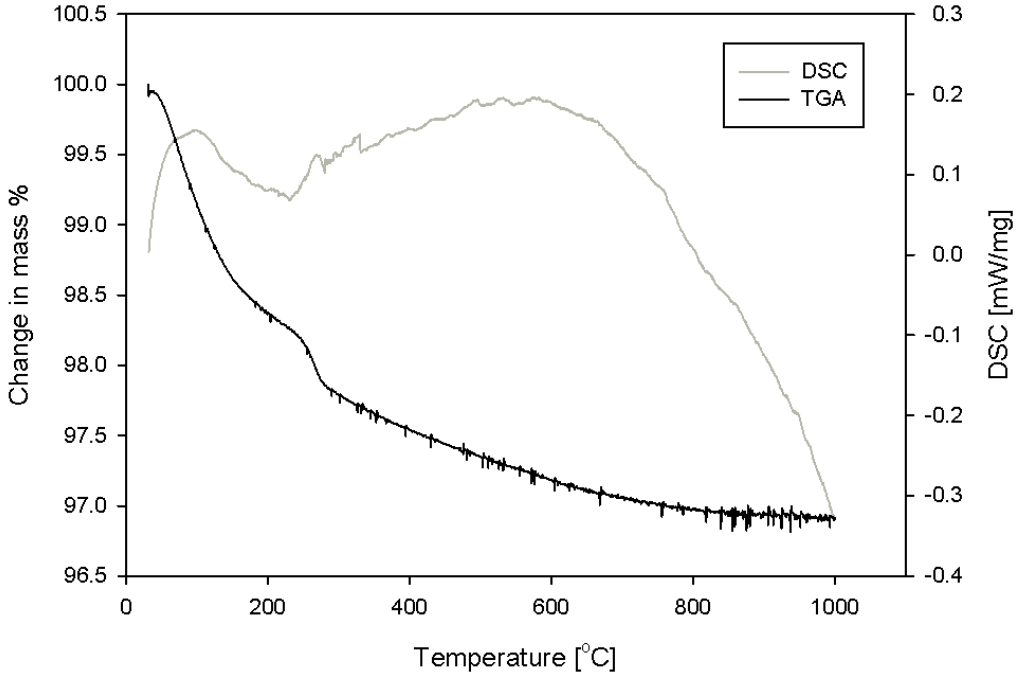

Figure 15: TGA and DSC analysis for alumina B, bulk fraction.

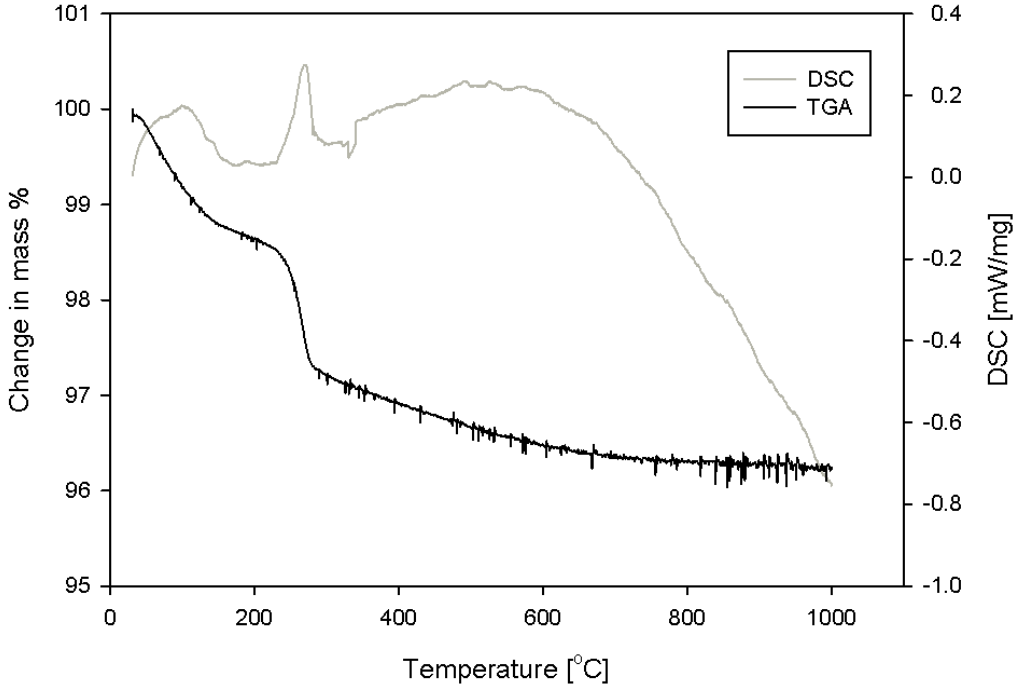

Figure 16: TGA and DSC analysis for alumina B, -45μm fraction.

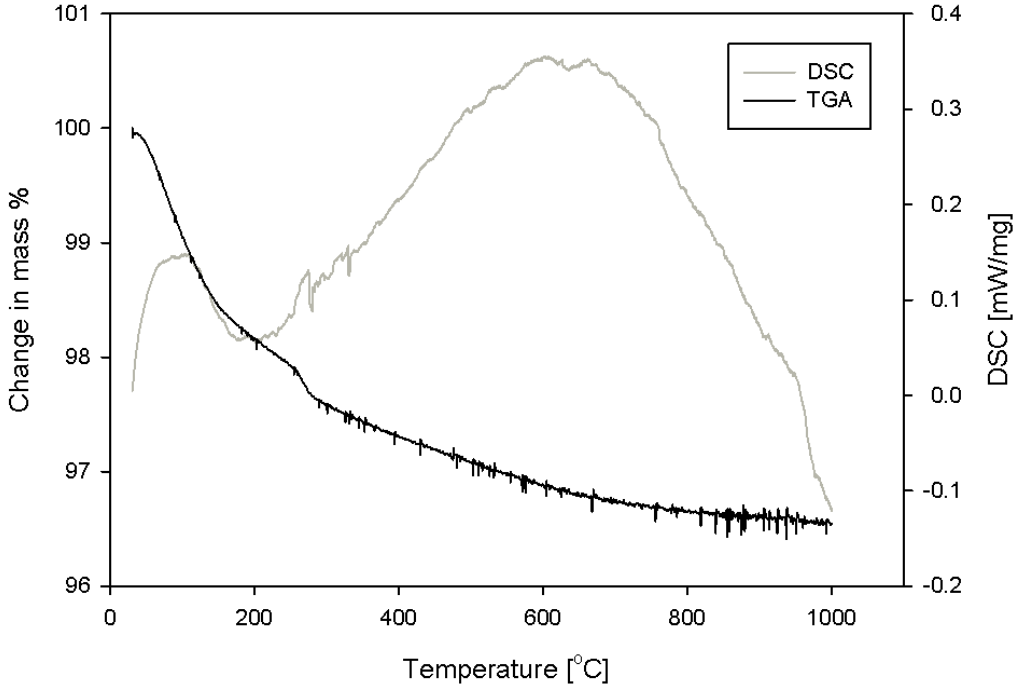

Figure 17: TGA and DSC analysis for alumina B, +150μm fraction.

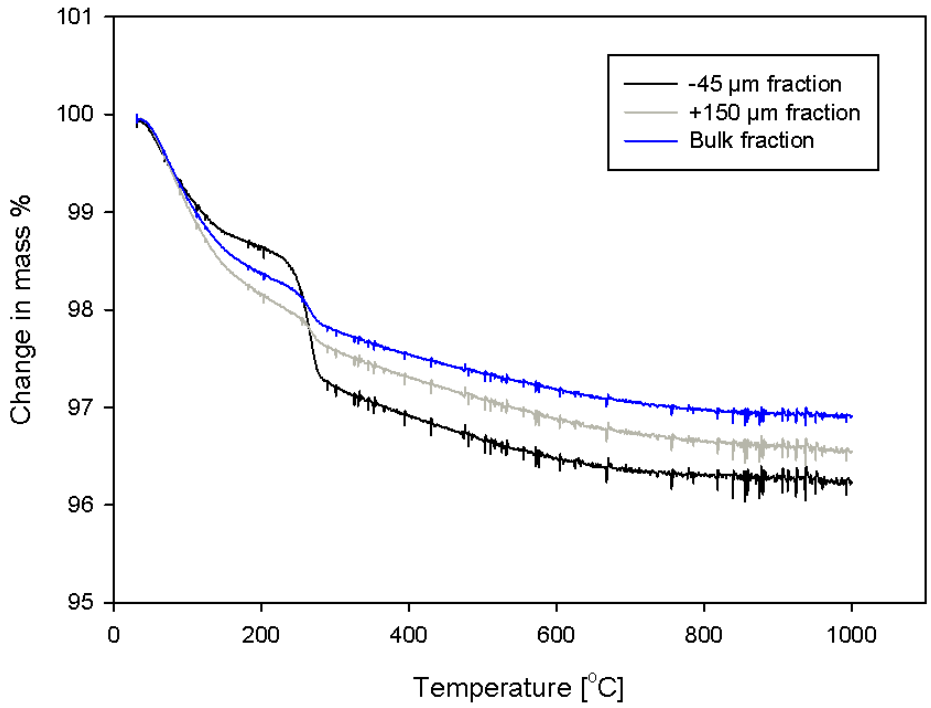

Figure 18: A comparison of the changes in mass for the three size fractions of alumina B. The graphs show that alumina B contains both physisorbed moisture and gibbsite. -45μm fraction alumina B contains more gibbsite than +150μm and bulk fractions.

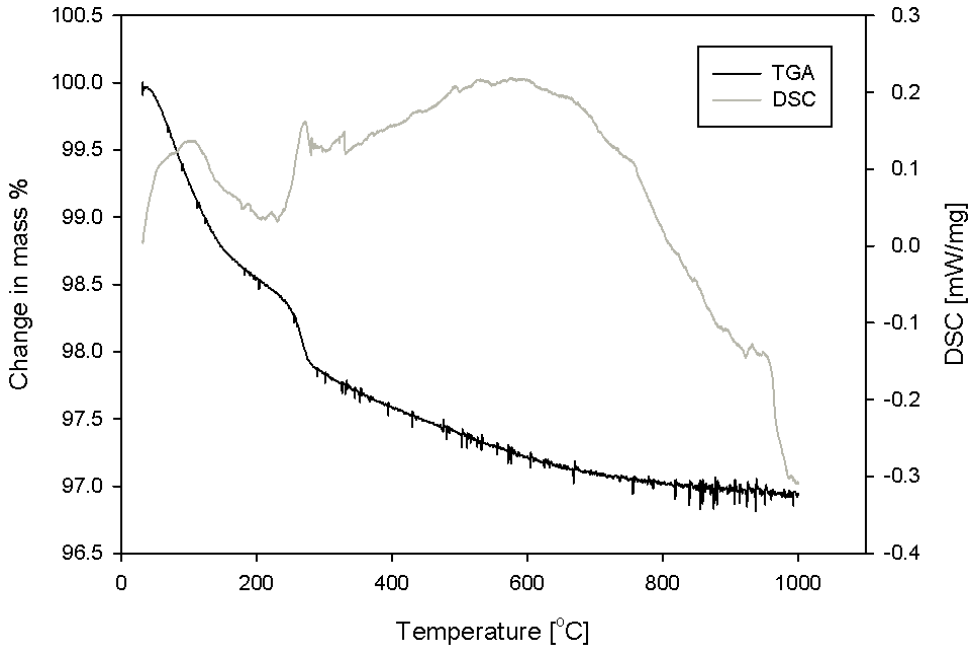

Figure 19: TGA and DSC analysis for alumina C, bulk fraction. It can be seen that alumina C behaves similarly to bulk fraction alumina B. The sample both contains physisorbed moisture and gibbsite.

5.1.4 X-Ray Diffraction on the Industrial Aluminas

Figures 20, 21, 22, 23 and 24 show the diffractograms of the hydrate alumina A, the calcined alumina A, all fractions of alumina A, all fractions of alumina B and bulk fraction of alumina C, respectively. The Eva software has been used to detect the phases with corresponding diffraction lines. An attempt was made to quantify the different phases by using Rietveld refinement in the Topas software. The result of this work is shown in Appendix G.

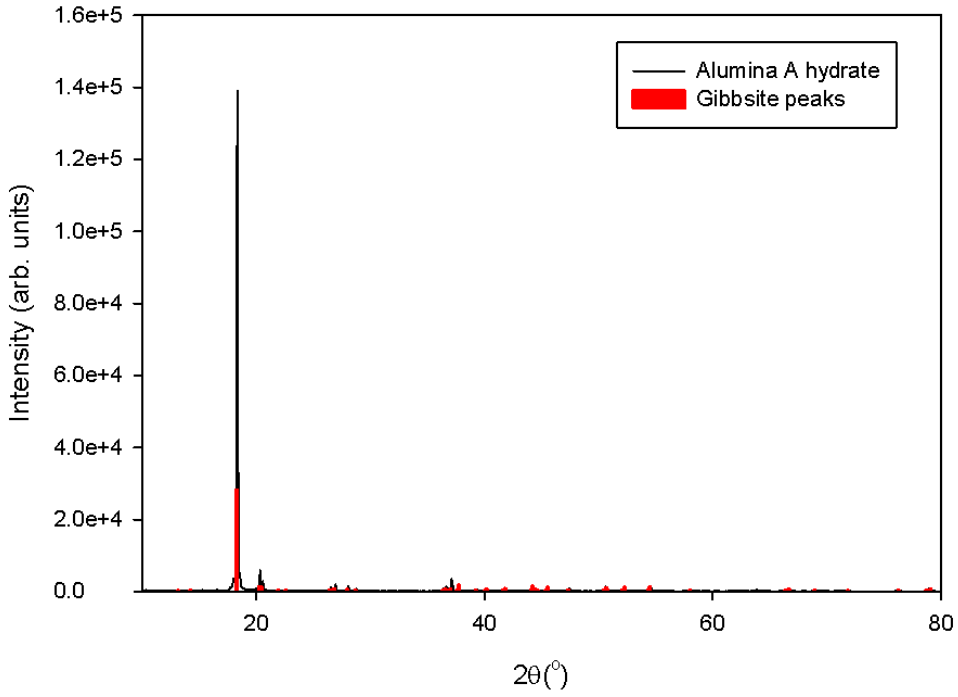

Figure 20: XRD diffractogram with diffraction lines for hydrate alumina A [33]. Gibbsite was the only identified phase in this diffractogram.

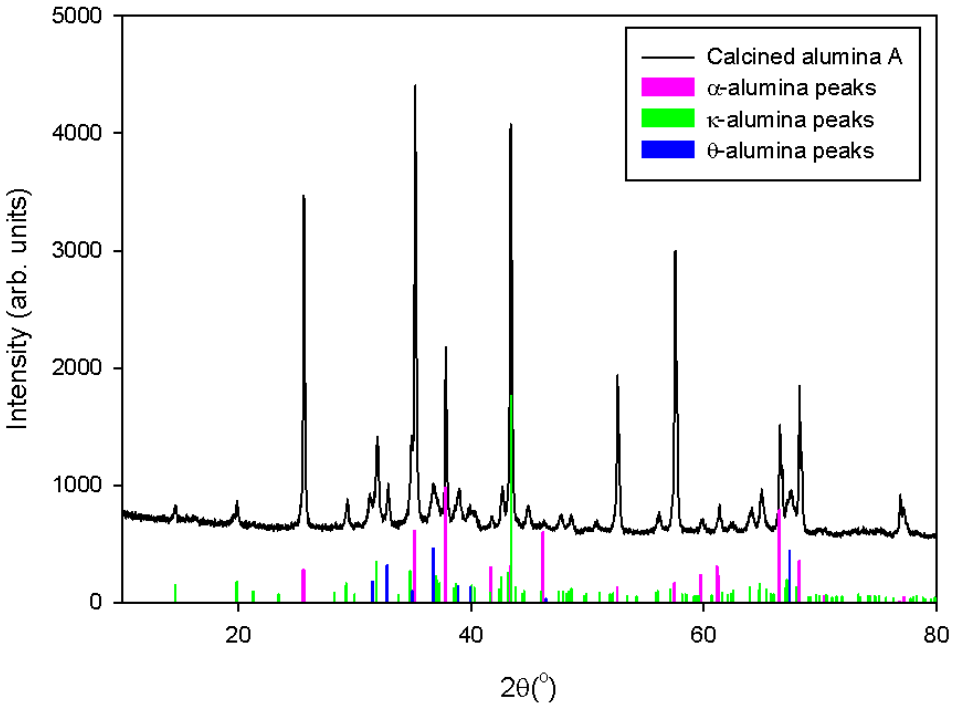

Figure 21: XRD diffractogram with diffraction lines for calcined alumina A [34, 35, 36]. The diffraction lines show that α-, θ- and κ-alumina were present.

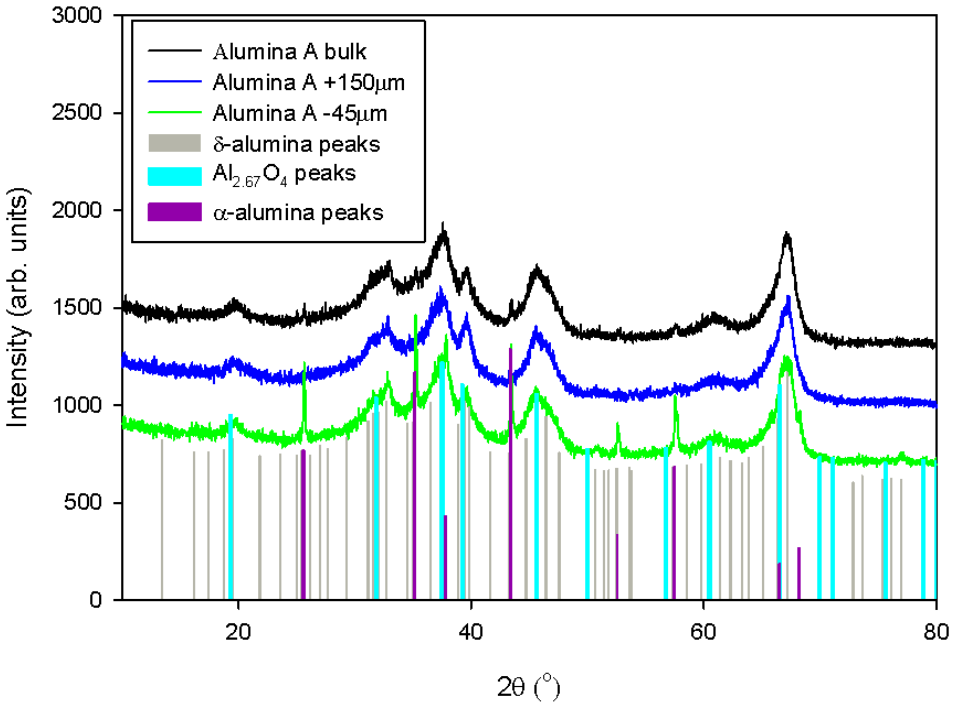

Figure 22: XRD diffractogram with diffraction lines for alumina A, all fractions [34, 37, 38]. The diffraction lines show that spinel $Al_{2.67}O_4$, α- and δ-alumina were present.

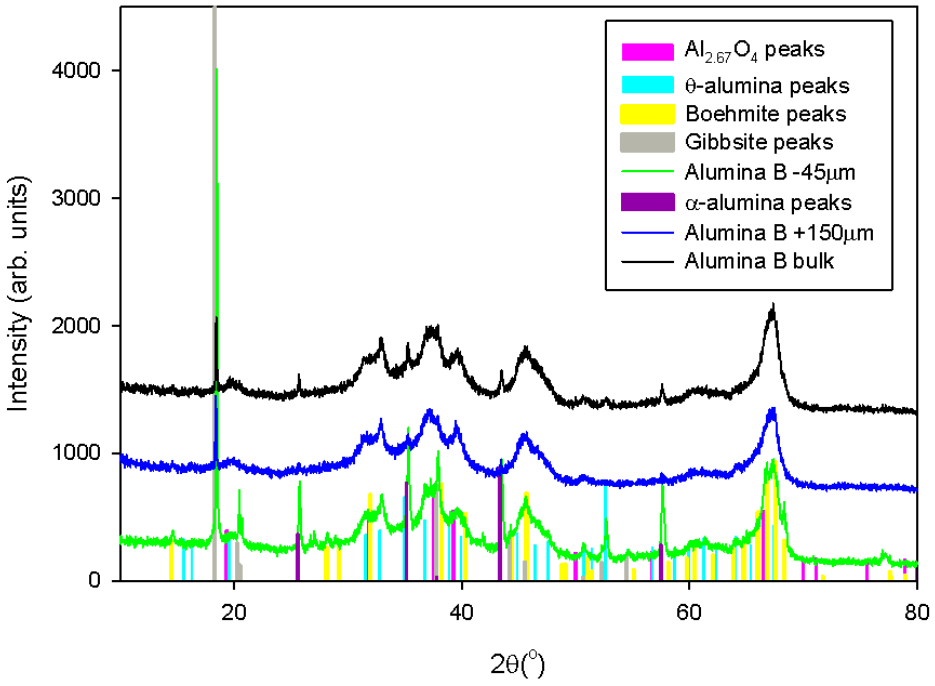

Figure 23: XRD diffractogram with diffraction lines for alumina B, all fractions [38, 36, 34, 33, 39]. The diffraction lines show that spinel $Al_{2.67}O_4$, gibbsite, α and θ alumina were present for all alumina B samples. For the -45μm fraction, boehmite was also detected.

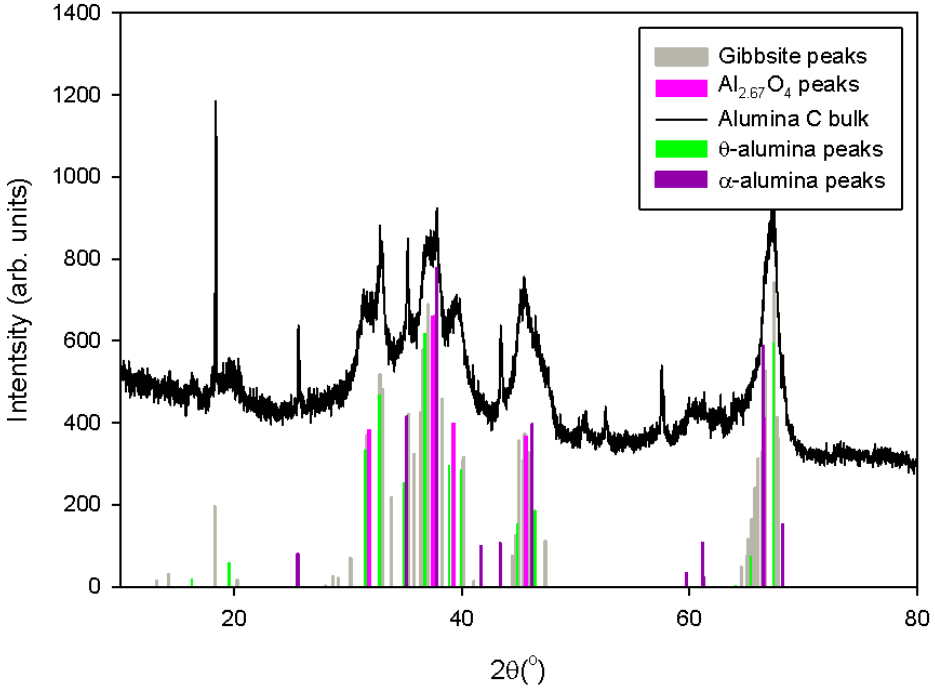

Figure 24: XRD diffractogram with diffraction lines for alumina C, bulk fraction [33, 38, 36, 34]. The diffraction lines show that spinel $Al_{2.67}O_4$, gibbsite, α- and θ-alumina were found present.

5.2 HF Formation and Moisture Behaviour when Adding Industrial Aluminas to a Cryolitic Melt

5.2.1 Testing Methodology and Reproducibility upon Addition of Industrial Aluminas to a Cryolitic Melt

The three following experiments were performed to check the methodology and reproducibility for measuring HF formation and H_2O concentration with the laser.

Experiment 1 - Addition of Calcined Alumina A and Mixtures of Hydrate and Calcined Alumina A

Figure 25 shows the results after five additions (addition 1-4 and 7) of alumina A that had been calcined in the laboratory at Hydro Porsgrunn and stored at 160°C at NTNU. Addition 5 consisted of a mixture of 85.7% calcined alumina A and 14.3% hydrate alumina A. Addition 6 consisted of a mixture of 86.2% calcined alumina A and 13.8% hydrate alumina A. Hydrate alumina A was kept at room temperature, as its low surface area greatly inhibits moisture adsorption. The "irregularities" between additions are caused by the changing of gas tubes and feeder.

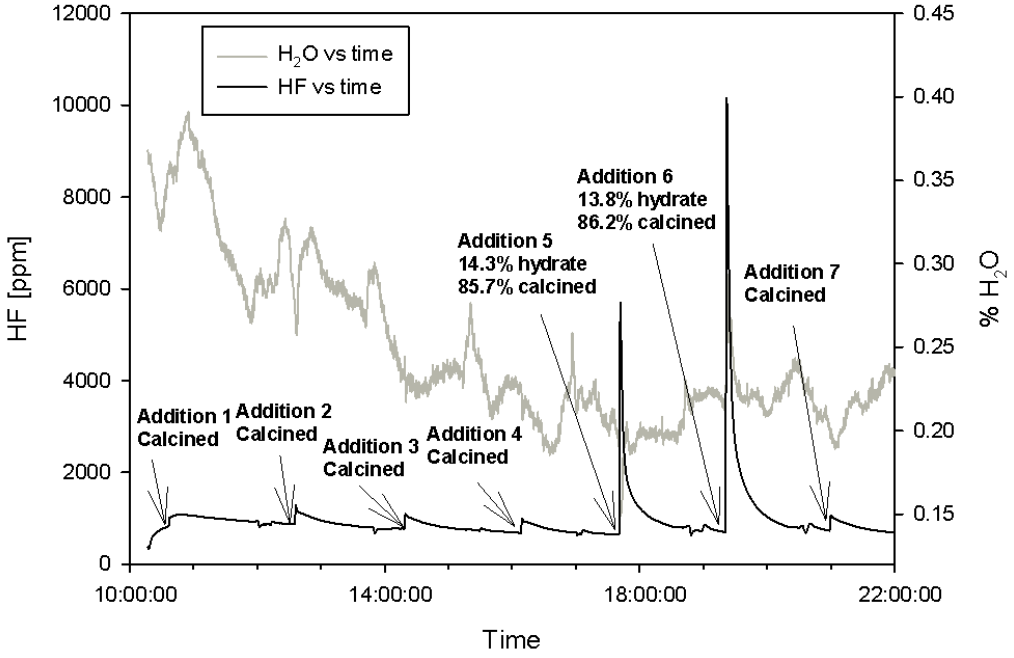

Figure 25: Experiment 1: Addition of calcined alumina A (additions 1-4 and 7) and 85.7% and 86.2% calcined alumina A and 14.3% and 13.8% hydrate of alumina A (high in gibbsite) (additions 5 and 6, respectively).

Table 8 shows a summary of the addition quantities of alumina, the alumina type and quality, and the addition order. A flexible tube was used as part of the alumina feed system as shown in Figure 8a. Some alumina sticks on the walls of this flexible silicon tube. To correct for this loss in alumina, the tube was weighed before and after addition of alumina. The loss in alumina has been substracted from the original amount of alumina weighed out. The flexible tube was changed in between each alumina addition.

Table 8: Experiment 1: Addition quantities of alumina. *denotes that it was forgotten to weigh the flexible tube before adding alumina.

Addition number	Quality	Type	Quantity weighed out [g]	Quantity after loss [g]
1	Alumina A	Calcined	0.2088	*
2	Alumina A	Calcined	0.2087	0.1725
3	Alumina A	Calcined	0.2061	0.1910
4	Alumina A	Calcined	0.2006	0.1553
5	Alumina A	Hydrate	0.0300	
5	Alumina A	Calcined	0.1800	
5	Alumina A	14.3%H/85.7%C mix	0.2100	0.1539
6	Alumina A	Hydrate	0.0289	
6	Alumina A	Calcined	0.1802	
6	Alumina A	13.8%H/86.2%C mix	0.2091	0.1505
7	Alumina A	Calcined	0.2040	0.1647

Table 9 shows the addition sequence, the amounts of HF, calculated from hydrogen mass balance (HMB) for H_2O from LOI and TGA data, as well as the actual amount of HF found in the experiment through Riemann sums. The possible HF formation has been calculated by using the total LOI and TGA values found for hydrate alumina A from room temperature to 1000°C and the LOI and TGA values for calcined alumina A from 160-1000°C, see Tables 4 and 7. A calculation example is given in Appendix H. When doing these calculations it is assumed that an equal amount of hydrate and calcined alumina sticks to the walls of the flexible silicon tube. Hence, it is assumed that the composition of the mixtures remains the same. This procedure will also be followed in experiment 2.

The amount of HF formed during the experiment was found using Riemann sums [40] to calculate the area under the HF curve for 30 minutes after each alumina addition. A calculation example for Riemann sums is given in Appendix E. When doing the calculations, the baseline of HF obtained before each addition has been subtracted from the total amount of HF. The value of this baseline is also shown in Table 9. This procedure will be followed in all eight experiments.

Table 9: Experiment 1: The addition sequence, the amounts of HF, calculated from HMB for H_2O from LOI and TGA data and the quantities of HF found for the experiment calculated through Riemann sums with corresponding baselines.

Addition sequence	HF from H LOI [g]	HF from H TGA [g]	Amount HF from experiment [g]	Baseline [ppm]
Calcined	$8.5{\cdot}10^{-4}$	$9.7{\cdot}10^{-4}$	$6.0{\cdot}10^{-4}$	825
Calcined	$8.8{\cdot}10^{-4}$	$1.0{\cdot}10^{-3}$	$4.2{\cdot}10^{-4}$	875
Calcined	$9.8{\cdot}10^{-4}$	$1.1{\cdot}10^{-3}$	$4.2{\cdot}10^{-4}$	775
Calcined	$7.9{\cdot}10^{-4}$	$9.0{\cdot}10^{-4}$	$4.2{\cdot}10^{-4}$	685
14.3%H/85.7%C	$1.8{\cdot}10^{-2}$	$1.8{\cdot}10^{-2}$	$2.9{\cdot}10^{-3}$	650
13.8%H/86.2%C	$1.7{\cdot}10^{-2}$	$1.7{\cdot}10^{-2}$	$5.4{\cdot}10^{-3}$	705
Calcined	$8.4{\cdot}10^{-4}$	$9.6{\cdot}10^{-4}$	$4.4{\cdot}10^{-4}$	730

Experiment 2 - Addition of Mixtures of Hydrate and Calcined Alumina A

Figure 26 shows the results when adding various mixtures of hydrate and calcined alumina A. Unfortunately, the first gas tube used in this experiment broke into two pieces sometime in the time period from 9:00-10:20. This was discovered when the gas tube was changed. The gas tubes are made of alsint (dry Al_2O_3). Approximately 5g of alsint fell into the cryolitic melt and was dissolved. Hence, the chemistry and composition of the melt was changed. It was decided to continue the experiment, despite of this incident.

To experiment with the effect of N_2 gas flow, the gas flow was doubled through the furnace during addition 7. The gas flow was increased at 19:17, causing the HF baseline to drop through increased dilution of the gas.

During addition 8 it was discovered that the gas flow through the system was poor. The flexible PFA tube leading the gas from the gas tube into the laser was blocked due to condensation. The tube was cleaned using pressurized air, and a new addition of the same mixture composition as addition 8 was added to the furnace (addition 9). During the procedure of cleaning the PFA tube, the furnace was open and HF gas from addition 8 leaked out of the system into the fume cupboard.

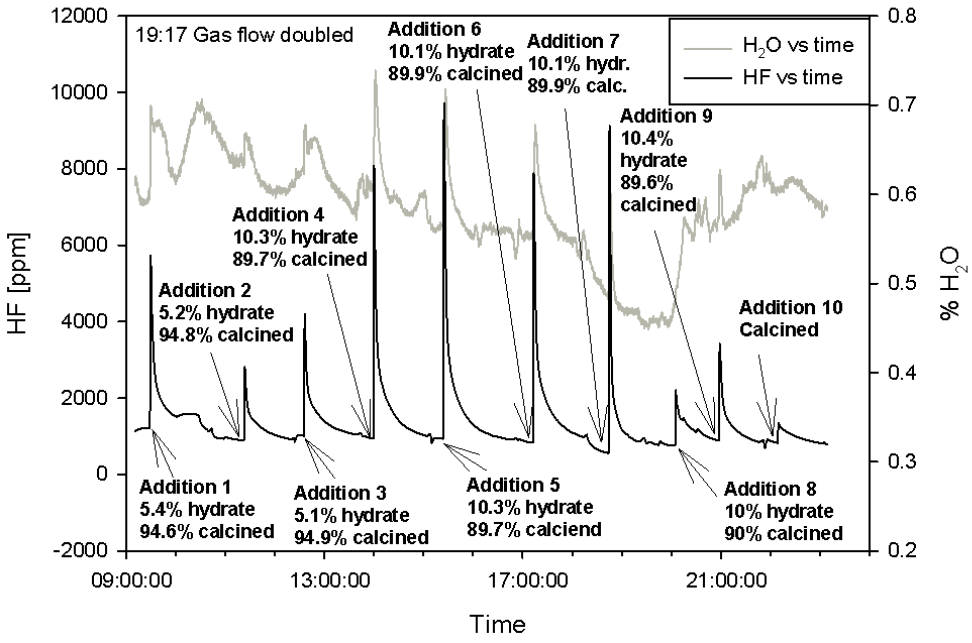

Figure 26: Experiment 2: Addition of various mixtures of hydrate and calcined alumina A (addition 1-9). Addition 10 was pure calcined alumina A.

Table 10 shows a summary of the quantities of the alumina additions. The quantity after loss refers to the loss of alumina in the silicon tube as earlier described.

Table 11 shows the addition sequence, the amounts of HF, calculated from HMB for H_2O from LOI and TGA data, as well as the actual amount of HF found in the experiment through Riemann sums [40]. The baseline in front of each alumina addition is also shown in the table. Note that no value for the amount of HF from experiment has been obtained in addition 8 due to the problems with the PFA tube.

Table 10: Experiment 2: Addition quantities of alumina.

Addition number	Quality	Type	Quantity weighed out [g]	Quantity after loss [g]
1	Alumina A	Hydrate	0.0109	
1	Alumina A	Calcined	0.1899	
1	Alumina A	5.4%H/94.6%C mix	0.2008	0.1725
2	Alumina A	Hydrate	0.0103	
2	Alumina A	Calcined	0.1896	
2	Alumina A	5.2%H/94.8%C mix	0.1999	0.1673
3	Alumina A	Hydrate	0.0102	
3	Alumina A	Calcined	0.1905	
3	Alumina A	5.1%H/94.9%C mix	0.2007	0.1662
4	Alumina A	Hydrate	0.0207	
4	Alumina A	Calcined	0.1803	
4	Alumina A	10.3%H/89.7%C mix	0.2010	0.1728
5	Alumina A	Hydrate	0.0206	
5	Alumina A	Calcined	0.1798	
5	Alumina A	10.3%H/89.7%C mix	0.2004	0.1694
6	Alumina A	Hydrate	0.0205	
6	Alumina A	Calcined	0.1832	
6	Alumina A	10.1%H/89.9%C mix	0.2037	0.1812
7	Alumina A	Hydrate	0.0202	
7	Alumina A	Calcined	0.1796	
7	Alumina A	10.1%H/89.9%C mix	0.1998	0.1712
8	Alumina A	Hydrate	0.0100	
8	Alumina A	Calcined	0.0899	
8	Alumina A	10.0%H/90.0%C mix	0.0999	0.0786
9	Alumina A	Hydrate	0.0104	
9	Alumina A	Calcined	0.0897	
9	Alumina A	10.4%H/89.6%C mix	0.1001	0.0746
10	Alumina A	Calcined	0.2009	0.1771

Table 11: Experiment 2: The addition sequence, the amounts of HF, calculated from HMB for H_2O from LOI and TGA data and the quantities of HF found for the experiment calculated through Riemann sums with corresponding baselines. Note that for addition 7 the N_2 gas flow was doubled.

Addition sequence	HF from H LOI [g]	HF from H TGA [g]	Amount HF from experiment [g]	Baseline [ppm]
5.4%H/94.6%C	$8.1{\cdot}10^{-3}$	$8.2{\cdot}10^{-3}$	$2.7{\cdot}10^{-3}$	1125
5.2%H/94.8%C	$7.5{\cdot}10^{-3}$	$7.6{\cdot}10^{-3}$	$1.5{\cdot}10^{-3}$	897
5.1%H/94.9%C	$7.3{\cdot}10^{-3}$	$7.5{\cdot}10^{-3}$	$2.1{\cdot}10^{-3}$	1020
10.3%H/89.7%C	$1.5{\cdot}10^{-2}$	$1.5{\cdot}10^{-2}$	$4.3{\cdot}10^{-3}$	940
10.3%H/89.7%C	$1.4{\cdot}10^{-2}$	$1.4{\cdot}10^{-2}$	$4.8{\cdot}10^{-3}$	935
10.1%H/89.9%C	$1.5{\cdot}10^{-2}$	$1.5{\cdot}10^{-2}$	$4.3{\cdot}10^{-3}$	840
10.1%H/89.9%C	$1.4{\cdot}10^{-2}$	$1.4{\cdot}10^{-2}$	$3.6{\cdot}10^{-3}$	557
10.0%H/90.0%C	$6.4{\cdot}10^{-3}$	$6.5{\cdot}10^{-3}$	N/A	N/A
10.4%H/89.6%C	$6.3{\cdot}10^{-3}$	$6.4{\cdot}10^{-3}$	$1.6{\cdot}10^{-3}$	890
Calcined	$9.0{\cdot}10^{-4}$	$1.0{\cdot}10^{-3}$	$6.6{\cdot}10^{-4}$	830

Experiment 3 - Addition of Primary Alumina A with Various Heat Treatment

Figure 27 shows the results from experiment 3. After the two previous experiments, it was decided to make it routine to add a batch of calcined alumina A at the beginning and end of every experiment. This procedure was followed for experiments 3-8. The aim of experiment 3 was to test the influence of various heat treatments on primary alumina A, bulk fraction. Three additions each were made of room temperature alumina A, alumina A that had been kept at 160°C for two hours and alumina A that had been kept at 350°C for two hours. The order of was randomised. Table 12 shows a summary of the addition order, heat treatment of each addition and mass loss during heat treatment. As calcined alumina A was always kept in an incubator at 160°C, no value for mass before heat treatment was obtained for these samples. LOI values were calculated to create a basis for comparison of the LOI characterisation earlier reported. These LOI data will create the basis for the amounts of HF, calculated from HMB for H_2O. The LOI values reported here are either LOI(RT-160°C) or LOI(RT-350°C), depending on the heat treatment.

The amount of alumina added to the melt, after all losses have been accounted for, is shown in Table 13. The table shows the addition sequence, the amounts of HF, calculated from HMB for H_2O from LOI and TGA data as well as the actual amount of HF found in the experiment through Riemann sums. The average LOI values found on the day of the experiment for LOI(RT-160°C) and LOI(RT-350°C) have been used when calculating the amount of moisture in the samples. The value for the remaining water from 350-1000°C has been taken from the LOI measurements presented in Table 4. The corresponding baseline of HF before each alumina addition is also shown in the table.

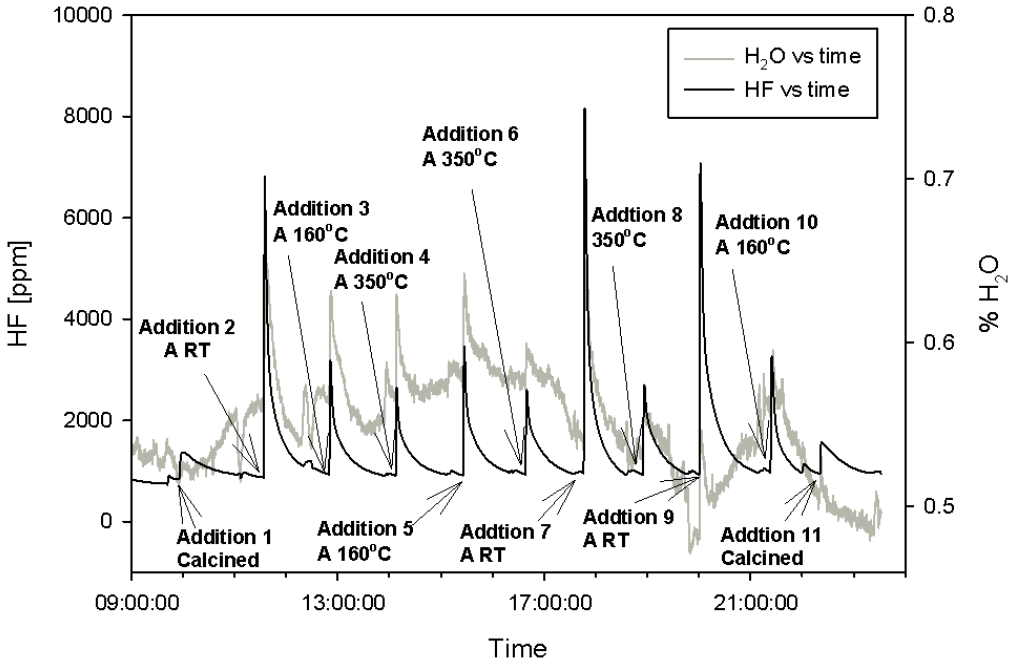

Figure 27: Experiment 3: Addition of primary alumina A, bulk fraction, with various pre-treatment, i) stored at room temperature (RT), ii) stored at 160°C for two hours and iii) stored at 350°C for two hours.

Table 12: Experiment 3: Summary of addition order, heat treatment and mass loss during heat treatment.

Addition number	Alumina quality	Heat treatment °C	Mass before heat treatment [g]	Mass after heat treatment [g]	LOI %
1	Calcined	160	N/A	0.1502	N/A
2	A	RT	0.1496	N/A	N/A
3	A	160, 2hrs	0.1508	0.1477	2.06
4	A	350, 2hrs	0.1505	0.1468	2.46
5	A	160, 2hrs	0.1505	0.1475	1.99
6	A	350, 2hrs	0.1500	0.1465	2.33
7	A	RT	0.1502	N/A	N/A
8	A	350, 2hrs	0.1510	0.1472	2.52
9	A	RT	0.1509	N/A	N/A
10	A	160, 2hrs	0.1502	0.1478	1.60
11	Calcined	160	N/A	0.1503	N/A

Table 13: Experiment 3: The addition sequence, the amounts of HF, calculated from HMB for H_2O from LOI and TGA data and the quantities of HF found for the experiment calculated through Riemann sums with corresponding baselines..

Addition sequence	Alumina added [g]	HF from H LOI [g]	HF from H TGA [g]	Amount HF from experiment [g]	Baseline [ppm]
Calcined	0.1258	$6.4{\cdot}10^{-4}$	$7.3{\cdot}10^{-4}$	$9.9{\cdot}10^{-4}$	850
A RT	0.1320	$9.0{\cdot}10^{-3}$	$4.8{\cdot}10^{-3}$	$4.1{\cdot}10^{-3}$	868
A 160°C	0.1206	$3.2{\cdot}10^{-3}$	$2.2{\cdot}10^{-3}$	$1.8{\cdot}10^{-3}$	930
A 350°C	0.1142	$1.6{\cdot}10^{-3}$	$1.3{\cdot}10^{-3}$	$1.5{\cdot}10^{-3}$	906
A 160°C	0.1202	$3.2{\cdot}10^{-3}$	$2.2{\cdot}10^{-3}$	$2.1{\cdot}10^{-3}$	911
A 350°C	0.1174	$1.7{\cdot}10^{-3}$	$1.4{\cdot}10^{-3}$	$1.7{\cdot}10^{-3}$	928
A RT	0.1341	$9.2{\cdot}10^{-3}$	$4.8{\cdot}10^{-3}$	$4.4{\cdot}10^{-3}$	953
A 350°C	0.1181	$1.7{\cdot}10^{-3}$	$1.4{\cdot}10^{-3}$	$1.8{\cdot}10^{-3}$	925
A RT	0.1360	$9.3{\cdot}10^{-3}$	$4.9{\cdot}10^{-3}$	$5.0{\cdot}10^{-3}$	927
A 160°C	0.1221	$3.2{\cdot}10^{-3}$	$2.2{\cdot}10^{-3}$	$1.5{\cdot}10^{-3}$	967
Calcined	0.1262	$6.5{\cdot}10^{-4}$	$7.3{\cdot}10^{-4}$	$1.0{\cdot}10^{-3}$	941

5.2.2 Comparison of HF Formation when Adding Aluminas with Various Gibbsite Concentrations

The aim of experiment 4 and 5 was to compare bulk fractions of alumina A, B and C when it comes to HF formation. Alumina A is low in gibbsite, while alumina B and C are high in gibbsite. Both primary and secondary alumina was tested.

Experiment 4 - Addition of Primary Alumina A, B and C, Bulk Fractions

Figure 28 shows the results when adding primary alumina A, B and C, bulk fractions, to the cryolitic melt. All samples had been heat treated at 160°C for two hours prior to the addition. Calcined alumina A was added to the melt as the first and the last batch. The addition order of alumina was randomized.

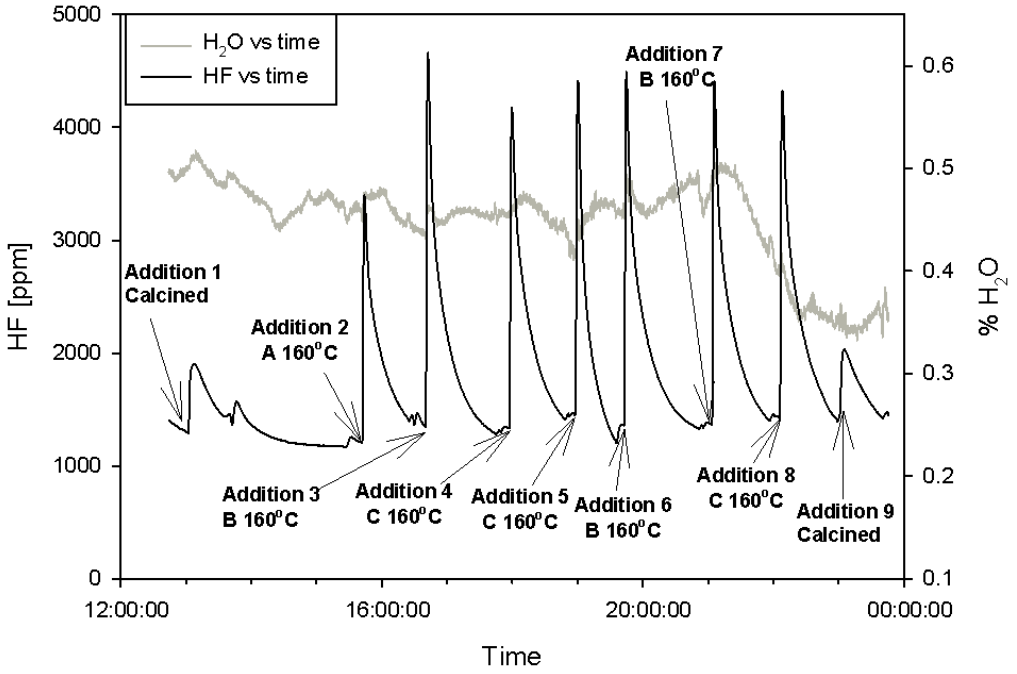

Figure 28: Experiment 4: Addition of primary alumina A, B and C, bulk fraction, heat treated at 160°C for two hours.

Table 14 shows a summary of the addition order, heat treatment, mass before and mass after heat treatment. The LOI values for the mass loss during the heat treatment have been calculated.

Table 15 shows the addition sequence and the amounts of HF, calculated from HMB for H_2O from LOI(160-350°C)+LOI(350-1000°C) and TGA data from 160-1000°C from Tables 4 and 7. The actual HF formation found in the experiment calculated by using Riemann sums [40] is also shown in Table 15 together with the corresponding baseline of HF. The amount of alumina added to the melt is reported in the table. The area under the graph was not calculated for 30 minutes on addition 5. The curve hit the given baseline of 1446 after 27 minutes and the Riemann calculation was terminated at that point to avoid negative values.

Table 14: Experiment 4: Summary of addition order, heat treatment and mass loss during heat treatment.

Addition number	Alumina quality	Heat treatment °C	Mass before heat treatment [g]	Mass after heat treatment [g]	LOI RT-160°C %
1	Calcined	160	N/A	0.1509	N/A
2	A	160, 2hrs	0.1507	0.1463	2.92
3	B	160, 2hrs	0.1509	0.1464	2.98
4	C	160, 2hrs	0.1506	0.1472	2.26
5	C	160, 2hrs	0.1499	0.1465	2.27
6	B	160, 2hrs	0.1499	0.1458	2.74
7	B	160, 2hrs	0.1500	0.1462	2.53
8	C	160, 2hrs	0.1507	0.1470	2.46
9	Calcined	160	N/A	0.1502	N/A

Table 15: Experiment 4: The addition sequence, the amounts of HF, calculated from HMB for H_2O from LOI and TGA data and the quantities of HF found for the experiment calculated through Riemann sums with corresponding baselines.

Addition sequence	Alumina added [g]	HF from H LOI [g]	HF from H TGA [g]	Amount HF from experiment [g]	Baseline [ppm]
Calcined	0.1340	$6.8{\cdot}10^{-4}$	$7.8{\cdot}10^{-4}$	$1.0{\cdot}10^{-3}$	1295
A 160°C	0.1201	$2.9{\cdot}10^{-3}$	$2.2{\cdot}10^{-3}$	$2.5{\cdot}10^{-3}$	1206
B 160°C	0.1222	$4.8{\cdot}10^{-3}$	$4.5{\cdot}10^{-3}$	$3.4{\cdot}10^{-3}$	1340
C 160°C	0.1263	$5.5{\cdot}10^{-3}$	$5.0{\cdot}10^{-3}$	$3.2{\cdot}10^{-3}$	1332
C 160°C	0.1249	$5.4{\cdot}10^{-3}$	$4.9{\cdot}10^{-3}$	$2.1{\cdot}10^{-3}$	1446
B 160°C	0.1274	$5.0{\cdot}10^{-3}$	$4.7{\cdot}10^{-3}$	$3.3{\cdot}10^{-3}$	1360
B 160°C	0.1287	$5.0{\cdot}10^{-3}$	$4.7{\cdot}10^{-3}$	$3.2{\cdot}10^{-3}$	1365
C 160°C	0.1186	$5.1{\cdot}10^{-3}$	$4.7{\cdot}10^{-3}$	$3.2{\cdot}10^{-3}$	1425
Calcined	0.1198	$6.1{\cdot}10^{-4}$	$7.0{\cdot}10^{-4}$	$8.5{\cdot}10^{-4}$	1450

Experiment 5 - Addition of Secondary Alumina A, B and C, Bulk Fractions

Figure 29 shows the results from experiment 5. In the experiment, bulk fractions of secondary alumina A, B and C were added to the melt with a randomized addition order. Calcined alumina A was added as the first and last batch.

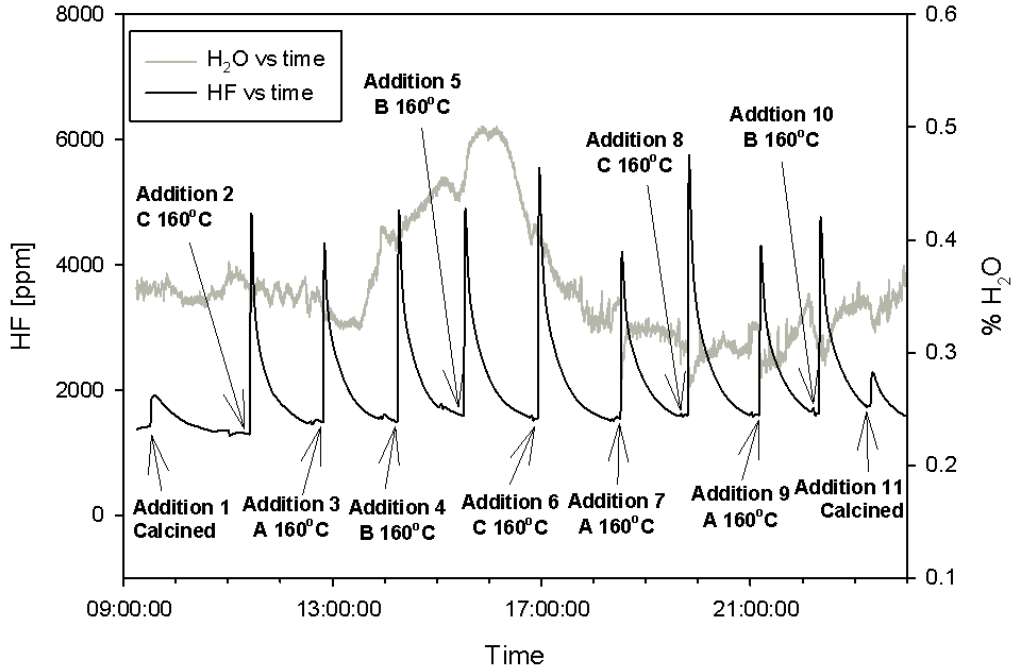

Figure 29: Experiment 5: Addition of secondary bulk alumina A, B and C, heat treated at 160°C for two hours.

Table 16 shows a summary of the addition order, the heat treatment and the mass loss during the heat treatment of experiment 5. LOI values have been calculated for the mass loss during heating to create a basis for comparison of the values given in Table 6. “sec” denotes that the alumina added is secondary alumina.

Table 17 shows the amounts of HF, calculated by using HMB for H_2O from LOI and TGA data. The LOI and TGA values found for primary alumina creates the basis for these calculation. It is assumed that the TGA and LOI values found for primary alumina are compatible with the moisture content in the secondary alumina. The table shows the addition sequence, addition quantity of alumina and the calculated amount of HF formed during the experiment when using Riemann sums [40] with the corresponding baselines. The area under the graph was not calculated for 30 minutes on addition 11. The curve hit the given baseline of 1740 after 25 minutes and the calculation was terminated at that point to avoid negative values.

Table 16: Experiment 5: Summary of addition order, heat treatment and mass loss during heat treatment.

Addition number	Alumina quality	Heat treatment °C	Mass before heat treatment [g]	Mass after heat treatment [g]	LOI RT-160°C %
1	Calcined	160	N/A	0.1503	N/A
2	C sec	160, 2hrs	0.1515	0.1484	2.05
3	A sec	160, 2hrs	0.1506	0.1470	2.39
4	B sec	160, 2hrs	0.1507	0.1467	2.65
5	B sec	160, 2hrs	0.1508	0.1465	2.85
6	C sec	160, 2hrs	0.1506	0.1471	2.32
7	A sec	160, 2hrs	0.1510	0.1470	2.65
8	C sec	160, 2hrs	0.1507	0.1474	2.19
9	A sec	160, 2hrs	0.1503	0.1465	2.53
10	B sec	160, 2hrs	0.1507	0.1475	2.12
11	Calcined	160	N/A	0.1499	N/A

Table 17: Experiment 5: The addition sequence, the amounts of HF, calculated from HMB for H_2O from LOI and TGA data and the quantities of HF found for the experiment calculated through Riemann sums with corresponding baselines.

Addition sequence	Alumina added [g]	HF from H LOI [g]	HF from H TGA [g]	Amount HF from experiment [g]	Baseline [ppm]
Calcined	0.1259	$6.4{\cdot}10^{-4}$	$7.3{\cdot}10^{-4}$	$9.0{\cdot}10^{-4}$	1416
C sec, 160°C	0.1366	$5.9{\cdot}10^{-3}$	$5.4{\cdot}10^{-3}$	$3.5{\cdot}10^{-3}$	1296
A sec, 160°C	0.1291	$3.1{\cdot}10^{-3}$	$2.3{\cdot}10^{-3}$	$3.1{\cdot}10^{-3}$	1485
B sec, 160°C	0.1316	$5.1{\cdot}10^{-3}$	$4.8{\cdot}10^{-3}$	$3.6{\cdot}10^{-3}$	1497
B sec, 160°C	0.1305	$5.1{\cdot}10^{-3}$	$4.8{\cdot}10^{-3}$	$3.7{\cdot}10^{-3}$	1588
C sec, 160°C	0.1299	$5.6{\cdot}10^{-3}$	$5.1{\cdot}10^{-3}$	$4.2{\cdot}10^{-3}$	1545
A sec, 160°C	0.1281	$3.1{\cdot}10^{-3}$	$2.3{\cdot}10^{-3}$	$3.1{\cdot}10^{-3}$	1543
C sec, 160°C	0.1346	$5.8{\cdot}10^{-3}$	$5.3{\cdot}10^{-3}$	$4.3{\cdot}10^{-3}$	1592
A sec, 160°C	0.1292	$3.1{\cdot}10^{-3}$	$2.3{\cdot}10^{-3}$	$3.1{\cdot}10^{-3}$	1596
B sec, 160°C	0.1318	$5.2{\cdot}10^{-3}$	$4.8{\cdot}10^{-3}$	$3.5{\cdot}10^{-3}$	1628
Calcined	0.1258	$6.4{\cdot}10^{-4}$	$7.3{\cdot}10^{-4}$	$5.2{\cdot}10^{-4}$	1740

5.2.3 Comparison of HF Formation when Adding Aluminas with Various Powder Size Fractions

These experiments were performed to test the difference in HF formation potential for alumina powder with fine powder size fraction: -45μm, vs. coarse powder size fraction: +150μm. Both primary and secondary alumina was tested. It was also of interest to test the difference in HF formation for alumina A and B.

Experiment 6 - Addition of Primary Alumina A and B, -45μm and +150μm Fractions

Figure 30 shows the results from experiment 6. In experiment 6, primary alumina A and B, size fractions +150μm and -45μm, were added to the melt. The samples were heat treated at 160°C for two hours. Calcined alumina A was added to the melt as the first and the last batch. The gas out tube was blocked at 10:12 hours and was changed at 10:27 hours. This is the reason for the increase in HF in this time period. At 19:20 hours the feeder tube was changed together with the gas out tube and the feeder. The HF concentration increased after changing the feeder tube and this was probably due to addition of moisture adsorbed on the new feeder tube. Other "irregularities" on the graph between the alumina additions are caused by changing of gas tube and feeder.

Table 18 shows a summary of the addition order, heat treatment and mass loss during heat treatment. The LOI values have been added to create a comparison to the results given in Table 4.

Table 19 shows the amounts of HF, calculated from HMB for H_2O from LOI and TGA data. The HF formation found during the experiment is also reported in the table, using Riemann sums with the corresponding baseline. The HF concentration reached the baseline 24 minutes after addition 2, and the calculation was terminated at that point. The experiment was terminated 18 minutes after addition 13 and the Riemann sum calculation was terminated after 18 minutes.

Table 18: Experiment 6: Summary of addition order, heat treatment and mass loss during heat treatment.

Addition number	Alumina quality	Heat treatment °C	Mass before heat treatment [g]	Mass after heat treatment [g]	LOI RT-160°C %
1	Calcined	160	N/A	0.1501	N/A
2	A +150μm	160, 2hrs	0.1497	0.1451	3.07
3	B -45μm	160, 2hrs	0.1501	0.1463	2.53
4	B +150μm	160, 2hrs	0.1511	0.1462	3.24
5	A -45μm	160, 2hrs	0.1500	0.1461	2.60
6	A -45μm	160, 2hrs	0.1498	0.1456	2.80
7	B +150μm	160, 2hrs	0.1498	0.1447	3.40
8	A +150μm	160, 2hrs	0.1511	0.1473	2.51
9	B -45μm	160, 2hrs	0.1510	0.1472	2.52
10	B +150μm	160, 2hrs	0.1803	0.1751	2.88
11	A +150μm	160, 2hrs	0.1510	0.1468	2.78
12	B -45μm	160, 2hrs	0.1505	0.1467	2.52
13	Calcined	160	N/A	0.1505	N/A

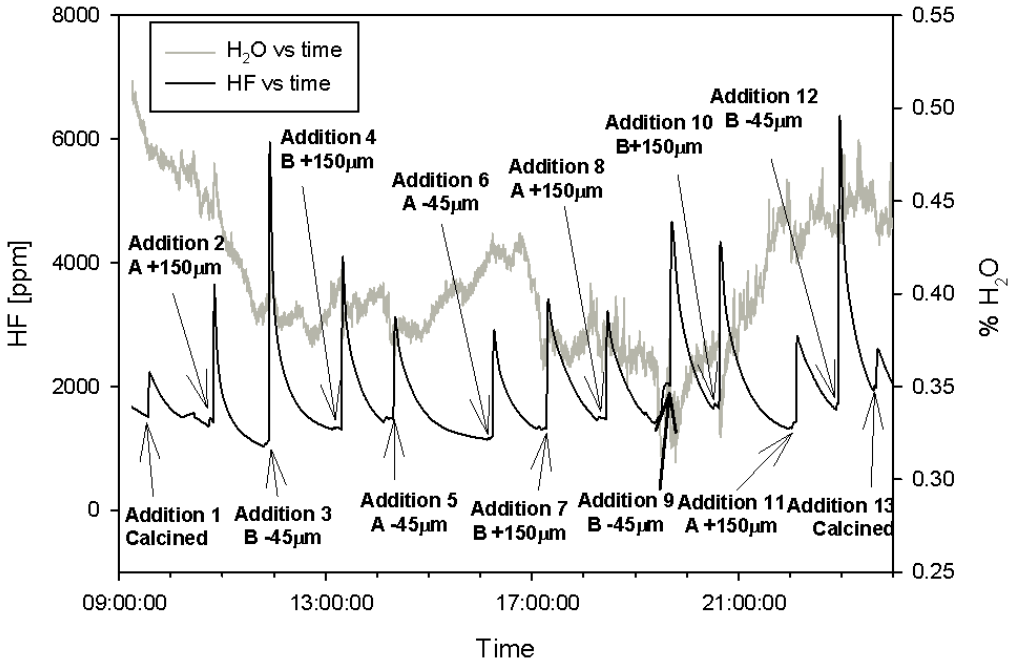

Figure 30: Experiment 6: Addition of primary alumina A and B, size fractions +150μm and -45μm. The samples were heat treated at 160°C for two hours.

Table 19: Experiment 6: The addition sequence, the amounts of HF, calculated from HMB for H_2O from LOI and TGA data and the quantities of HF found for the experiment calculated through Riemann sums with corresponding baselines.

Addition sequence	Alumina added [g]	HF from H LOI [g]	HF from H TGA [g]	Amount HF from experiment [g]	Baseline [ppm]
Calcined	0.1295	$6.6{\cdot}10^{-4}$	$7.5{\cdot}10^{-4}$	$9.2{\cdot}10^{-4}$	1514
A +150μm 160°C	0.1138	$3.8{\cdot}10^{-3}$	$3.0{\cdot}10^{-3}$	$1.2{\cdot}10^{-3}$	1414
B -45μm 160°C	0.1298	$8.8{\cdot}10^{-3}$	$7.3{\cdot}10^{-3}$	$4.3{\cdot}10^{-3}$	1122
B +150μm 160°C	0.1335	$6.5{\cdot}10^{-3}$	$5.4{\cdot}10^{-3}$	$3.0{\cdot}10^{-3}$	1305
A -45μm 160°C	0.1244	$3.8{\cdot}10^{-3}$	$2.6{\cdot}10^{-3}$	$2.0{\cdot}10^{-3}$	1476
A -45μm 160°C	0.1194	$3.7{\cdot}10^{-3}$	$2.5{\cdot}10^{-3}$	$2.2{\cdot}10^{-3}$	1192
B +150μm 160°C	0.1169	$5.7{\cdot}10^{-3}$	$4.8{\cdot}10^{-3}$	$3.2{\cdot}10^{-3}$	1328
A +150μm 160°C	0.1178	$4.0{\cdot}10^{-3}$	$3.1{\cdot}10^{-3}$	$2.3{\cdot}10^{-3}$	1467
B -45μm 160°C	0.1286	$8.7{\cdot}10^{-3}$	$7.2{\cdot}10^{-3}$	$2.9{\cdot}10^{-3}$	2010
B +150μm 160°C	0.1132	$5.5{\cdot}10^{-3}$	$4.6{\cdot}10^{-3}$	$3.2{\cdot}10^{-3}$	1650
A +150μm 160°C	0.1056	$3.6{\cdot}10^{-3}$	$2.8{\cdot}10^{-3}$	$2.3{\cdot}10^{-3}$	1425
B -45μm 160°C	0.1311	$8.9{\cdot}10^{-3}$	$7.4{\cdot}10^{-3}$	$4.7{\cdot}10^{-3}$	1725
Calcined	0.1261	$6.4{\cdot}10^{-4}$	$7.3{\cdot}10^{-4}$	$5.8{\cdot}10^{-4}$	1980

Experiment 7 - Addition of Secondary Alumina A and B, -45μm and +150μm Fractions

Figure 31 shows the results from experiment 7. In the experiment, additions of secondary alumina A and B, powder fractions +150μm and -45μm, were added to the cryolitic melt. The gas out tube was blocked from 11:39-11:58 hours and 19:15-19:31 hours, and this is the reason for the increase in HF during these two time intervals. After addition 4, poor gas flow between the furnace and the laser was observed. The gas out tube was changed and the flexible PFA tube leading the gas into the laser was flushed with pressurized air. After addition 11, poor gas flow was again observed. It is assumed that the reason for this is that the particles in the -45μm fractions are very light and may enter the gas flow into the gas tube instead of the melt. This will cause blockage of the gas flow inside the flexible PFA tube.

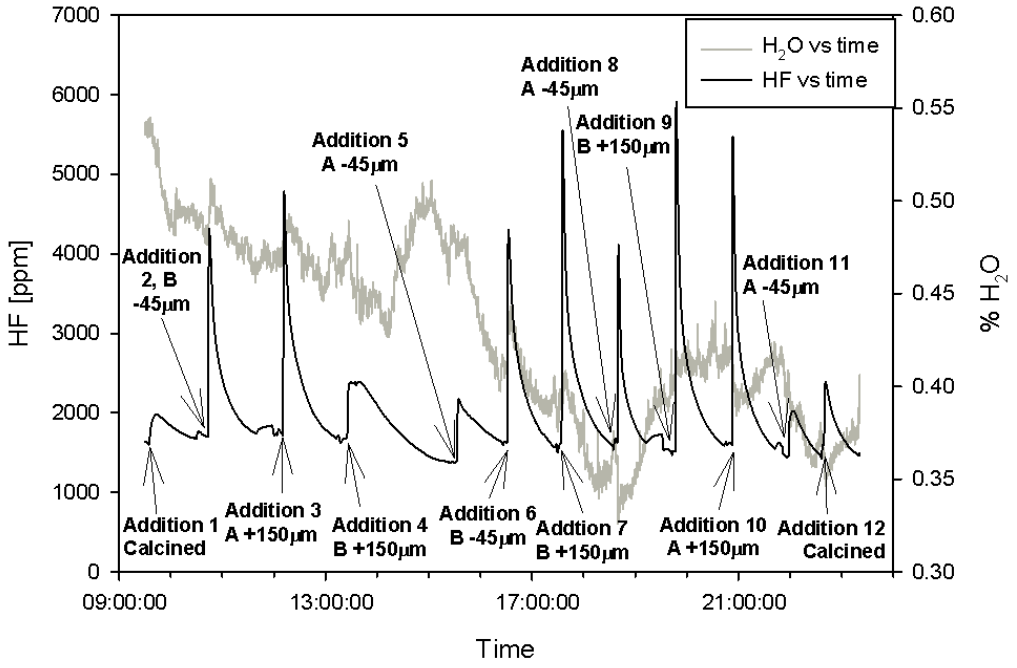

Figure 31: Experiment 7: Addition of secondary alumina A and B, size fractions +150μm and -45μm, heat treated at 160°C for two hours.

Table 20 shows a summary of the addition order, heat treatment and mass loss of sample during heat treatment.

Table 21 shows the amounts of HF, calculated from HMB for H_2O from LOI and TGA data. The LOI and TGA values found for primary alumina creates the basis for these calculations. It is assumed that the TGA and LOI values found for primary alumina are compatible with the moisture content in the secondary alumina. The calculated amount of HF found in the experiment is also shown, with the corresponding baseline. The quantity of alumina added to the system is also reported in the table.

Table 20: Experiment 7: Summary of addition order, heat treatment and mass loss during heat treatment.

Addition number	Alumina quality	Heat treatment °C	Mass before heat treatment [g]	Mass after heat treatment [g]	LOI RT-160°C %
1	Calcined	160	N/A	0.1501	N/A
2	B -45μm sec	160, 2hrs	0.1500	0.1471	1.93
3	A +150μm sec	160, 2hrs	0.1503	0.1463	2.66
4	B +150μm sec	160, 2hrs	0.1505	0.1472	2.19
5	A -45μm sec	160, 2hrs	0.1503	0.1472	2.06
6	B -45μm sec	160, 2hrs	0.1508	0.1481	1.79
7	B +150μm sec	160, 2hrs	0.1500	0.1473	1.80
8	A -45μm sec	160, 2hrs	0.1502	0.1475	1.80
9	B +150μm sec	160, 2hrs	0.1512	0.1477	2.31
10	A +150μm sec	160, 2hrs	0.1506	0.1470	2.39
11	A -45μm sec	160, 2hrs	0.1500	0.1459	2.73
12	Calcined	160	N/A	0.1510	N/A

Table 21: Experiment 7: The addition sequence, the amounts of HF, calculated from HMB for H_2O from LOI and TGA data and the quantities of HF found for the experiment calculated through Riemann sums with corresponding baselines.

Addition sequence	Alumina added [g]	HF from H LOI [g]	HF from H TGA [g]	Amount HF from experiment [g]	Baseline [ppm]
Calcined	0.1217	$6.2\cdot10^{-4}$	$7.1\cdot10^{-4}$	$7.6\cdot10^{-4}$	1600
B -45μm 160°C	0.1410	$9.6\cdot10^{-3}$	$7.9\cdot10^{-3}$	$2.6\cdot10^{-3}$	1700
A +150μm 160°C	0.1345	$4.5\cdot10^{-3}$	$3.5\cdot10^{-3}$	$3.1\cdot10^{-3}$	1717
B +150μm 160°C	0.1312	$6.4\cdot10^{-3}$	$5.3\cdot10^{-3}$	N/A	N/A
A -45μm 160°C	0.1325	$4.1\cdot10^{-3}$	$2.8\cdot10^{-3}$	$1.5\cdot10^{-3}$	1388
B -45μm 160°C	0.1387	$9.4\cdot10^{-3}$	$7.8\cdot10^{-3}$	$2.8\cdot10^{-3}$	1620
B +150μm 160°C	0.1317	$6.4\cdot10^{-3}$	$5.4\cdot10^{-3}$	$3.3\cdot10^{-3}$	1625
A -45μm 160°C	0.1386	$4.3\cdot10^{-3}$	$2.9\cdot10^{-3}$	$1.5\cdot10^{-3}$	1623
B +150μm 160°C	0.1363	$6.6\cdot10^{-3}$	$5.5\cdot10^{-3}$	$3.6\cdot10^{-3}$	1513
A +150μm 160°C	0.1234	$4.2\cdot10^{-3}$	$3.3\cdot10^{-3}$	$2.9\cdot10^{-3}$	1590
A -45μm 160°C	0.1338	$4.1\cdot10^{-3}$	$2.8\cdot10^{-3}$	$8.2\cdot10^{-4}$	1480
Calcined	0.1260	$6.4\cdot10^{-4}$	$7.3\cdot10^{-4}$	$7.3\cdot10^{-4}$	1605

5.2.4 Testing of Alumina with a High Level of Physisorbed Moisture versus Alumina with a High Level of Gibbsite

This experiment was performed to test the significance of physisorbed moisture vs. gibbsite when it comes to HF formation. Moist primary alumina A, bulk fraction, was prepared by the method described in section 5.1.1. The moist alumina was compared with bulk fraction of primary alumina B (high in gibbsite).

Experiment 8 - Addition of Moist Primary Alumina A, Mixtures of Moist Primary Alumina A and Dry Primary Alumina A and Primary Alumina B

Figure 32 shows the results from experiment 8. Note that after addition 2, the HF concentration was higher than the maximum measuring range of the laser. Addition 2 was pure moist alumina A. Addition 3 and 5 were mixtures of moist alumina A and dry primary alumina A, bulk fraction (dried at 160°C for two hours). Alumina B was added as the 4th and the 6th addition. Calcined alumina A was added as the first and last batch. The last batch was added only ten minutes after the previous addition. The reason for this was to test if addition of "inert" powder would release HF that could be dissolved in the melt. The gas out tube was blocked at 13:44-14:27 hours, causing the slight increase in HF concentration measured by the laser at that time interval. Other "irregularities" between the additions were caused by changing of gas out tube and feeder.

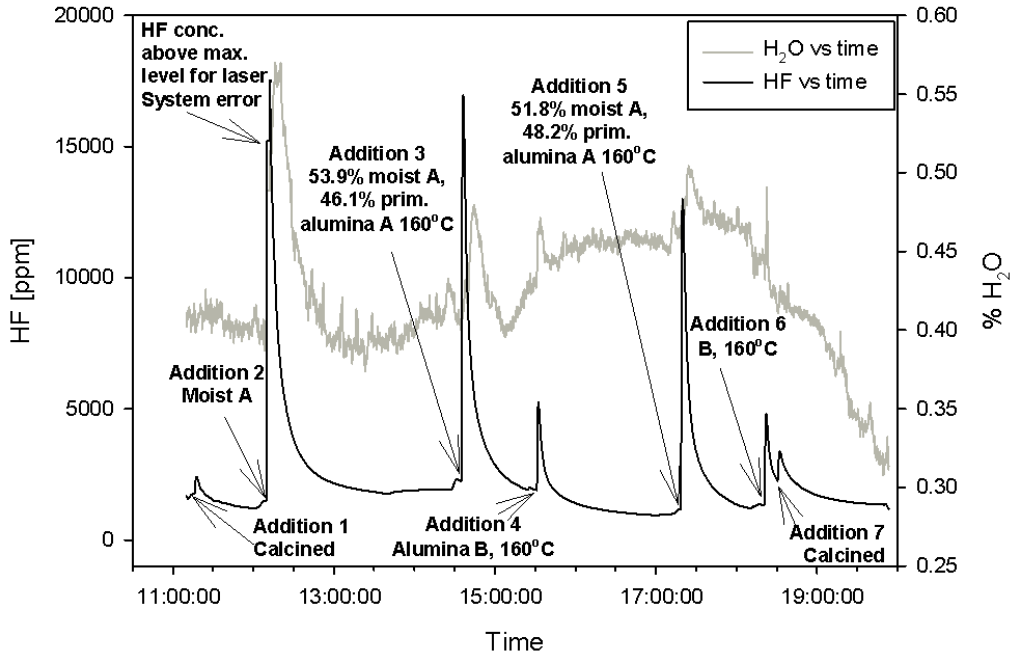

Figure 32: Experiment 8: Addition of moist alumina A, mixtures of moist alumina A and alumina A, alumina B, primary bulk fractions, with various heat treatment.

Table 22 summarizes the addition order, the heat treatment and the quantity of alumina added. The amounts of HF, calculated from HMB for H_2O from LOI data (given in Tables 4 and 5) are also given in the table. No calculation was done for TGA, since TGA testing was not performed on the moist alumina. Riemann sums were used to calculate the amount of HF formed in the experiment with the corresponding baselines.

Table 22: Experiment 8: Summary of alumina quality, alumina addition, heat treatment, mass of addition, calculated amount of HF from LOI and Riemann with corresponding baselines.

Addition number	Quality	Heat treat. °C	Alumina added [g]	Amount HF from LOI [g]	Amount HF from exp. [g]	Baseline [ppm]
1	Calcined	160	0.1262	$6.5{\cdot}10^{-4}$	$1.8{\cdot}10^{-4}$	1777
2	Moist A	No	0.0851	$2.9{\cdot}10^{-2}$	N/A	N/A
3	53.9% moist A	No	0.0935	$1.8{\cdot}10^{-2}$	$8.6{\cdot}10^{-3}$	2240
3	46.1% A	160, 2 hrs				
4	B	160, 2 hrs	0.1227	$4.8{\cdot}10^{-3}$	$1.2{\cdot}10^{-3}$	1900
5	51.8% moist A	No	0.0832	$1.5{\cdot}10^{-2}$	$7.3{\cdot}10^{-3}$	1184
5	48.2% A	160, 2 hrs				
6	B	160, 2 hrs	0.1198	$4.7{\cdot}10^{-3}$	$1.5{\cdot}10^{-3}$	1337
7	L	160	0.1257	$6.4{\cdot}10^{-4}$	$2.8{\cdot}10^{-4}$	2496

6 Discussion

6.1 Characterisation of the Aluminas

6.1.1 Loss on Ignition

The results from the loss on ignition testing are shown in Tables 4 - 6. Table 4 shows the results when performing LOI on hydrate. The LOI(RT-160°C) value is only 0.1%. Hydrate alumina has a low surface area and adsorbs very little moisture from the ambient air. A mass loss of 28.89% was found for hydrate alumina A in the temperature interval of 160-350°C. This mass loss consists mainly of moisture loss from gibbsite (in a sample of pure gibbsite the stoichiometric water content is calculated to be 29.36%). The LOI(350-1000°C) value of 5.72% is mainly due to boehmite transforming into anhydrous transition aluminas, before finally forming α-alumina.

The total mass loss (LOI(RT-1000°C)) for calcined alumina A was found to be 0.73%. However, the standard deviation greatly exceeds this. To account for this error it was hypothesised that one of the samples was left for a while at room temperature outside the desiccator after heating to 1000°C before weighing. The sample would then be able to readsorb moisture. Calcined alumina should ideally contain no moisture since it should have transformed completely into α-alumina. However, the transformation of lower transition aluminas into α-alumina is dependent not only on heating to 1200°C, but also on the hold time at that temperature. 1.5 hours may have been insufficient in so far as to transform all transition aluminas into anhydrous α-alumina. The samples of calcined alumina may also have picked up some moisture during shipment.

The LOI testing on primary alumina A, B and C (reported in Table 4), clearly shows that alumina B and C contain more H_2O than alumina A. This is valid for all size fractions and all temperature intervals. B and C have more physisorbed, chemisorbed and structural hydroxyl water. When comparing B and C internally, the LOI values in the temperature intervals 160-350°C and 350-1000°C also indicate that alumina B contains more under-calcined matter than alumina C. The increased quantity of moisture found in both alumina B and C compared to A yields a higher HF formation potential. The higher levels of moisture reported from 160-350°C in alumina B and C indicate a higher gibbsite level in alumina B and C, when compared to A.

It is important to remember that LOI(RT-160°C) will change according to the ambient moisture content as the samples are not kept in completely closed containers. The LOI testing reported in Table 4 was performed in February and March in a time period of very cold and dry weather. The LOI values reported in Tables 12, 14, 16, 18 and 20 were performed in May during warmer and humid weather. The LOI values reported in these tables show that more moisture had been adsorbed on the alumina from March to May due to the weather conditions. However, the values are not directly comparable due to the sample sizes of 3g vs. 0.15g.

Table 5 shows the results when doing LOI testing on moist alumina A. The alumina had been kept in a desiccator filled with water for three days. The amount of physisorbed moisture (LOI(RT-160°C)) had increased substantially to 13.69%. LOI(160-350°C) and LOI(350-1000°C) had both increased compared to the values reported for alumina A bulk fraction in Table 4, but not to the same extent as LOI(RT-160°C). The increased LOI(160-350°C) indicates that some of the physisorbed water may have formed irreversibly bound gibbsite as suggested by Hyland et al [14].

Table 6 shows the results when performing LOI on secondary alumina. It should be mentioned that it is not common to run LOI testing on secondary alumina. The reason for this is that

LOI is usually used as a measure of the moisture content in an alumina sample. When heating secondary alumina, adsorbed fluorides and carbon dust will be released together with the moisture in the sample. Hence, LOI on secondary alumina will not measure the moisture content in the alumina only, but a mixture of several volatiles. The motivation for doing LOI testing on the secondary alumina was to have some feeling with the quantity of volatiles in the aluminas. An interesting discovery made when performing the LOI testing on the secondary alumina was that the LOI values reported in Table 6 for -45μm fractions of alumina A and B from RT-160°C and 160-350°C did not deviate much from the reported values for primary alumina A and B, -45μm fractions in Table 4, indicating that the scrubber efficiency of the fines are poor. On both alumina A and B -45μm fractions, an increased LOI(350-1000°C) is observed. The observed increased LOI(350-1000°C) may be explained due to a high level of carbon dust in the fines.

The higher values of mass loss for the other secondary aluminas (bulk and +150μm fractions) compared to LOI values reported for primary aluminas, both bulk and +150μm fractions indicate adsorbed fluorides and carbon dust evaporating together with moisture.

6.1.2 Thermal Gravimetric Analysis and Differential Scanning Calorimetry

TGA and DSC were performed on the primary aluminas, all size fractions. In the Figures both TGA and DSC results are reported. The results are shown in Table 7 and Figures 9 - 18. Table 7 creates a basis for comparison to Table 4. The major trends found in Table 4 are also found in Table 7. Alumina B and C show greater H_2O evaporation than alumina A. The hydrate and calcined alumina A TGA results are reproducible when compared with LOI on the same samples.

Too much emphasis should not be put into the differences in the numbers between LOI and TGA. The reason for this is that TGA is not directly comparable to LOI due to the lack of hold time at two hours at 160, 350 and 1000°C (except for one of the hydrate samples). As can also be seen in Figures 9 - 18, there is a lot of noise in the measurements creating uncertainties in the exact percent mass loss at the specific temperatures.

Figure 9 shows a comparison of the hydrate sample being heated with dwell time for two hours at 160, 350 and 1000°C respectively. As can be seen in the figure, the difference between the mass loss with and without dwell times is not very large. It was decided to run the rest of the tests without dwell times to reduce the time spent on each test. The hydrate sample shows a massive decrease in mass from approximately 220-320°C. A corresponding peak is observed on the DSC graph, indicating that it is the evaporation of H_2O that causes the mass loss. Evaporation of H_2O is an endothermic reaction. It is reasonable to assume that the mass loss observed from 220-320°C comes from evaporation of moisture from gibbsite [24]. No mass loss is observed for the hydrate sample from RT-220°C showing that the amount of physisorbed moisture is low. The mass loss observed from approximately 350-550°C is boehmite transforming into transition aluminas [24].

A small mass loss for the calcined sample is observed in Figure 10; however, the TGA curve shows a lot of noise during the measurement. The decrease on the DSC curve from approximately 550-1000°C can be considered a result of this noise.

Figures 11 - 14 show the results from the TGA and DSC results for alumina A, all powder size fractions. All alumina A size fractions show a trend where the largest drop in mass happens between RT-160°C. This drop comes from evaporation of physically adsorbed moisture. The DSC curve also shows a peak in Figures 11 - 13 at approximately 100°C. In correspondence with

the discussion given for the calcined sample, the peaks on the DSC curve around 600°C are caused by noise in the instrument.

Figures 15 - 18 show the results from the TGA and DSC results for alumina B, all powder size fractions. These graphs show somewhat different behaviour compared to the TGA and DSC graphs for alumina A, all fractions. Figures 15 - 18 show the same drop in mass from RT-160 as the alumina A graphs do. However, for alumina B, there is an extra drop in mass from approximately 220-300°C. This drop is also supported by a peak on the DSC curve, most evident in Figure 16. This mass loss is evaporation of moisture in gibbsite. In correspondence with the discussion given for the calcined sample, the peaks on the DSC curve around 600°C are caused by noise in the instrument. In Figure 18, it is interesting to see that the mass loss curve of the -45μm sample goes from evaporating least moisture compared to the bulk and +150μm fractions, to losing more moisture. This happens around 255°C, and indicate that the -45μm fraction contains more gibbsite than the +150μm and bulk fractions.

Figure 19 shows the results when performing TGA and DSC on alumina C. Alumina C shows the same behaviour as alumina B, bulk fraction.

6.1.3 LOI Temperature Intervals

The chosen temperature intervals to run the LOI testing were RT-160°C, 160-350°C and 350-1000°C. The basis for choosing these temperature intervals was was to allow better distinction between physically adsorbed moisture, gibbsite and structural hydroxyl moisture. The results from the TGA testing show that the chosen temperature intervals did give a better division between the different types of moisture present in the alumina than the traditional time intervals used in industry: RT-300°C and 300-1000°C. This is in accordance with the proposed redefinition of the alumina specification sheet by Perander et al [17].

6.1.4 X-Ray Diffraction

The X-ray diffractograms for hydrate and calcined alumina A and alumina A, B and C, all size fractions are shown in Figures 20 - 24. The corresponding diffraction lines are also included. The intensities have been shifted for illustrative purposes.

Figure 20 shows that the main component in the hydrate sample is gibbsite. This finding is also supported by both the TGA and LOI measurements. Figure 21 shows the diffractogram for the calcined sample. The diffractions lines show that α-, θ- and κ-alumina are present in the sample. These findings do not correspond with any of the proposed production routes in Figure 4. However, this sample has been calcined in the laboratory and not by any of the production lines in the figure and may explain why there is no correspondence with the findings in the diffractogram for the calcined sample, compared with the literature. Another observation is that both the hydrate and the calcined sample create narrow peaks with relatively high intensities, indicating that the samples are crystalline.

Figure 22 shows the diffractogram for alumina A, all powder size fractions. The peaks were identified to be an $Al_{2.67}O_4$ spinel alumina phase, as well as α- and δ-alumina. At first glance, alumina A does not seem to follow any proposed production routes in Figure 4. But, on closer inspection, the structure of γ-alumina allows the suggestion that this $Al_{2.67}O_4$-alumina is related to the γ-alumina. γ-alumina has a disordered spinel structure [41]. With this in mind, the suggested production route for alumina A from Figure 4 follows the blue arrow.

Figures 23 - 24 shows the diffractograms for alumina B all fractions, and C bulk fraction. For samples alumina B bulk and +150μm fractions and alumina C bulk fraction, the same phases are found: θ- and α-alumina, $Al_{2.67}O_4$-alumina and gibbsite. For the -45μm fraction of alumina B, boehmite was also found. This finding is in accordance with the reported findings of Perander et al [29] indicating that the -45μm fraction is even more under-calcined than the larger size fractions. The phases found during XRD indicate that both alumina B and C have followed the blue production route. The findings also indicate the alumina B and C are more under-calcined than alumina A.

For all industrial aluminas (A, B and C, all size fractions) the intensities of the peaks were low and the peaks were relatively wide. This indicates that the samples are rather amorphous.

A lot of work was put into optimizing the procedure when doing XRD. However, the method was far from perfect and more work should be put into optimizing the sample preparation and the understanding of the different phases. It is very difficult to interpret the data for the industrial aluminas due to the many phases present and the mixture of amorphous and more crystalline phases. The amorphous phases will cause low but wide peaks, and other peaks may "hide" underneath these peaks. An attempt was made to run Rietveld refinement on the results, but it was very difficult to find a good curve fit. The result from the attempt to run Rietveld refinement is shown in Appendix G.

6.2 Testing of Laser

Extensive testing of the laser was performed before experimentation could start. This was part of the proposed further work in the project work performed by the author, autumn 2010 [7]. Increased understanding of the moisture measurements by the laser were needed when performing the experiments.

It was found that the laser measured a large offset compared to the expected H_2O concentration when the work with testing of the laser started. This was verified by placing an FTIR unit in series with the laser in accordance with the results given in Figure A.1. A service was performed on the laser by Ove Bjorøy from NEO, and the offset was to a large extent removed. Figure A.2 show the offset of the laser before manual calibration was found to be 0.2935. There is reason to believe that this offset is due to the closed space around the laser, as this space is not flushed by N_2 in the outer circuit. The laser was manually calibrated on the basis of Figure A.2, the procedure is shown in Appendix A. This calibration greatly increased the understanding of the apparatus, and furthermore proved vital for the success of the experiments.

6.3 HF Formation and Moisture Behaviour when Adding Industrial Aluminas to a Cryolitic Melt

6.3.1 Laboratory Setup

The laboratory setup has by and large been put together from scratch. A lot of work has been put into planning, building and optimizing the laboratory setup. Some major improvements were made to the setup, with the outer nickel crucible with lid being the most important. The nickel crucible made it easier to place the Pt-crucible inside the furnace. The nickel crucible stood steady in the furnace and the lid was well placed on top of it, removing the possibility to shift around or fall into the Pt-crucible. The lid also made positioning of the feeder and gas out

tube much easier. The nickel crucible with lid was not completely closed, so some gas from the experiment would still enter the furnace volume. However, the control with gas, alumina addition and positioning inside the furnace was greatly improved by the outer nickel crucible with lid.

Another improvement made to the system was that a nickel sheet was placed inside the Pythagoras tube. This way the inside of the furnace tube was covered in nickel metal. This caused more stable baselines throughout the experiments, as it is assumed that HF is not adsorbed as much by nickel as on the ceramic made Pythagoras tube.

The flow into the furnace was better controlled after the introduction of the flow meters. The flow meters kept a steady and well defined flow of gas into the system.

The feeder system was optimized by introducing a Y-shaped tube made of glass. A photo of the feeder system is shown in Figure 8 in the Experimental Chapter. Through one of the necks of the Y a small flow of N_2 gas was used to keep the feeder tube open. The other neck was used to add the alumina. The Y shape of the tube minimized the loss of alumina on the way down to the melt; hence, increasing the control of the quantity of alumina added to the system. For further optimization of the system, a system where it is not found necessary to open up the furnace before every new batch of alumina added to the system, should be considered. A closed system will get no interference from HF formation caused by the moist air added to the system, in accordance with Equation 2. On the practical level, however, a system that is to be kept closed from ambient air through an entire experiment will run into trouble with condensation, causing gas out tubes to become blocked. A closed system would need major alterations compared to the current laboratory setup used in these experiments.

6.3.2 Activities in the Cryolitic Melt and Partial Pressure of HF

The activities of NaF, AlF_3 and Al_2O_3 in experiment 3 have been calculated by using the model made by Solheim and Sterten [30]. The temperature used in the calculations was 1273K, in correspondence with the temperature used in the experiments. The ΔG for Reaction 3 at 1273K has been found to be -28137.2J/mol by using FactSage, thermodynamic software.

Equation 5 can be used to model a plot that shows how the partial pressures of HF over H_2O will change when the activity and wt% of alumina changes for a given activity of AlF_3. Figure 33 shows the results of this modelling. The activities of Al_2O_3 and AlF_3 used when calculating the partial pressures of HF over H_2O are given in Table 23. A start concentration of 0.6 wt% Al_2O_3 is assumed on the basis of previous work [7]. From Figure 33 it can be seen that the partial pressure of HF will decrease with increasing alumina wt% and activity, if the partial pressure of H_2O is kept constant.

6.3.3 Addition Order

In experiments 3-8, several alumina additions were made to each cryolitic melt. The addition order of the various alumina qualities was randomized. It does not seem as if the addition order has any influence on the experimental results. The only exception being some relatively high quantities of HF found during the first addition of calcined alumina to the melt. As already discussed, the explanation of the relatively high HF quantity for some of the first additions might be due to the findings in Table 23 and Figure 33, where the partial pressure of HF is seen to decrease with increasing wt% of alumina (when keeping the partial pressure of H_2O constant).

Table 23: Calculated activities for NaF, AlF_3 and Al_2O_3 for experiment 3 by using the model made by Solheim and Sterten [30].

Addition number	Wt% Al_2O_3	Activity AlF_3	Activity NaF	Activity Al_2O_3
0	0.60	$2.77 \cdot 10^{-3}$	0.204	$2.30 \cdot 10^{-3}$
1	0.68	$2.76 \cdot 10^{-3}$	0.204	$3.25 \cdot 10^{-3}$
2	0.77	$2.75 \cdot 10^{-3}$	0.204	$4.45 \cdot 10^{-3}$
3	0.85	$2.74 \cdot 10^{-3}$	0.203	$5.76 \cdot 10^{-3}$
4	0.93	$2.73 \cdot 10^{-3}$	0.203	$7.25 \cdot 10^{-3}$
5	1.00	$2.73 \cdot 10^{-3}$	0.203	$8.71 \cdot 10^{-3}$
6	1.08	$2.72 \cdot 10^{-3}$	0.203	$1.06 \cdot 10^{-2}$
7	1.17	$2.71 \cdot 10^{-3}$	0.203	$1.29 \cdot 10^{-2}$
8	1.25	$2.71 \cdot 10^{-3}$	0.203	$1.51 \cdot 10^{-2}$
9	1.34	$2.70 \cdot 10^{-3}$	0.203	$1.79 \cdot 10^{-2}$
10	1.42	$2.69 \cdot 10^{-3}$	0.203	$2.06 \cdot 10^{-2}$
11	1.50	$2.69 \cdot 10^{-3}$	0.203	$2.34 \cdot 10^{-2}$

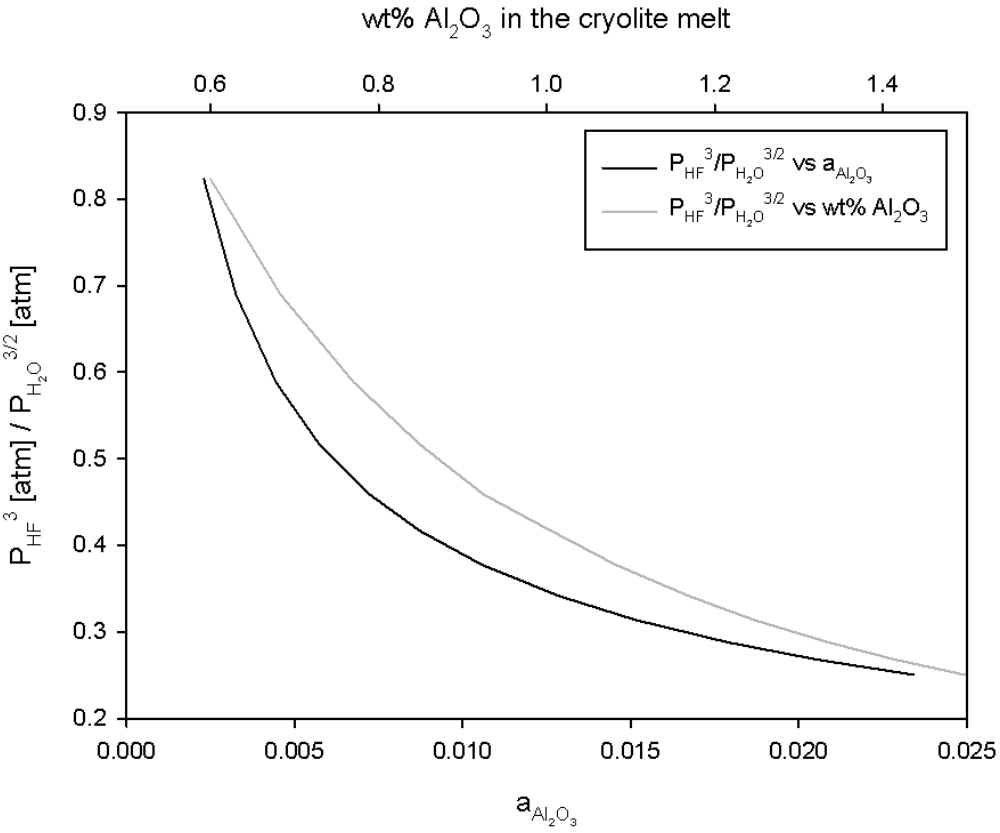

Figure 33: Partial pressure of HF over partial pressure of H_2O vs. the activity and wt% of alumina.

Another possibility is that the calcined alumina may have had time to pick up moisture from ambient air before being added to the melt in some of the cases.

Dando et al [6] experienced that addition order did not influence on the HF formation measured when they performed electrolysis experiments where alumina was added to a cryolitic melt. These experiments also suggest that alumina addition order does not influence on the HF formation results even though no electrolysis has been performed in the present work. Gas flow and blockage of gas tubes are more crucial parameters on the results found for HF formation.

6.3.4 Comments on the Method of Calculating Riemann Sums and Conversion Efficiency of HF from H_2O

When calculating the quantity of HF formed after each addition in the experiments, it was decided to do Riemann sum calculations for 30 minutes after each addition. Exceptions were made to this rule when the line of HF hit the baseline before 30 minutes had passed. The optimal way of calculating the HF quantity would have been to wait for every addition to hit the baseline. However, it was prioritized to fit as many additions of alumina as possible in each experiment. To be able to do this, the baseline stabilization time was forfeited. Usually the area under the graph after 30 minutes would be negligible. Another consideration to make was that the gas tubes leading the gas out of the system were blocked approximately every two hours. By choosing to wait for every baseline there was always the risk of having to wait for too long, so that the gas flow was blocked before the baseline was hit.

Haupin and Kvande [5] has predicted that approximately 25% of the H_2O equilibrium concentration in Equation 3 will form HF. Comparing the ratio between the calculated HF quantities possible, when assuming that all hydrogen found when performing LOI and TGA would form HF, and the quantity of HF found in the experiments; it is evident that several of the HF amounts found in the experiments are higher than 25% compared to the calculated amount of HF from TGA and LOI values. The calculations based on LOI and TGA values are not based on any equilibrium H_2O. Instead, they are based on the actual amount of H_2O found present in each sample. Also, Haupin and Kvande's model was based on a real electrolysis cell producing aluminium. The wt% of alumina present in a real electrolysis cell is higher than that obtained in these experiments. The conditions inside a closed laboratory furnace are substantially different from the conditions inside an electrolysis cell producing aluminium.

6.3.5 General Comments on Moisture Behaviour during the Experiments

In experiments 2-3 and 8, the laser measures an increase in H_2O concentration in correspondence with addition of alumina. This behaviour of moisture is relatively reasonable considering that the aluminas added to the melt in experiment 2 and 8 had a very high moisture content. The reason why experiment 3 also shows this behaviour is less understood considering that this behaviour was not observed in, for instance, experiment 4. The work laid down to increase the understanding of the moisture content did pay off to a certain extent, since it became possible to observe trends to a greater extent within an experiment.

However, the real increased understanding of moisture in alumina came from performing LOI, TGA, DSC and XRD on the alumina samples. It was also the LOI and TGA values that laid the basis for calculating the expected HF formation for each addition. The uncertainty in the H_2O

measurements are still considered too large to be able to quantify the amount of H_2O from the alumina being flashed off vs. reacting to form HF.

6.3.6 Continuous Stirred Tank Reactor

The modelling of a continuous stirred tank reactor (CSTR) has been used to show the ideal HF evacuation of the crucible. The details for the calculations are shown in Appendix I. Figure 34 shows the modelled evacuation of addition 6 in experiment 2 compared to the real evacuation observed in the experiment. During this alumina addition, the flow of N_2 gas was 98.79NmL/min and this gas flow is referred to as normal flow. Figure 35 shows the modelled evacuation of addition 7 in experiment 2 compared to the real evacuation observed in the experiment. During this alumina addition, the flow of N_2 gas was 197.60NmL/min and this gas flow is referred to as double flow. Figure 36 shows the modelled evacuation of addition 3 in experiment 8 compared to the real evacuation observed in the experiment. This addition gave a high peak, due to the high amount of surface adsorbed H_2O in the sample. Figure 37 shows the modelled evacuation of addition 4 in experiment 8 compared to the real evacuation observed in the experiment. This addition gave a low peak compared to addition 3.

Figures 34 and 35 show the modelled and real evacuation of HF observed in the experiment with normal and double flow into the furnace. As expected in the modelled case, the HF evacuation happens twice as fast when the flow into the system is doubled. The most interesting observation from these figures is to see that the real evacuation observed in the two cases follow the modelled trend. The real HF evacuation never reaches a level of zero ppm HF, but the graphs do follow the same trend where the curves flatten approximately at the same time after addition as in the modelled cases.

Figures 36 and 37 show the modelled and real evacuation of HF when adding an alumina quality with a high HF formation potential vs. an alumina quality that has a lower HF formation potential due to the difference in LOI in the two samples. HF is fully evacuated after approximately 9 minutes in Figure 36 according to the CSTR modelled curve. The real evacuation curve shows a flattening of the HF concentration at approximately 13 minutes. This deviation from the modelled example may come from the substantial flash of HF formed in the instance when the alumina reached the cryolitic melt. Some parts of this HF may exit the nickel crucible and enter the large furnace area, to later re-enter the nickel crucible causing a slower evacuation of HF. If this is the case, then the problem would have been solved by having a completely closed system that did not allow the gas to enter anywhere other than out of the gas tube. Having a completely closed crucible, however, would be difficult to implement in practice. In Figure 37, the trend of flattening into a baseline of the real curve happens approximately at the same time as an observed flattening of the modelled curve.

As mentioned previously, one of the reasons for deviation between the real and the modelled cases when comparing CSTR modelling to the real evacuation observed in the experiments may be HF gas entering the furnace volume and then re-entering the crucible. If this did not happen, the peak would have been higher after the alumina addition; but in theory, the sums of the areas below the curve should be equal if all HF that entered the furnace volume is emptied through the crucible before a new addition is made. Another reason for deviation between the observed and modelled case is that some HF may dissolve into the cryolitic melt and slowly be released. This may explain why the baseline is so high, and why it takes so long to reach a steady baseline of HF after every addition.

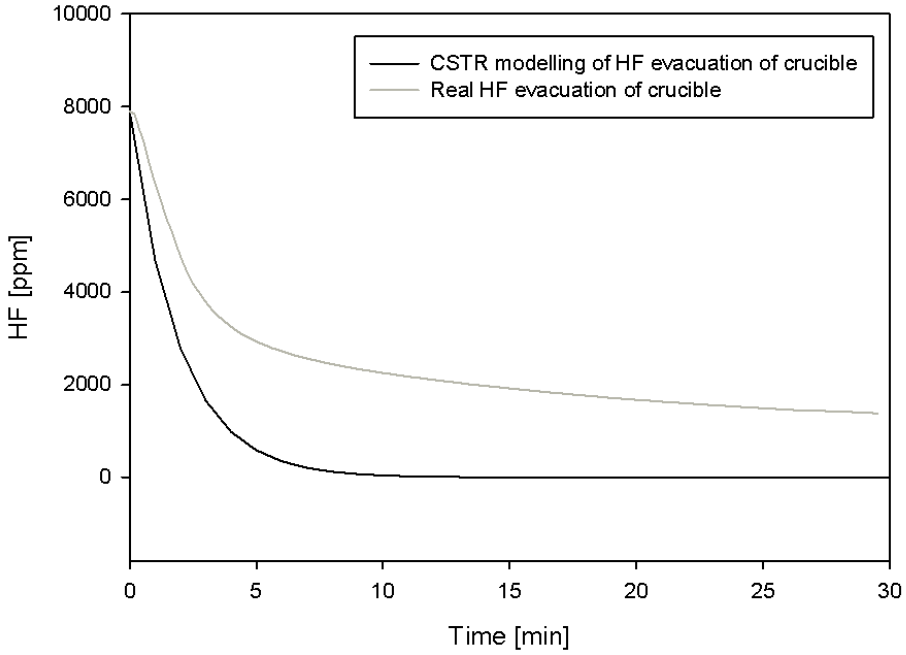

Figure 34: CSTR modelled evacuation of HF compared to the real evacuation of HF measured in the experiment for addition 6 in experiment 2. "Normal" N_2 gas flow was purged through the system.

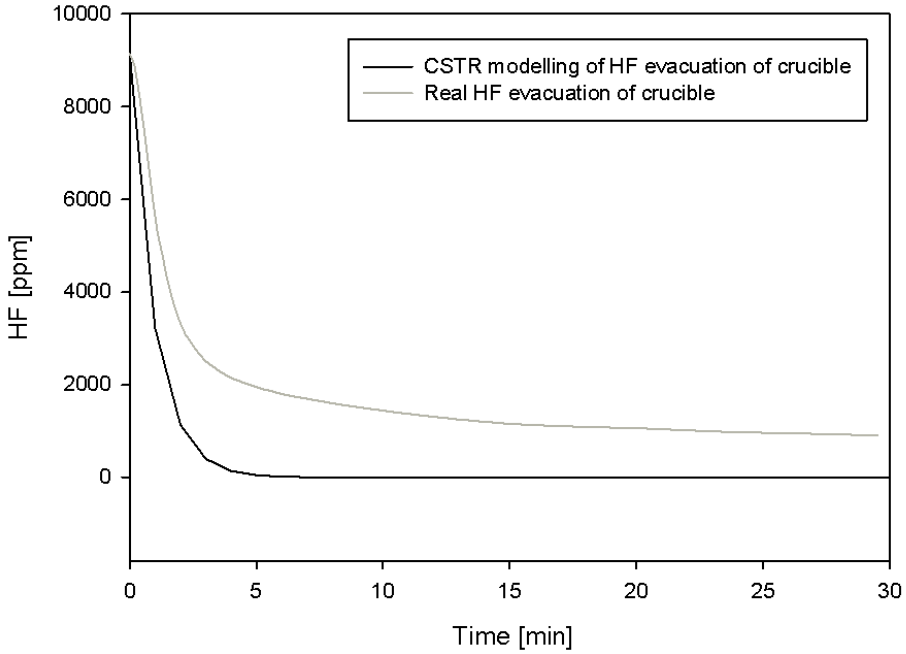

Figure 35: CSTR modelled evacuation of HF compared to the real evacuation of HF measured in the experiment for addition 7 in experiment 2. "Double" N_2 gas flow was purged through the system.

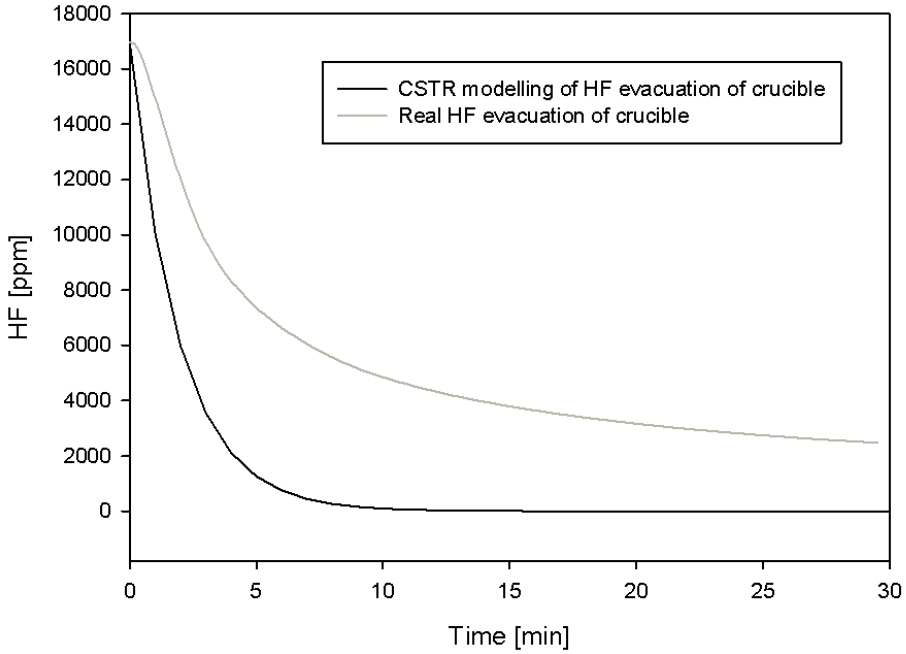

Figure 36: CSTR modelled evacuation of HF compared to the real evacuation of HF measured in the experiment for addition 3 in experiment 8. The high amount of physisorbed moisture caused a high peak.

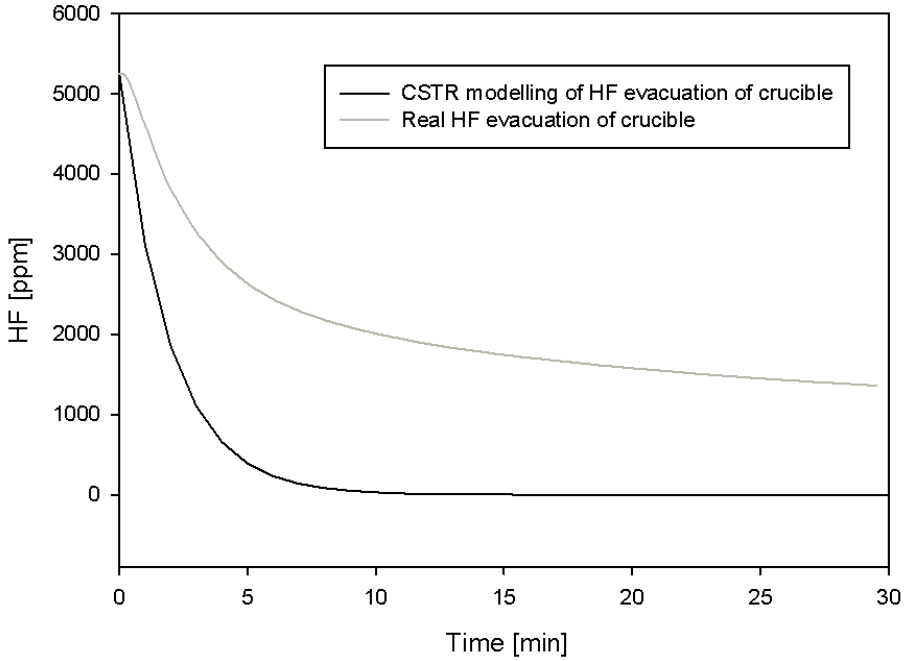

Figure 37: CSTR modelled evacuation of HF compared to the real evacuation of HF measured in the experiment for addition 4 in experiment 8. The sample had a lower HF formation potential due to less moisture in the sample hence creating a lower peak.

6.3.7 Testing Methodology and Reproducibility when Adding Industrial Aluminas to a Cryolitic Melt

Experiments 1-3 was performed to test the reproducibility when adding several batches of alumina of various quality to a cryolitic melt.

Experiment 1

The results for experiment 1 presented in Figure 25, and Tables 8 and 9 show that the addition of calcined alumina A was very reproducible. Addition 1, however, deviates to a certain extent and forms more HF than additions 2-4 and 7. Figure 33 and Table 23 show that the expected HF formation can be higher for the first alumina addition to a cryolitic melt depending on the starting concentration of Al_2O_3 formed by reaction between moisture in the melt and AlF_3.

The calculated amount of HF (using Riemann sums shown in Table 9) for additions 5 and 6 in experiment 1 deviate a lot from each other, even though the expected HF formation from LOI and TGA calculations for the two additions show that the HF formation for the two additions should be equal. An explanation to this observed deviation is that it is difficult to make a representative mixture of hydrate and calcined alumina. The amount of hydrate sample weighed out to create the hydrate/calcined mixture is very small, and this may cause samples that are not representative of the hydrate powder. When weighing out samples it is better to take out many small portions from the container with powder instead of one big portion. Since the amount of hydrate is so small, it becomes difficult to take out many small portions.

Experiment 2

The results from experiment 2 are shown in Figure 26 and Tables 10 and 11. In experiment 2 more hydrate/calcined mixtures were made. In addition, it was experimented with changing the gas flow and addition quantities.

A mixture of approximately 5% hydrate, 95% calcined alumina A was prepared for additions 1-3. In accordance with the discussion given for experiment 1, it is difficult to make a representative sample when the amount of hydrate to be weighed out is so small. The first addition may also experience increased HF formation due to the findings in Figure 33 and Table 23.

The gas flow was doubled before addition 7 to see the effect of gas flow on the measurements. One problem that occurs in the laboratory cell with increased gas flow is increased condensation in the gas tube, eventually leading to blockage of the gas flow. When increasing the gas flow the HF gas will become diluted; however, the final amount of HF formation should remain the same. The quantity of HF found for addition 7 should be the same as for additions 4-6. Additions 4-6 show very reproducible results for HF formation. Addition 7 deviates somewhat, however, when the gas flow is doubled this may cause more of the produced HF gas to enter the furnace volume from the crucible. The effect of gas flow inside the furnace is not well understood and has not been examined further.

In addition 9, the addition quantity was reduced and the expected HF formation from addition 9 should be approximately $1.8 \cdot 10^{-3}$g when comparing to the HF formation values and alumina addition quantities found from additions 4-6. The HF quantity found after addition 9 was in reasonable accordance with this expected value.

The quantity of HF for the calcined alumina sample in addition 10 is considered reasonable.

As mentioned previously, a part of the alsint tube leading the gas out of the furnace fell into the melt. This incident does not seem to have affected the results to a large extent.

Experiment 3

The results from experiment 3 are shown in Figure 27 and Tables 12 and 13. The aim of experiment 3 was to determine the effect of various heat treatments on the same alumina quality. Additions of alumina A stored at room temperature and heated for 2 hours at 160 and 350°C were added to the melt. A procedure of adding calcined alumina A as the first and last batch to the melt was introduced.

The results shown in Table 13 from the experiment show that there is a clear difference between the room tempered sample and the samples heat treated at 160 and 350°C. The room tempered sample clearly forms more HF than the heat treated samples. The difference in HF quantity between the samples heat treated at 160 and 350°C is not so clear. This result supports the findings during TGA, LOI and XRD characterisation; that alumina A does not contain a substantial amount of gibbsite. Figure 27 does show, however, that the peaks for alumina heat treated at 160°C are higher than the peaks for alumina heat treated at 350°C. The findings in experiment 3 for HF formation are in contrast with the literature that suggest that structural hydroxyl contributes more to HF formation than physisorbed moisture [2]. In this laboratory setup, the physisorbed moisture contributes to the HF formation to a large extent and is not flashed off before entering the melt.

LOI(RT-160°) and LOI(RT-350°C) reported in Table 12 laid the basis for the calculated theoretical possible amount of HF from the hydrogen mass balance found from LOI values, reported in Table 13. When comparing the LOI values given in Table 4 with the LOI values in Table 12 it is interesting to see that the LOI(RT-160°C) has increased. The numbers are not directly comparable due to the large difference in the sample size (3g vs 0.15g). However, it may be that the warmer weather with higher humidity has caused higher LOI(RT-160°C) for alumina A. This is natural since the LOI testing was performed in February/March, while the melt experiments were performed in May. Ideally, the LOI and TGA testing should be performed on the same day as the melt experiments.

The calcined samples gave reasonable HF amounts, compared to the findings in experiment 1. This shows that the results found from experiment to experiment are fairly reproducible.

6.3.8 Comparison of HF Formation when Adding Aluminas with Various Gibbsite Concentrations

The aim for experiments 4 and 5 was to compare HF formation when adding aluminas with various gibbsite consentrations. It has been shown, through LOI, TGA, DSC and XRD testing, that alumina B and C contain gibbsite, whilst alumina A contains hardly any. In experiments 4 and 5 alumina A, B and C have been heat treated to 160°C for two hours, to remove physisorbed H_2O, and then added to a cryolitic melt. In experiment 4, primary alumina was added to the melt and in experiment 5 secondary alumina was added.

Experiments 4 and 5

The results for experiment 4 are given in Figure 28 and Tables 14 and 15. The trend is that for primary aluminas; alumina A forms less HF than alumina B and C. Alumina C forms less HF than alumina B. The difference in HF quantities between B and C are, however, negligible if assuming that the HF quantity found from addition 5 is considered an outlier. This result is expected when looking into the calculated amounts of HF by using LOI and TGA values, reported in Table 15. The much higher LOI for alumina B and C compared to A also explain the higher HF formation.

The results for experiment 5 are given in Figure 29 and Tables 16 and 17. In this experiment secondary alumina A, B and C were added to the melt in a randomized addition order. Once again, it is observed that alumina A forms less HF than alumina B and C. But now the situation has changed for secondary aluminas B and C compared to primary alumina. From Table 17 it is clear that secondary alumina C forms more HF than secondary alumina B. One hypothesis is that there are some properties within alumina C that gives it better scrubber efficiency than alumina B, and that this extra HF is released upon addition to the cryolitic melt. Testing this hypothesis was outside the scope of this master work.

Comparing the results from experiments 4 and 5, show that secondary alumina form more HF than primary alumina. This is not surprising considering that secondary alumina already holds a quantity of HF after being used in the dry scrubber to adsorb fluorides. This quantity of HF will be released upon addition to a cryolitic melt.

6.3.9 Comparison of HF Formation when Adding Aluminas with Various Powder Size Fractions

The aim of experiments 6 and 7 was to compare the HF formation potential with powder sizes. Alumina A and B, size fractions +150μm and -45μm were added to the melt. Both primary and secondary alumina was investigated. The samples were heat treated at 160°C for two hours before addition to the melt.

Experiments 6 and 7

Figure 30 and Tables 18 and 19 show the results from experiment 6. In experiment 6, primary alumina was investigated. From the results it is once again obvious that alumina B forms more HF than alumina A. This is in accordance with the characterisation results (LOI, TGA and XRD). By investigating the quantities of HF formed, it cannot be concluded whether +150μm or -45μm alumina A form more HF (when assuming that the result found for alumina A +150μm addition 2 can be considered an outlier). From the calculated amounts of HF they both seem to have a relatively similar HF formation potential. The HF formation potential of alumina A -45μm and +150μm fractions seem relatively similar when comparing LOI and TGA results for the two samples (see Table 4 and Figure 14).

When it comes to primary alumina B, however, it seems clear that the -45μm fraction forms more HF than the +150μm fraction (when assuming that the result found for alumina B addition 9 can be considered an outlier). When investigating the LOI values and TGA findings for alumina B in Table 4 and Figure 18, it is observed that alumina B -45μm did contain more gibbsite than the +150μm fraction. Hence, the conclusion that alumina B -45μm fraction forms more HF than the +150μm fraction is supported by the characterisation findings.

Figure 31 and Tables 20 and 21 show the results from experiment 7. In experiment 7 secondary alumina A and B, -45μm and +150μm fractions were investigated. Alumina A +150μm forms less HF than alumina B +150μm. However, secondary alumina A +150μm forms more HF than primary alumina A of the same size fraction indicating that fluorides adsorbed on the secondary alumina flashes off and contributes to the HF formation concentrations measured by the laser. Alumina B -45μm forms more HF than alumina A -45μm. Both secondary alumina A and B -45μm fractions form less HF than primary alumina A and B -45μm. This indicates first of all poor scrubber efficiency for the small fraction secondary alumina. It also indicates that a substantial amount of the small fraction secondary alumina consists of carbon that burns off. Hence, all the small fraction secondary alumina powder does not only contain alumina, but also

carbon. Carbon will not contribute to HF formation. Both secondary alumina A and B +150μm forms more HF than secondary alumina A and B -45μm.

When performing the experiments with the different powder size fractions, one problem was that all of the -45μm fraction powders did not enter the melt. Instead it went with the gas flow into the gas tube and further into the 1/16" PFA tubing. As a result the PFA tubing was blocked by this alumina dusting. More work should be performed to optimize the additions of fine fraction alumina. One idea is to block the gas flow of carrier N_2 gas at the instant of addition, allowing the alumina to pass into the melt before turning the carrier gas back on.

6.3.10 Testing of Alumina with a High Level of Physisorbed Moisture versus Alumina with a High Level of Gibbsite

Experiment 8

Experiment 8 was performed to test the HF formation potential of physisorbed moisture vs. gibbsite. Moist primary alumina A was prepared to create a sample with a high amount of physisorbed moisture. Primary alumina B, heat treated at 160°C for two hours represented the sample high in gibbsite.

Figure 32 and Table 22 show the results of experiment 8. From both the figure and the table, it is evident that the sample with a high amount of surface adsorbed moisture forms a substantial amount of HF. From this experiment it seems clear that physisorbed moisture does contribute to HF formation in contrast with what has been suggested in the literature [2]. With the laboratory setup used in these experiments, the distance from the feeder to the bath is very short (approximately 1cm). It may be so, although not very likely, that the physisorbed H_2O on the alumina does not have time to flash off before entering the melt. Reasons for arguing that the physisorbed moisture would have time to flash off are i) The samples are very small, hence it does not need a lot of heating time to evaporate the relatively loosely bonded physisorbed moisture, ii) The feeder tube is hot, so even though the distance from the bath to the feeder is short, the alumina is being heated before in enters this open gap between the bath and the feeder and iii) It has been shown during previous work that moist air will contribute to the HF formation [7]. If the physisorbed moisture was flashed off, this moisture may still represent a source of hydrogen for HF formation as H_2O present in the ambient gas. The results in experiment 8 are in correspondence with the results found in experiment 3.

The last addition in experiment 3 was calcined alumina A. This batch was added only 10 minutes after the previous addition. The motivation for doing this was to test a hypothesis that some HF will dissolve in the melt and slowly be released from the bath. It is believed that dissolved HF in the bath may be the reason why the evacuation of HF after each addition is so slow, causing the observed long tail before reaching baseline. When adding "inert" alumina, like calcined alumina A, any dissolved HF might flash off from the melt. No conclusion can be drawn from the results of the last addition in experiment 8. The last batch of calcined alumina A form more HF than the first batch. However, this result is within the uncertainty parameters of the experiments. More experiments should be performed to test this hypothesis. One last comment to be made, is that both the HF amounts found in the experiment from calcined alumina and primary alumina B samples are substantially lower than what found in earlier experiments. No clear explanation for this has been found.

6.3.11 HF Formation as a Function of LOI

In Figure 38 found on the next page; mol HF (Riemann) vs. mol H_2O from LOI is plotted. The values for HF and H_2O have been divided by the amount of alumina added to remove any variations in alumina quantity added, creating relative values for HF and H_2O. This figure has been made to summarize all findings from experiments 1-8.

From the figure it can be seen that HF formation is, by and large, a function of LOI. Secondary alumina generally forms more HF than primary alumina. If a straight line is drawn from origin toward the data for secondary alumina, the gradient will approximately equal 2, indicating 100% conversion of all H (calculated from primary LOI data) in the H_2O found into HF. 100% conversion efficiency is not very likely to happen, moreover it indicates that the secondary alumina already holds some fluorides that are being released during addition to the cryolitic melt.

If a straight line is drawn from orgigin towards the star shaped points, most of the experimental data shows little deviation from the trend line: calcined alumina A, primary alumina A (RT), primary alumina A (160°C), primary alumina A and B +150μm fraction (160°C), primary alumina A and B -45μm fraction (160°C) and secondary alumina A and B +150μm fraction (160°C). This line has a slope of approximately 1, indicating 50% conversion of all H (calculated from primary LOI data) in the H_2O found, into HF.

A third straight line can be drawn from origin toward the cluster of test points represented by, amongst others, primary alumina B and C (160°C). This line has a slope of approximately 0.5, indicating that approximately 25% of the total amount of H found in H_2O (from primary LOI data) was converted into HF.

The two points of 14.3% hydrate/85.7% calcined and 13.8% hydrate/86.2% calcined alumina A, that lies far to the right in Figure 38 can be considered outliers. It is reason to believe that the weighing out of the two samples did not create representative mixture of the two alumina qualities.

From Figure 38 it is seen that the calcined alumina samples from all experiments form a cluster at the left bottom. Even though there is uncertainties in the measurements, the cluster indicate that the results from the experiments are relatively reproducible throughout the measuring campaign.

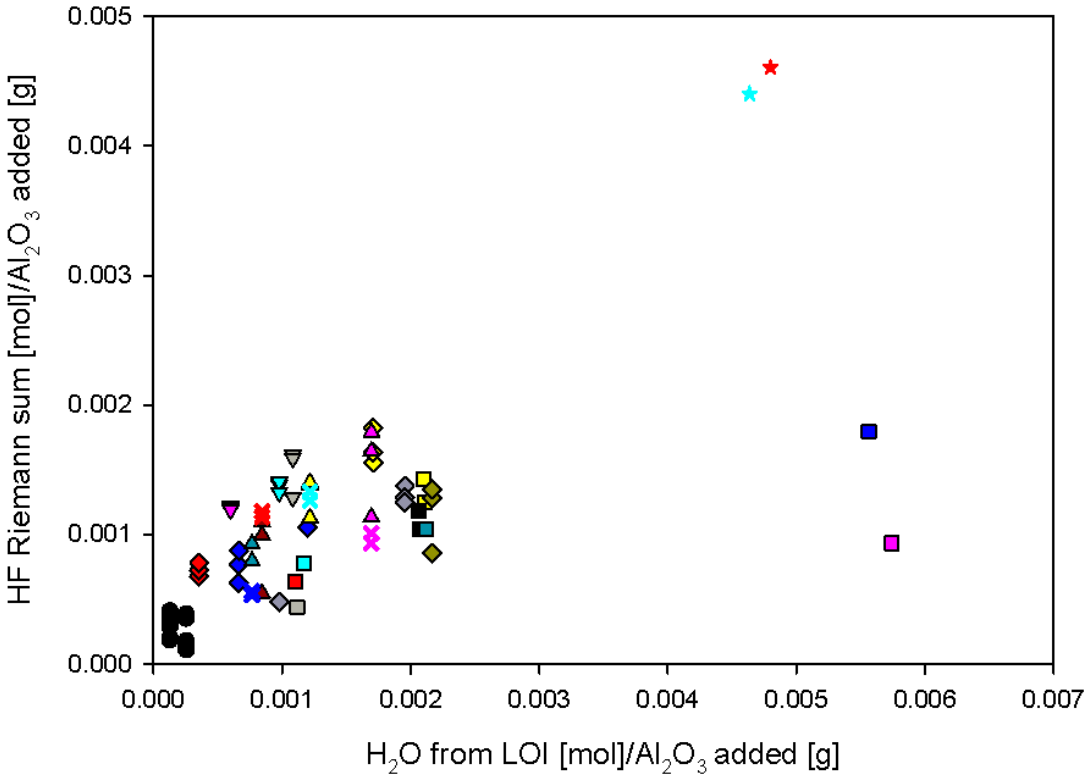

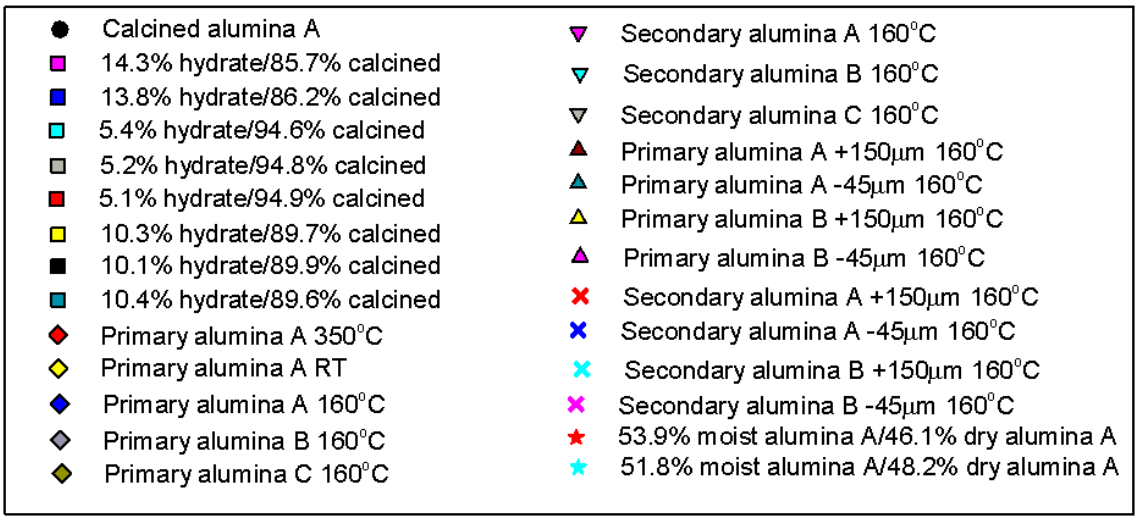

Figure 38: Mol HF vs. mol H_2O from LOI values. The LOI values are based on primary alumina from Tables 4 and 12. The HF and H_2O values plotted are divided by the amount of alumina added to remove any variations in alumina additions.

6.3.12 Relations between Laboratory Findings and Observed Fluoride Losses at the Smelter

This master (and project) work was initiated by the findings of a loss in aluminium fluoride from the electrolyte when using a certain alumina quality (alumina B) at Norsk Hydro Sunndal. The hypothesis was that increased HF formation caused the observed AlF_3 loss. Three alumina qualities have been investigated: A, B and C. Alumina A works satisfactory in the plant, and in the present work it has been shown that alumina A forms less HF than alumina B and C. It has also been found that alumina A contains hardly any gibbsite, in contrast with findings for alumina B and C. To examine the three alumina qualities, LOI has been performed. Both alumina B and C had higher LOI values than alumina A, indicating that the potential for HF formation for these two alumina qualities are higher. It has also been found that both the physisorbed and the more strongly bound structural hydroxyl moisture contribute to HF formation.

Alumina C is made by the same producer as alumina B, but did not show a loss in aluminium fluoride at the smelter. This master work has not found any clear differences in alumina B and C that can explain the different behaviour of the two at the smelter. It was found that secondary alumina C formed more HF than secondary alumina B. One hypothesis can be that the scrubber efficiency of alumina C may be better compared to alumina B. Testing this hypothesis has been outside the scope of this master work but should be looked further into. If this hypothesis fails, then the explanation may be found in parameters outside the alumina quality itself e.g. weather variations around the plant or storing conditions at the calciner.

7 Further Work

Some further work is suggested on the basis of the present work:

- Improve sample preparation for XRD testing and gain increased understanding on all theory behind the different phases in the alumina e.g. crystal structures and atomic positions.
- Optimization of the addition of small fraction aluminas to the cryolitic melt to eliminate the problem of alumina dust blocking the PFA tubing leading the gas into the laser.
- Increase the knowledge around the scrubber properties of the different aluminas. The key to answering the hypothesis on why alumina B causes loss in fluorides from the electrolyte completely may be a combination of the two: increased HF formation when using alumina B as well as poorer scrubber efficiency. In this work, only the HF formation itself has been studied.
- To increase the understanding of the moisture behaviour when performing alumina additions, for instance, when measuring the amount of H_2O being flashed off, two lasers should be used. One optimized for measuring HF and the other optimized for measuring H_2O. Due to the nature of the absorption lines of HF and H_2O in the laser, the water signal suffers and only trends can be seen in the present experimental results. No quantifications of H_2O can be done on the basis of the present experimental results.
- More experimental work to support the findings in this work. Time limitations did not allow for more experiments. More experimental data will create the basis for further processing of the data.

8 Conclusion

This work set out to test the hypothesis concerning the HF formation potentials of alumina A, B and C. During production, Hydro Sunndal had experienced unexpected high losses of aluminium fluoride from the electrolyte when using alumina B. Alumina A worked satisfactory in the plant. Alumina C was made from the same producer as alumina B, but did not show the characteristic drop in aluminium fluoride at the smelter. This problem formed the background for this work.

The experimental work was separated into two parts: A characterisation section where LOI, TGA, DSC and XRD were performed, and a section where the industrial aluminas were added to a cryolitic melt to measure the HF formation found for each alumina quality. Both primary and secondary alumina were investigated as well as bulk, fine and coarse fractions (-45μm and +150μm). No electrolysis was performed in the laboratory cryolitic melt during alumina addition.

The following summarizes the findings of this master work:

- A method and laboratory setup producing relatively reproducible results when it comes to measuring HF formation in different industrial aluminas, have been developed.
- By performing LOI and TGA techniques it was found that alumina A contained less H_2O than alumina B and C. It was also found that the amount of gibbsite in alumina A is negligible, whilst alumina B and C contain a substantial amount of gibbsite. XRD has been used to identify the phases in the aluminas.
- Increased LOI gives an increased HF formation potential. Hence, it has been found that alumina A forms less HF than alumina B and C. This is valid for both primary and secondary alumina. A correlation between LOI and HF formation has been found. For primary aluminas the conversion efficiencies of H_2O into HF has been found to be approximately 25-60%. Values found from the LOI testing have been used to determined the amount of H_2O theoretically available for HF formation.
- Primary alumina B forms slightly more HF than primary alumina C.
- Upon addition of coarse and fine fraction primary alumina, it was observed that both coarse and fine fractions of alumina B formed more HF than both size fractions of alumina A. The fines of primary alumina B formed more HF than the coarse fraction of B, whilst the coarse fraction of alumina A formed more HF than the fine fraction of alumina A.
- Secondary alumina forms more HF than primary alumina. This indicates that the fluorides adsorbed on the secondary alumina from the dry scrubber process are released upon addition of the aluminas to a cryolitic melt.
- Secondary alumina C forms more HF than secondary alumina B. This may indicate that secondary alumina C holds more HF from the scrubber process.
- Upon addition of coarse and fine fraction secondary alumina, it was observed that the coarse fraction formed more HF than the fine fractions, indicating better scrubber efficiency for the coarse particles. It was also observed that both fine and coarse fractions of secondary alumina B formed more HF than alumina A.
- The addition order of the aluminas has been found to have a minor impact on the experimental results.

- From the laboratory work it can be concluded that all types of moisture in the aluminas contribute to HF formation. This includes both physisorbed and chemistorbed moisture, as well as structural hydroxyls.
- The findings of this work cannot explain why there was an observed loss in AlF_3 when using alumina B as opposed to alumina C at the smelter. One explanation can be that alumina C may have better scrubber efficiency than alumina B. Examining this hypothesis has been outside the scope of this master work. If variations in scrubber efficiency for the two aluminas fails to explain the drop in AlF_3, the solution may be found in parameters outwit the alumina quality e.g. weather conditions at the time of production or storage conditions at the calciner.

References

[1] J. Thonstad, P. Fellner, G.M Haarberg, J. Híves, H. Kvande, and Å. Sterten. *Aluminium Electrolysis*. Aluminium-Verlag Marketing und Kommunikation GmbH, Düsseldorf, 3rd edition, 2001.

[2] M. Hyland, E. Patterson, and B. Welch. Alumina structural hydroxyl as continuous source of HF. *Light metals*, pages 361–366, 2004.

[3] W.E. Haupin. Principles of aluminium electrolysis. *Light metals*, pages 195–203, 1995.

[4] K. Radon, D. Nowak, and R. Heinrich-Ramm. Respiratory health and fluoride exposure in different parts of the modern primary aluminum industry. *Int Arch Occup Environ Health*, pages 297–303, 1999.

[5] W. Haupin and H. Kvande. Mathematical model of fluoride evolution from Hall-Héroult cells. *Light metals*, pages 257–263, 1993.

[6] N. Dando, X. Wang, J. Sorensen, and W. Xu. Impact of Thermal Pretreatment on Alumina Dissolution Rate and HF Evolution. *Light metals*, pages 541–546, 2010.

[7] C. Sommerseth. HF Formation Upon Addition of Different Industrial Aluminas to Cryolitic Baths, December 2010. Project Work in TMT4500, Norwegian University of Science and Technology.

[8] D.W. Richerson. *Modern Ceramic Engineering - Properties, Processing and Using in Design*. CRC Press, Boca Raton, FL, 3rd edition, 2006.

[9] A. Meyer. Personal communication. March. Norsk Hydro ASA, 2011.

[10] L.M. Perander. *Evolution of nano- and microstructure during the calcination of Bayer gibbsite to produce alumina*. PhD thesis, The University of Auckland, 2010.

[11] I. Tabsh and M. Dupuis. Modeling of Aluminum Reduction Cells Using Finite Element Analysis Techniques, December 2010. http://www.genisim.com/website/tms95.htm.

[12] K. Grjotheim and H. Kvande. *Introduction to Aluminium Electrolysis*. Aluminium-Verlag, Düsseldorf, 2rd edition, 1993.

[13] L.T. Kristiansen. Presentation at ntnu, hydrodagen 06.04.11. Norsk Hydro ASA, 2011.

[14] M.M. Hyland, A.R. Gillespie, and J.B. Metson. Predicting moisture content on smelter grade alumina from measurement of the water isotherm. *Light metals*, pages 113–117, 1997.

[15] P.C. Mørk. *Overflate og kolloidkjemi, grunnleggende prinsipper og teorier*. Norges teknisk-naturvitenskapelige universitet, Trondheim, 8th edition, 2004.

[16] A.A. Tsyganenko and P.P. Mardilovichb. Structure of alumina surfaces. *J. Chem. Soc.*, pages 4843–4852, 1996.

[17] L.M. Perander, M.A. Stam, M.M. Hyland, and J.B. Metson. Towards Redifining the Alumina Specifications Sheet - The Case of HF Emissions. *Light metals*, pages 285–290, 2011.

[18] N.R. Dando and R. Tang. Fluoride evolution/emission from aluminum smelting pots - impact of ore feeding and cover practices. *Light metals*, pages 363–366, 2005.

[19] K.S. Osen. Oppførsel av fukt i kryolittsmelter. Master's thesis, Norwegian University of Science and Technology, 2005.

[20] K.S. Osen, C. Rosenkilde, A. Solheim, and E. Skybakmoen. The behavior of moisture in cryolite melts. *Light metals*, pages 395–400, 2009.

[21] NEO Monitors AS. LaserGas^{TM} II SP and LaserGas^{TM} II SP Compact Monitors. User's reference, Version 1.4.

[22] P. Atkins, T. Overton, J. Rourke, M. Weller, and F. Armstrong. *Shriver and Atkins Inorganic Chemistry*. Oxford University Press, Oxford, 4th edition, 2006.

[23] R. Tilley. *Understanding Solids - The Science of Materials*. John Wiley and Sons, LTD, West Sussex, 1st edition, 2004.

[24] J.T. Wehrli and A.R. Kane. Application of Differential Scanning Calorimetry for Characterisation of Bayer Process Solids. *Light metals*, pages 175–184, 1993.

[25] K. Wefers and C. Misra. Oxides and hydroxides in aluminum. Technical Report 19, Alcoa Research Laboratories, 1987.

[26] K. Yamada, T. Harato, S. Hamano, and K. Horinouchi. Dehydration products of gibbsite by rotary kiln and stational calciner. *Light metals*, pages 157–171, 1984.

[27] V.J. Ingram-Jones, R.C.T. Slade, T.W. Davies, J.C. Southern, and S. Salvador. Dehydroxylation sequences of gibbsite and boehmite: study of differences between soak and flash calcination and of particle-size effects. *Journal of Materials Chemistry*, pages 73–79, 1996.

[28] B. Whittington and D. Ilievski. Determination of the gibbsite dehydration reaction pathway at conditions relevant to Bayer refineries. *Chemical Engineering Journal*, pages 89–97, 2004.

[29] L.M. Perander, Z.D. Zujovic, T.F. Kemp, M.E. Smith, and J.B. Metson. The Nature and Impacts of Fines in Smelter-Grade Alumina. *JOM*, pages 33–39, 2011.

[30] A. Solheim and Å. Sterten. Activity of alumina in the system NaF-AlF3-Al2O3 at NaF/AlF3 molar ratios ranging from 1.4 to 3. *Light metals*, pages 445–452, 1999.

[31] A. Solheim, E. Rolseth, E. Skybakmoen, L. Støen, Å. Sterten, and T. Støre. Liquidus temperatures for primary crystallization of cryolite in molten salt systems of interest for the aluminium electrolysis. *Met. trans.*, pages 739–744, 1996.

[32] R.E. Walpole, R.H. Myers, S.L. Myers, and K. Ye. *Probability and Statistics for Engineers and Scientists*. Pearson Education International, Upper Saddle River, 8th edition, 2007.

[33] H. Saalfeld and M. Z. Wedde. Refinement of the crystal structure of gibbsite, Al(OH)3. *Kristallogr., Kristallgeom., Kristallphys., Kristallchem.*, pages 129–135, 1974. PDF-4+ 2010 Database number: 04-011-1369.

[34] V.L. Cherginets, V.N. Baumer, S.S. Galkin, L.V. Glushkova, T.P. Rebrova, and Z.V. Shtitelman. Solubility of Al2O3 in some chloride-fluoride melts. *Inorg. Chem.*, pages 7367–7371, 2006. PDF-4+ 2010 Database number: 04-013-1687.

[35] B. Ollivier, R. Retoux, P. Lacorre, D. Massiot, and G. Ferey. Crystal structure of κ-alumina: an X-ray powder diffraction, TEM and NMR study. *J. Mater. Chem.*, pages 1049–1056, 1997. PDF-4+ 2010 Database number: 04-012-6907.

[36] R.S. Zhou and Snyder R.L. Structures and Transformation Mechanisms of the η, γ and θ Transition Aluminas. *Acta Crystallogr.*, pages 617–630, 1991. PDF-4+ 2010 Database number: 04-008-7261.

[37] S. Tsybulya and G. Kryukova. New X-ray powder diffraction data on delta-Al2O3. *Powder Diffraction*, pages 309–311, 2003. PDF-4+ 2010 Database number: 00-056-1186.

[38] W. Guse and H. Saalfeld. X-ray characterization and structure refinement of a new cubic alumina phase (alpha-Al2O3) with spinel-type structure. *Neues Jahrb. Mineral.*, page 217, 1990. PDF-4+ 2010 Database number: 04-005-4662.

[39] A.N. Christensen, M.S. Lehmann, and P. Convert. Deuteration of crystalline hydroxides. hydrogen bonds of gamma-AlOO(H, D) and gamma FeOO(H, D). *Acta Chem. Scand.*, page 303, 1982. PDF-4+ 2010 Database number: 01-074-6248.

[40] C.H. Edwards and D.E. Penney. *Calculus*. Pearson Education International, Upper Saddle River, 6th edition, 2002.

[41] M.-H. Lee, C.-F. Cheng, V. Heine, and J. Klinowski. Distribution of tetrahedral and octahedral A1 sites in gamma alumina. *Chemical physics letter*, pages 673–676, 1997.

[42] NEO Monitors AS. Lasergas II Troubleshooting and Service for trained personnel (for hardware version 1 and Software version 6). Version 2004-07-19.

[43] Relative humidity, August 2010. http://ww2010.atmos.uiuc.edu/(Gh)/home.rxml.

[44] Standards Australia. As 2879.1-2000 Alumina - Determination of loss of masse at 300 degrees Celsius and 1000 degrees.

[45] H.S. Fogler. *Elements of chemical reaction engineering*. Prentice-Hall Inc., New Jersey, USA, 4th edition, 2006.

A Testing Laser and Changing Settings and Gain

The aim of this appendix is to give a procedure on how to troubleshoot and deal with problems that might arise when working with the laser. The appendix has also been made to document what has been done to improve the laser measurements, especially when it comes to the H_2O concentrations, and how to recognize problems. The first section of this appendix chapter will show relevant work that laid the basis for changing the settings and gain of the laser. The gain and settings of the laser was changed to meet the requirements in the laboratory and this appendix shows what settings have been used, and how to change them.

A.1 Testing of Laser

Figure A.1 shows the deviation between the H_2O concentrations measured with an FTIR unit and the laser on the same system. The FTIR was placed in series with the laser. This work was performed to verify that the laser needed service. The laboratory setup when performing this test is shown in Figure 5.

A service was performed on the laser by personnel from NEO. After the service had been performed, the laboratory setup shown in Figure 5 was used to test the laser and verify that it was now reporting reasonable H_2O concentrations. A curve was made where the real vs. the measured H_2O concentrations was plotted. The result of this work has been shown in Figure A.2. The laser can be calibrated manually in the gmw61 program that follows the laser on the basis of curves like the one showed in Figure A.2. The equation found when running regression on the data is used for correcting for the offset of the laser and correcting for deviations in the slope of the line. If the relationship between the real and the measured H_2O value is non-linear, the settings of the laser may be wrong and a service on the instrument might be required. A procedure on how to check and update the settings and how to calibrate the laser are shown later in this appendix.

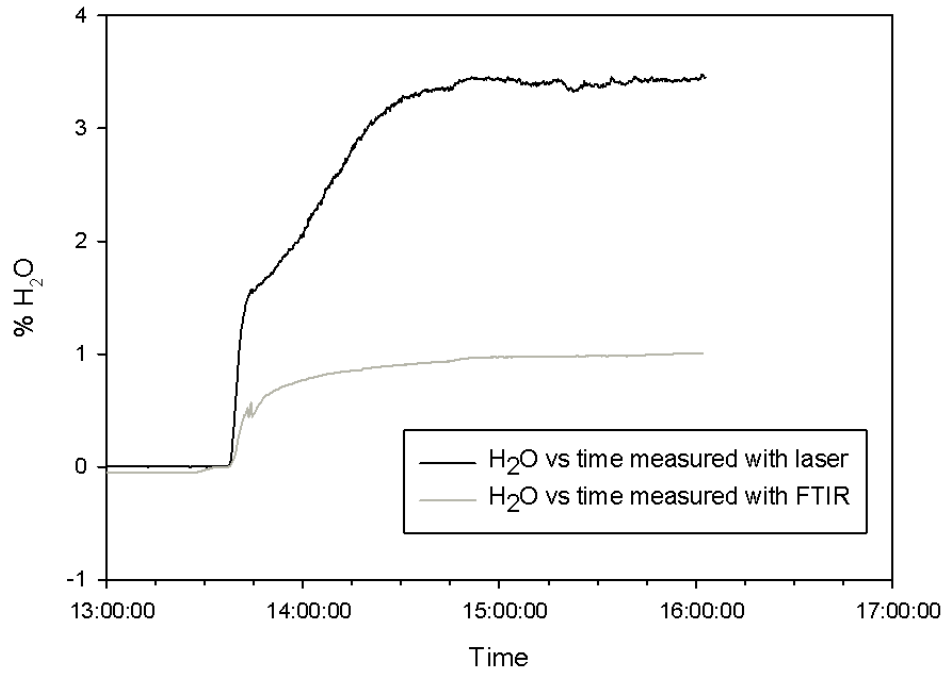

Figure A.1: The deviation found between the H_2O concentrations measured with the laser and FTIR in series.

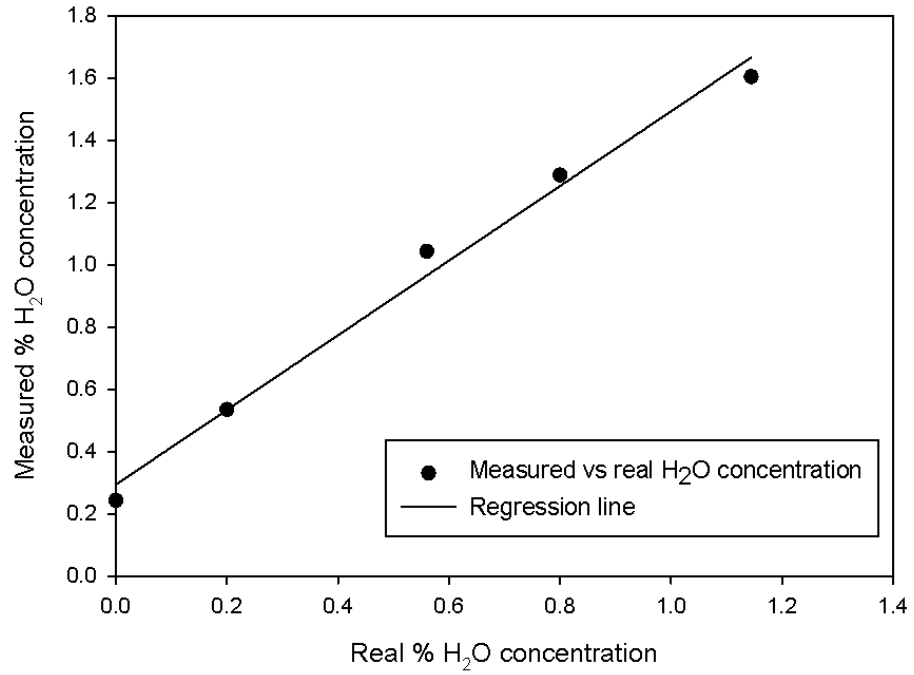

Figure A.2: Measured vs. real H_2O concentration. The equation of the regression line is: y=1.1994x+0.2935.

Different requirements are set for the laser when working in the laboratory compared to working with the laser in the industry. When measuring HF concentrations in the industry, it is important that the laser can measure concentrations as high as 3%. To enable measurements of HF concentrations as high as 3% the H_2O absorption line suffer. Hence, the H_2O measurements will become more uncertain. With the original gain settings of the laser, the settings and gain were optimised for industrial measurements. In the laboratory, it is more important that the laser are more sensitive for the H_2O measurements. The gain was changed so that the amplitude of the absorption line of HF was decreased, while the amplitude of the absorption line of H_2O was increased. The maximum HF concentration possible to measure with the laser now became approximately 1.7%. The accuracy of the moisture measurements is then increased. One weakness of this laser instrument, is that the absorption lines of H_2O and HF are relatively close to each other, and might affect each other. This appendix will show how to change the gain and the corresponding settings. The settings used when performing the laboratory measurements are shown.

A.2 Gain

The gain of the laser was changed from 0000 to 0010 in the electronics of the laser. To change the gain settings, the receiver box has to be opened and the switches has to be turned either off=0 or on=1. Figure A.3 shows the different gain settings that the instrument can have. [42] When changing the gain, the calibration factors and settings have to be changed.

Combination No.	SW3 1	SW3 2	SW3 3	SW3 4	Gain
0	0	0	0	0	11,00
1	1	0	0	0	17,80
2	0	1	0	0	26,45
3	1	1	0	0	33,25
4	0	0	1	0	50,23
5	1	0	1	0	57,03
6	0	1	1	0	65,69
7	1	1	1	0	72,49
8	0	0	0	1	111,00
9	1	0	0	1	117,80
10	0	1	0	1	126,45
11	1	1	0	1	133,25
12	0	0	1	1	150,23
13	1	0	1	1	157,03
14	0	1	1	1	165,69
15	1	1	1	1	172,49

0=OFF 1=ON

Figure A.3: Second harmonic gain switches [42].

A.3 Settings

The following section will show which settings that has to be used when changing the gain to 0010. The section will show how to change the settings manually.

To change the settings, the program gmw61.exe has to be opened. This program is found when opening the folder bin in the folder ng98 that can be found on the desktop of the computer that has the software for the laser installed. Figure A.4 shows the bin folder on the computer. When the program has been opened, a box will appear as shown in Figure A.5. When this box appears, press the LAN(TCP/IP) button. When the next box appears, click connect, as shown in Figure A.6. A new box, Figure A.7, will appear that either asks you to go into user or advanced mode. To change the settings it is necessary to go into advanced mode, and the password is r2d2. Figure A.8 shows the menu where it is possible to look at and change, the settings. It is also possible to create dump files, look at the state of the measurements in-situ from this menu. To change the settings back to the original 0000-gain settings: use the file called 0000-setting on the desktop of the computer following the laser and upload the settings. If this is not successful, contact NEO.

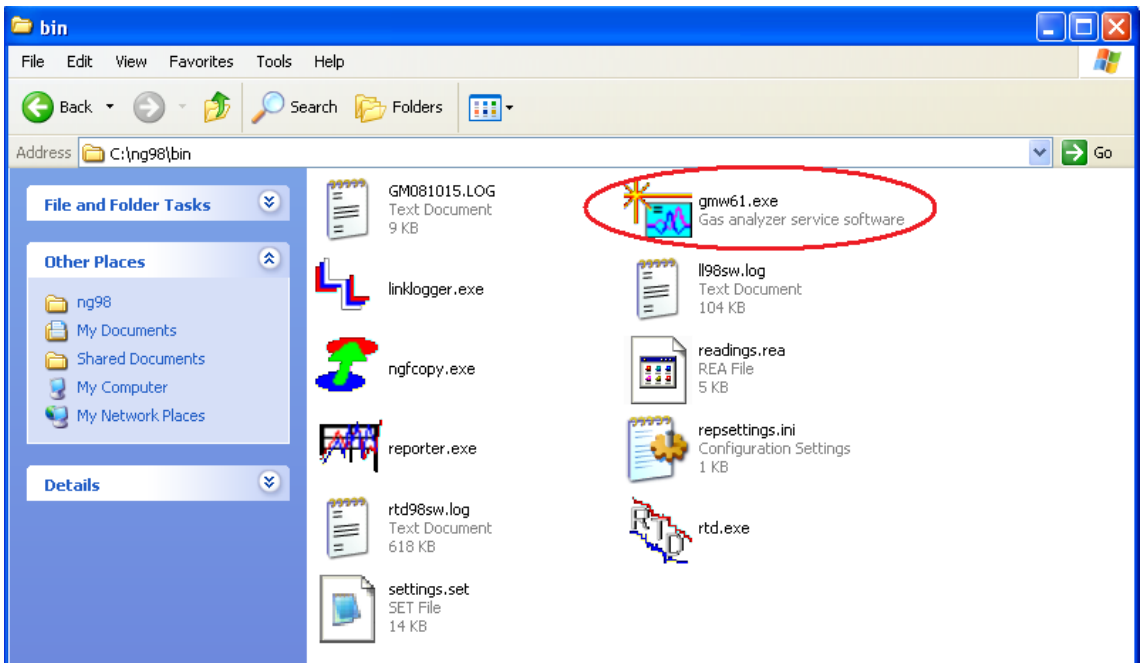

Figure A.4: The bin folder on the computer with the laser software. When changing the settings, the program gmw61.exe has to be opened.

Figure A.5: The box that appears when opening the gmw61.exe program. To move on, press the LAN(TCP/IP) button.

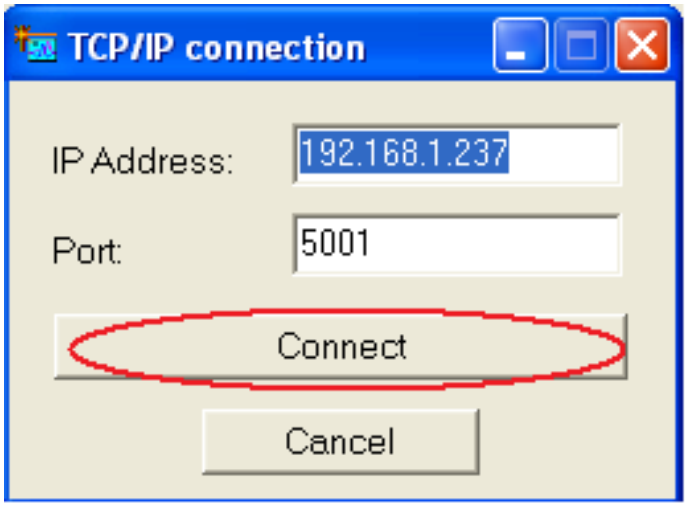

Figure A.6: Click connect when this box appears.

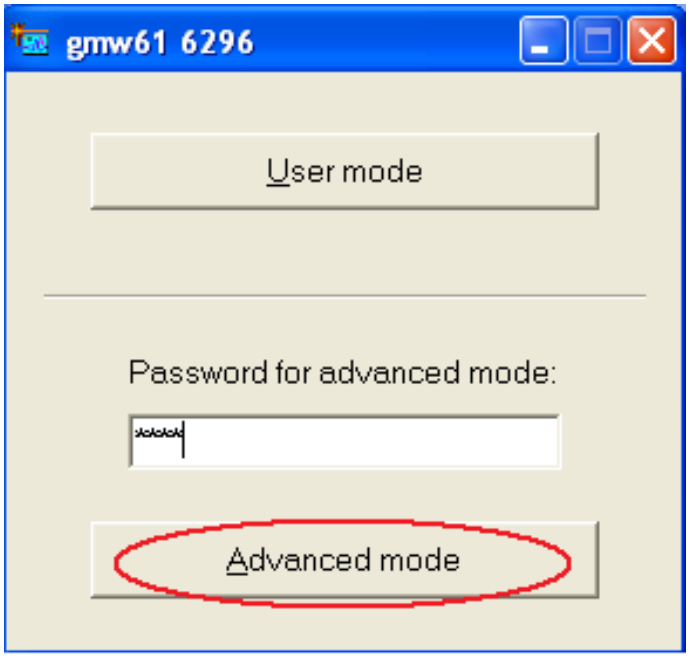

Figure A.7: To change the settings, use advanced mode. The password is r2d2.

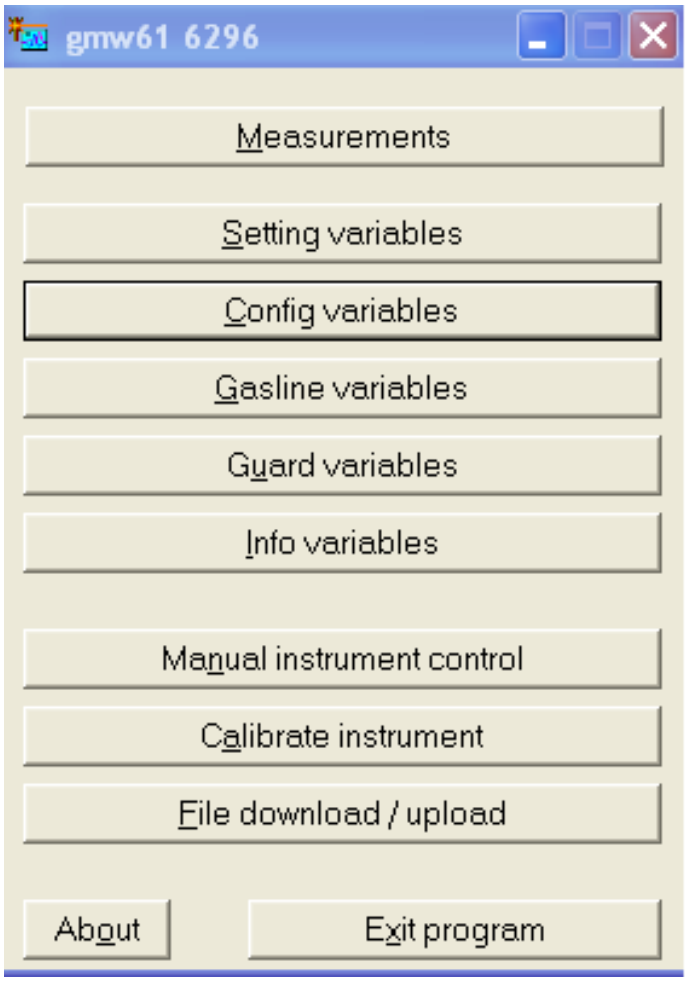

Figure A.8: The menu.

When the menu window shows up on the computer screen, several buttons can be pushed. If clicking the top button, named measurements, an overview on what the laser measures at that specific moment appears. Figure A.9 shows the measurement overview. An easy way to identify problems with the laser is by looking at the second harmonics signal. Push the second harmonic signal button to view the signal. Two plots of the second harmonic signal has been added to this appendix, Figure A.10 and A.11. These figures shows the second harmonic signal for HF and H_2O respectively. The HF signal should be placed at 15 on the x-axis and the H2O signal should be placed at 49 on the x-axis. If the signal deviates from this on the x-axis, something is seriously wrong with the settings, and the measured HF and H_2O levels will be wrong. More troubleshooting is then necessary to find out which settings that needs to be changed.

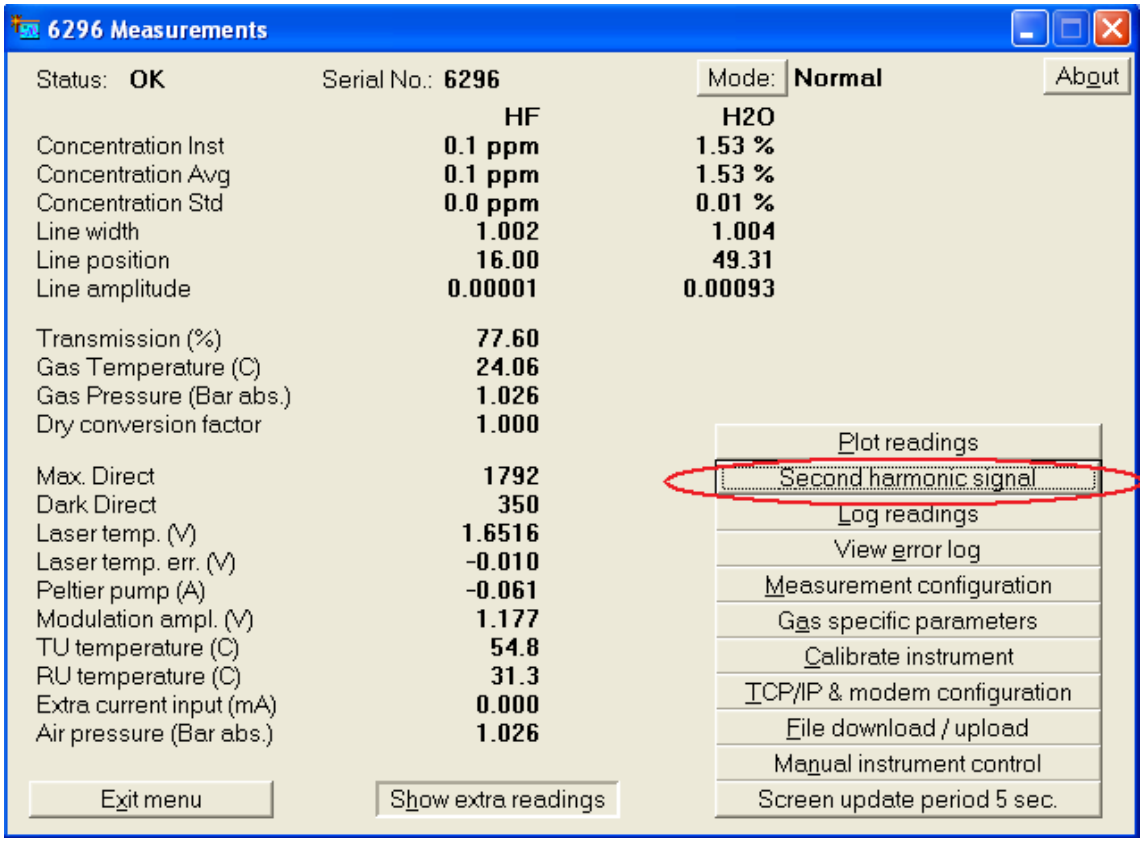

Figure A.9: The measurement overview. The red ellipse indicating the button to push to view the second harmonic signal and the positioning of the adsorption lines of HF at 15 and H_2O at 49, respectively.

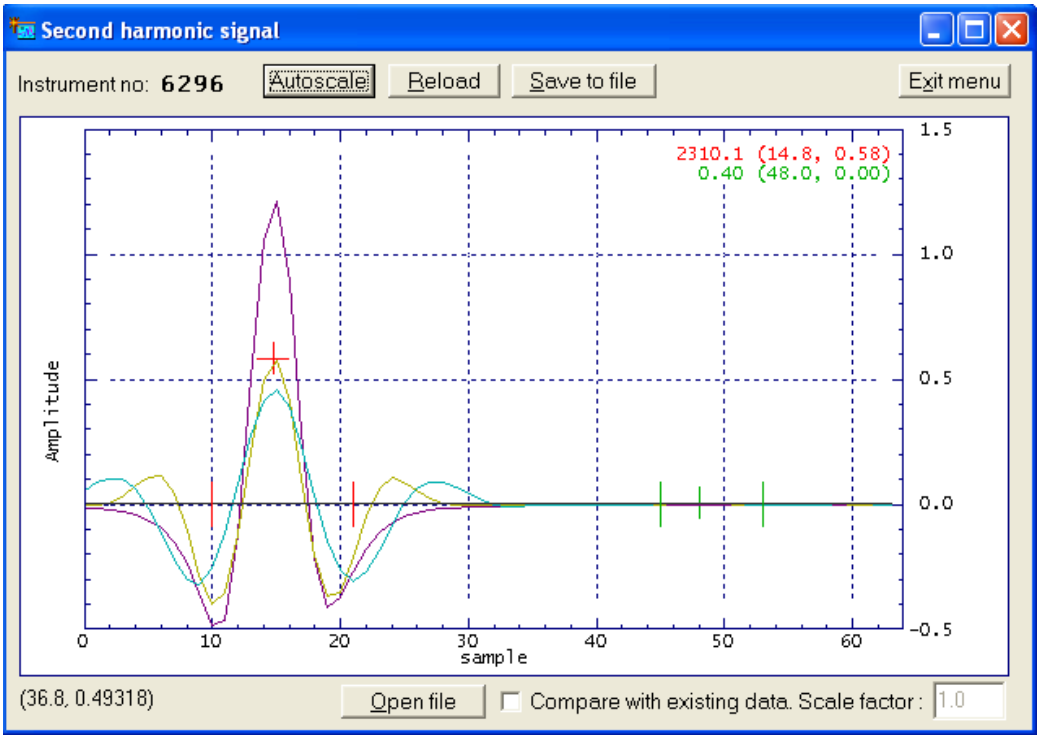

Figure A.10: The second harmonics signal of HF, showing a peak at 15 on the x-axis.

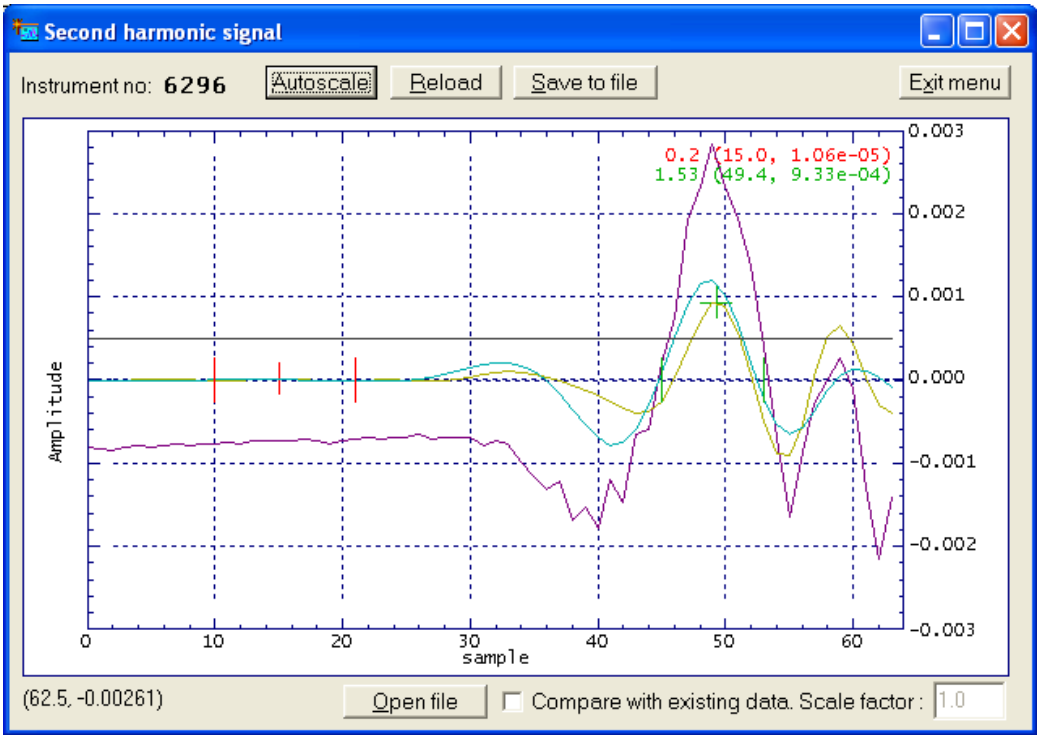

Figure A.11: The second harmonics signal of H_2O, showing a peak at 49 on the x-axis.

The settings that have been used when the gain was changed to 0010 are displayed in the following. In the menu showed in Figure A.8, the button Setting variables can be pushed. The setting variables will then appear, and Figures A.12, A.13, A.14 and A.15 show the setting variables used when the gain has been set to 0010. If loading new settings, always remember to push the button named “update instrument”.

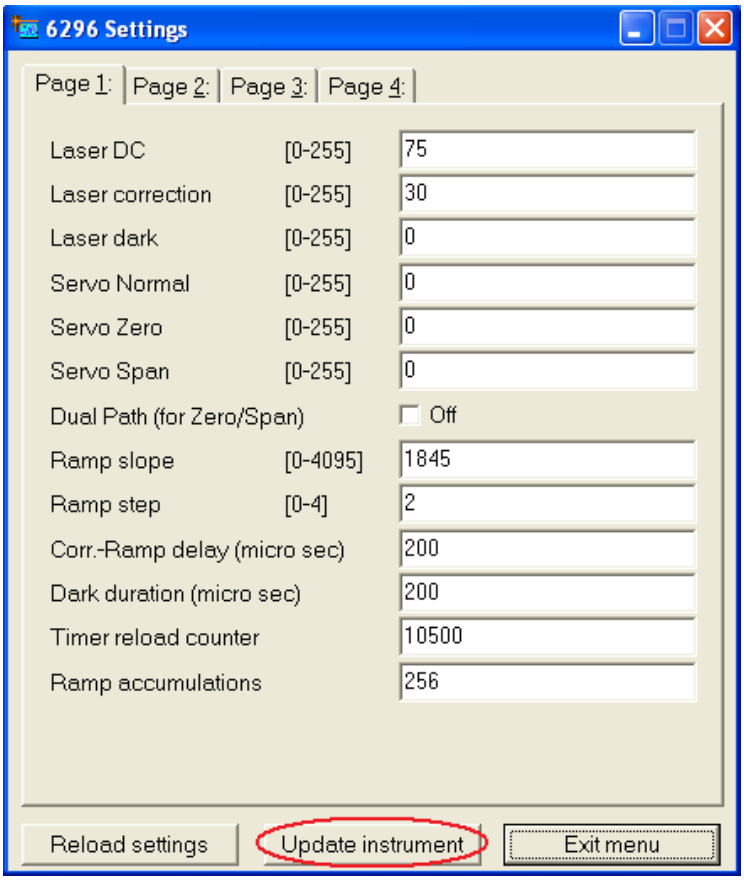

Figure A.12: Page 1 of the setting variables.

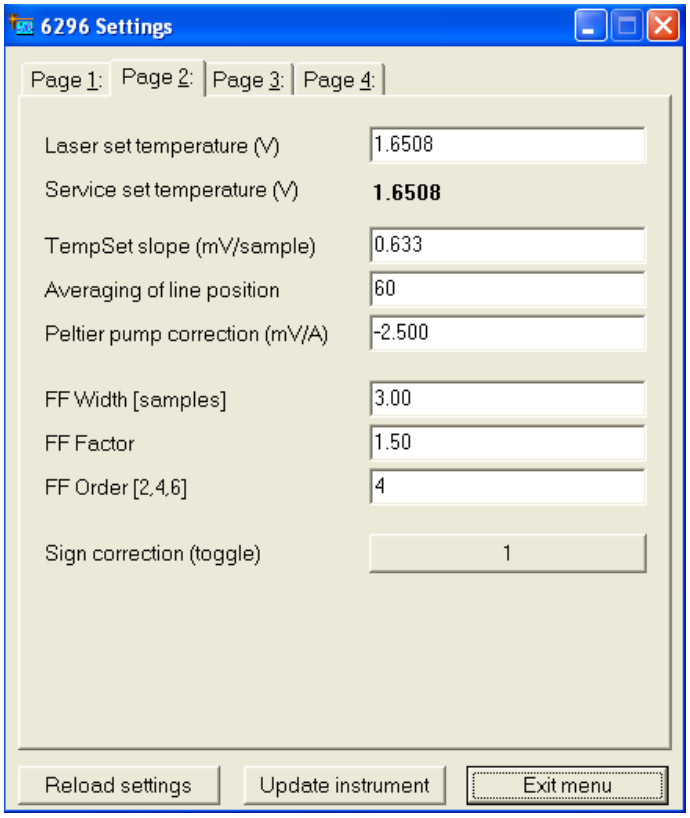

Figure A.13: Page 2 of the setting variables.

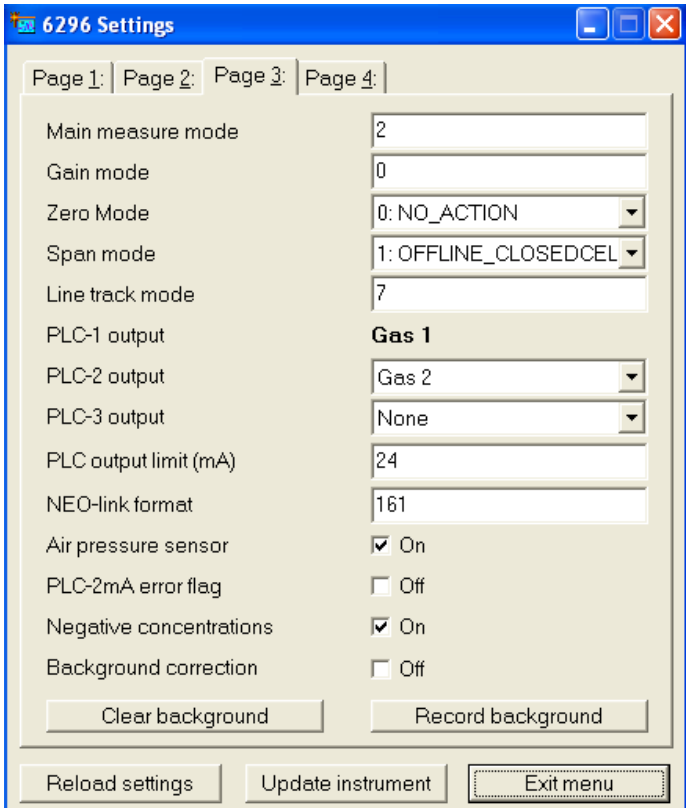

Figure A.14: Page 3 of the setting variables.

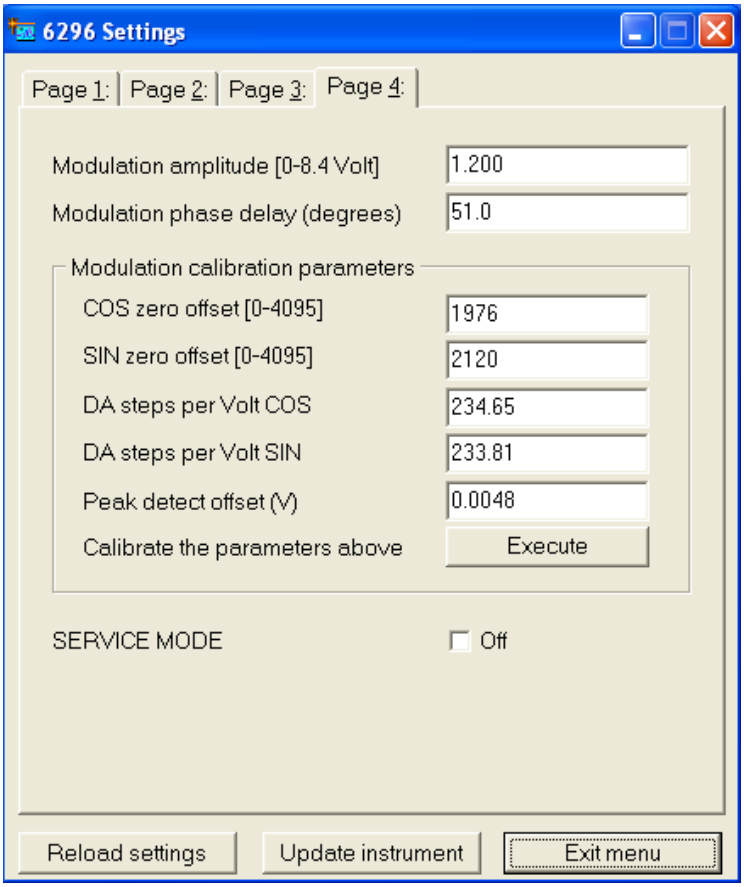

Figure A.15: Page 4 of the setting variables.

The next button on the menu in Figure A.8 is Config variables. The settings used for the config variables when the gain has been set to 0010, are shown in Figures A.16, A.17, A.18 and A.19. Remember to update instrument.

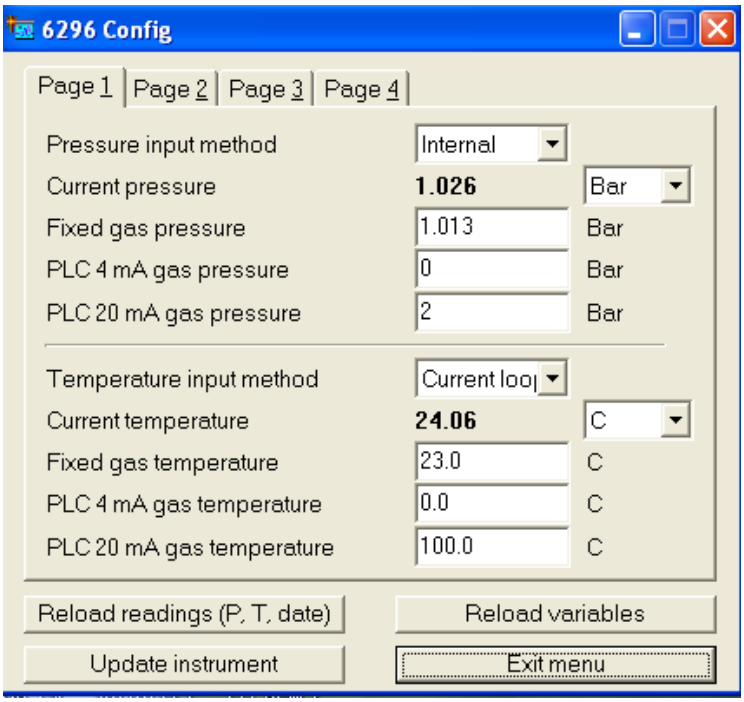

Figure A.16: Page 1 of the config variables.

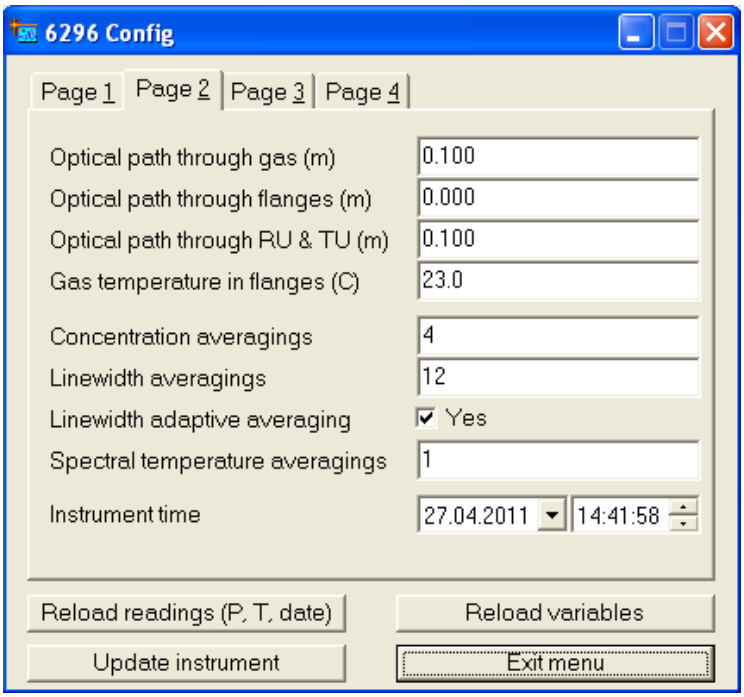

Figure A.17: Page 2 of the config variables.

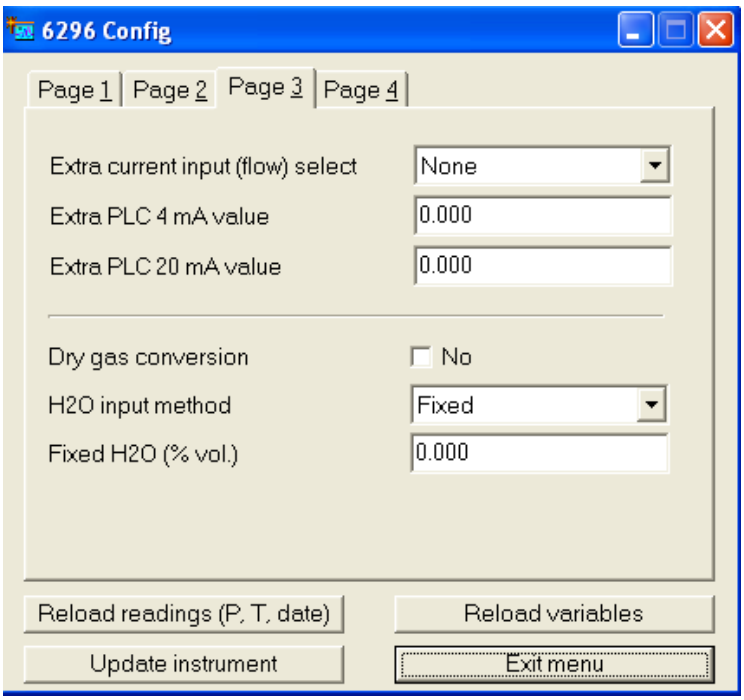

Figure A.18: Page 3 of the config variables.

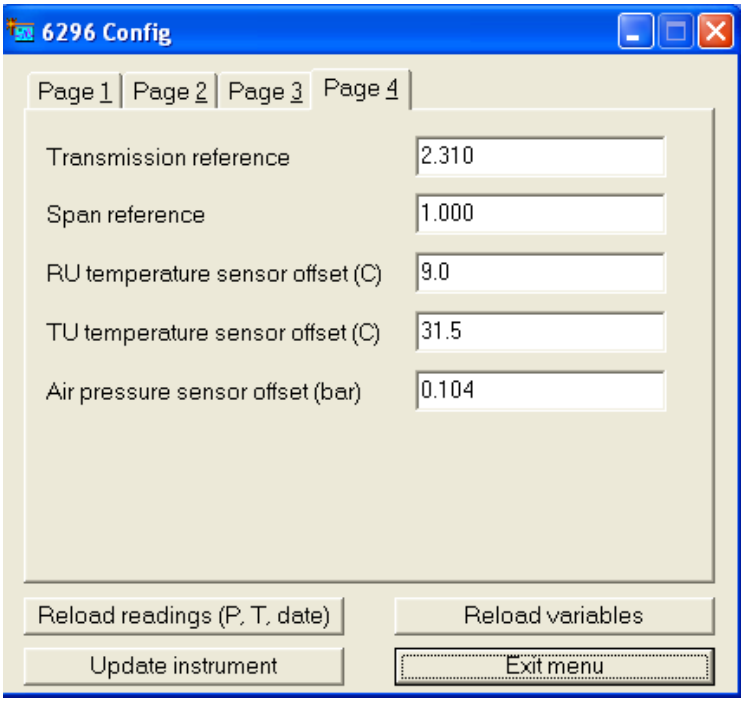

Figure A.19: Page 4 of the config variables.

The next button on the menu in Figure A.8 is Gasline variables. The gasline variables button has two options, HF and H_2O. The settings used for the Gasline variables for H_2O and HF_2O when the gain has been set to 0010, are shown in Figures A.20, A.21, A.22 and A.23, respectively. Remember to update instrument. When using gain 0010, the calibration constants of H_2O and HF is reduced (divide the original 0000 calibration constant) with a factor of 50.23/11=4.566 (from the gain in Figure A.3 for 0000 and 0010). A calculation example on how to calculate the calibration constant for H_2O is given in Equations A.1 and A.2. In the equations the calibration constant is labelled as C. This is only a calculated calibration constant, and the real calibration constant may deviate from the calculated. How to calibrate the instrument, and find the correct calibration factor is shown in section A.3.

$$C_{0010} = \frac{C_{0000}}{Gain_{0000}/Gain_{0010}} \tag{A.1}$$

$$517.61 = \frac{2363.6}{50.23/11} \tag{A.2}$$

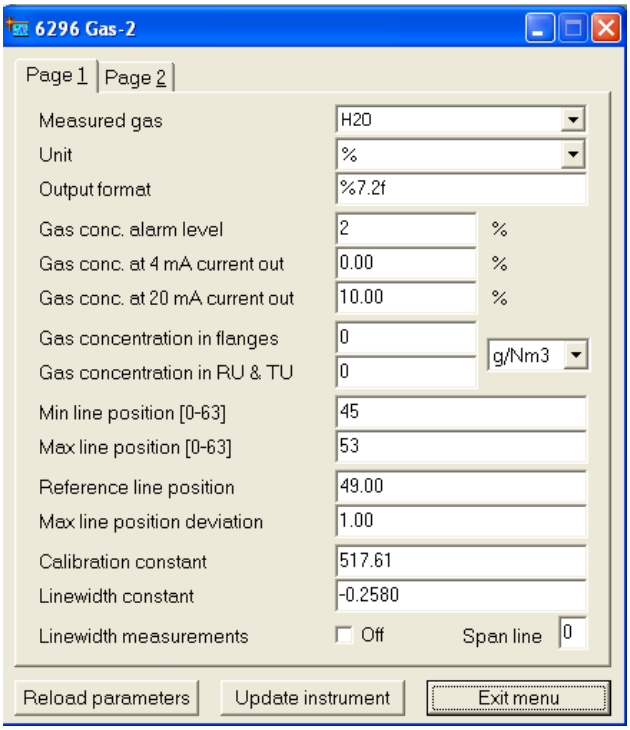

Figure A.20: Page 1 of the gasline variables for H_2O.

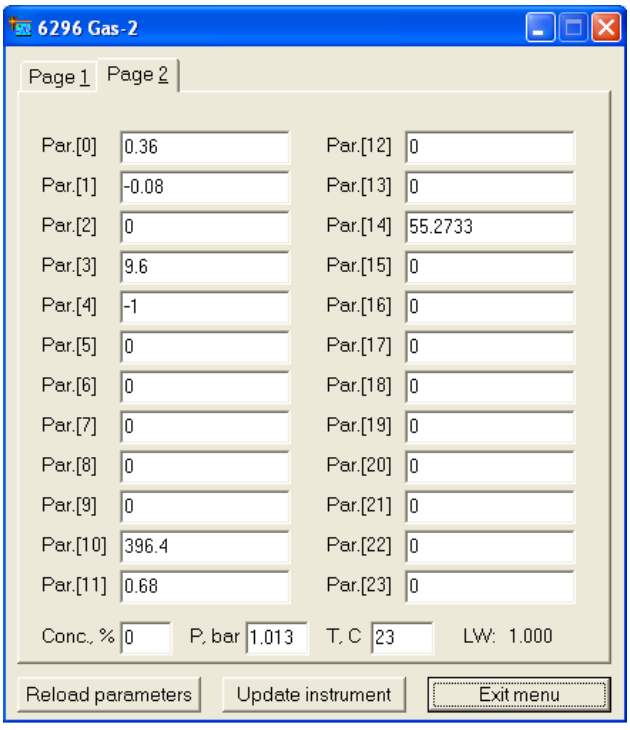

Figure A.21: Page 2 of the gasline variables for H_2O.

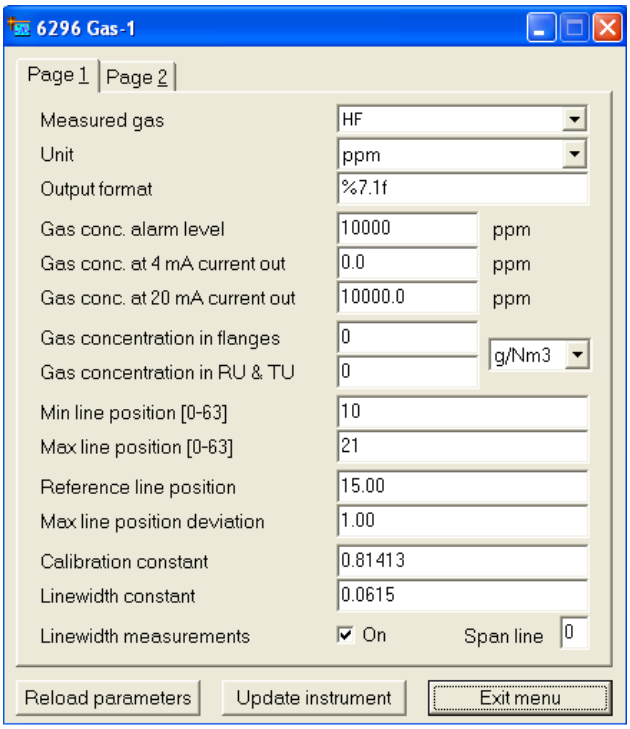

Figure A.22: Page 1 of the gasline variables for HF.

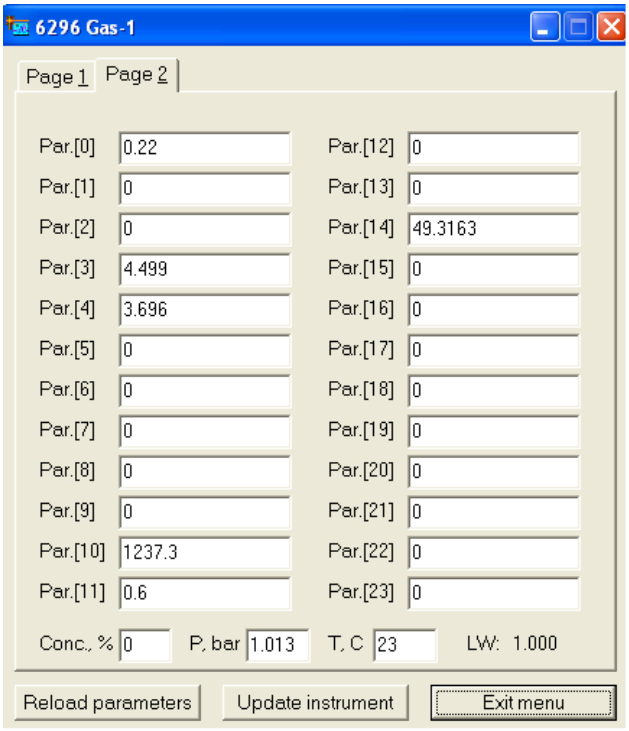

Figure A.23: Page 2 of the gasline variables for HF.

The next button on the menu in Figure A.8 is Guard variables. The settings used for the guard variables when the gain has been set to 0010, are shown in Figure A.24. Remember to update instrument.

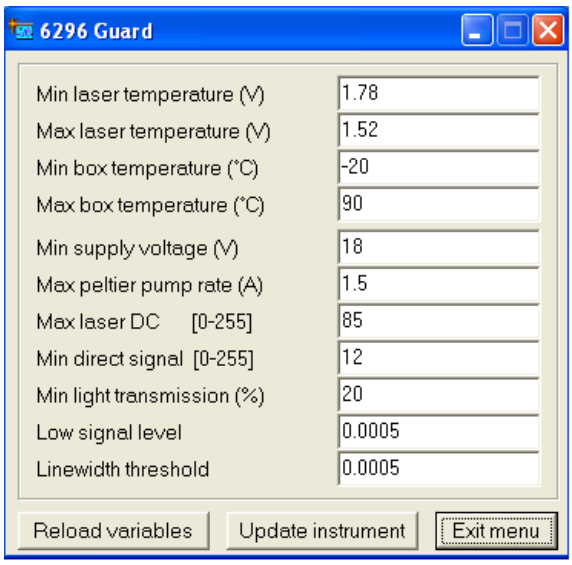

Figure A.24: The guard settings.

The next button on the menu in Figure A.8 is Info variables. The settings used for the info variables when the gain has been set to 0010, are shown in Figure A.25. Remember to update instrument.

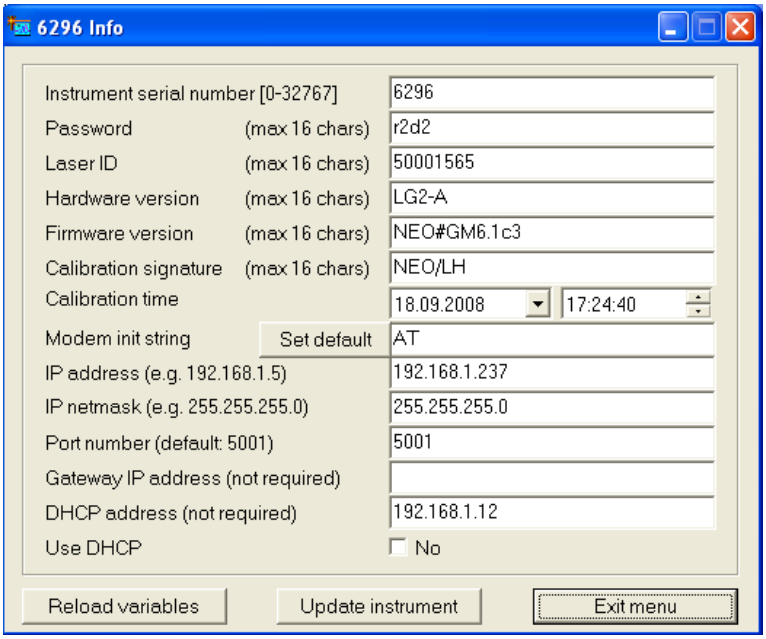

Figure A.25: The info settings.

A.4 How to Calibrate the Laser Instrument

Figure A.2 in the Results section, shows a linear relationship of the measured and the real H_2O concentrations when performing a calibration test of the instrument. The laboratory setup shown in Figure 5 was used, and moist N_2 gas with a known H_2O concentration was added to the laser. The N_2 gas was enriched with moisture by the bubble flasks. The water bath had a constant known temperature, and the concentration of H_2O in the gas could be calculated by using Figure B.1 in Appendix B. A regression line was made as shown in Figure A.2, and the equation of the regression line was used to change the offset of the H_2O concentration and change the slope of the line. Various dilutions of the moist gas was sent through the laser. The total gas flow was kept constant.

The regression line of the real vs. measured relationship of H_2O is shown in Figure A.2. The equation of the regression line was found to be y=1.1994x+0.2935. The calibration constant in Figure A.20 was changed from 517.61 with a factor of 1.1994. The new calibration constant value was found to be 431.56. The offset on the graph in Figure A.2 was corrected for by writing 0.2935 in the Gas concentration in RU & TU window in Figure A.2. Choose unit % and update the instrument. These calibration constant and gas concentration RU & TU values were used throughout the alumina additions to a cryolitic melt experiments. Equation A.3 shows how to calculate the new gain with use of the slope of the regression line.

The system was not calibrated for HF because the flow of the calibration gas from the gas cylinder (Figure 5 in the Experimental chapter) was difficult to control. No mass flow controllers could be used because the HF in the calibration gas could destroy them. However, the HF values were observed to be reasonable when testing with calibration gas.

$$C = \frac{517.61}{1.1994} \tag{A.3}$$

B Saturation Pressure

Figure B.1 shows a graph of the relation between H_2O saturation pressure and temperature [43]. This relation has been used for testing the moisture concentrations measured by the laser. Moisture enriched gas entered the laser with a known temperature. Using the relation in Figure B.1, the expected concentration of moisture could be calculated when assuming that the ambient pressure equal to 1 atm.

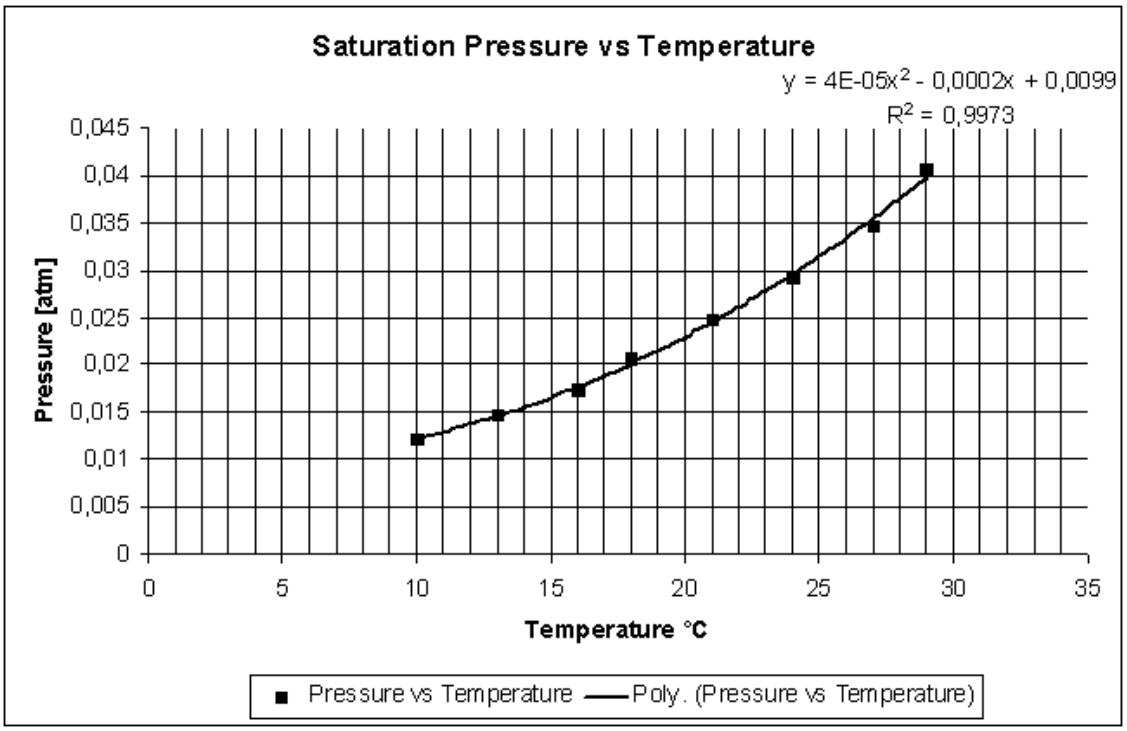

Figure B.1: Saturation pressure vs. temperature [43].

C Calibration of Flow Meters

The calibration curves of flow meter A and B are shown in Figures C.1, C.2 and C.3. Flow meter B has been calibrated both for N_2 and Ar gas. Flow meter A was only calibrated for N_2.

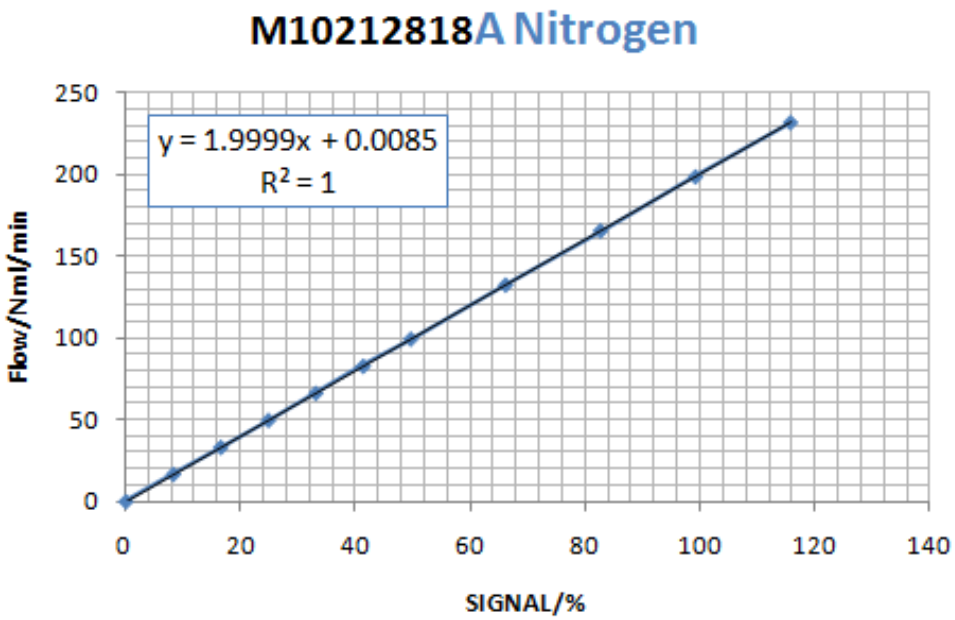

Figure C.1: Calibration curve for flow meter A. The flow meter was calibrated for N_2 gas. The corresponding regression line and equation is shown.

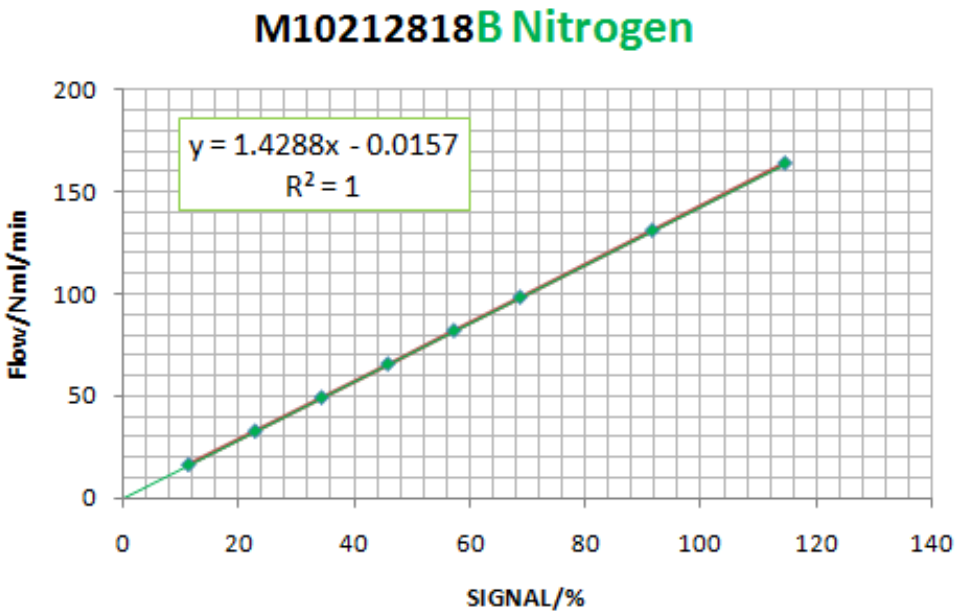

Figure C.2: Calibration curve for flow meter B. The flow meter was calibrated for N_2 gas. The corresponding regression line and equation is shown.

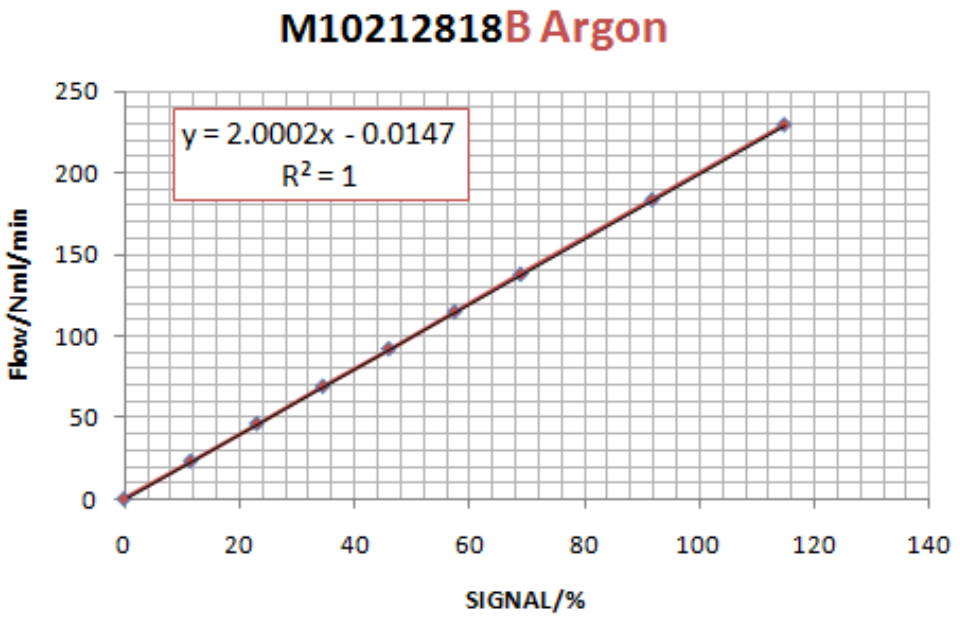

Figure C.3: Calibration curve for flow meter B. The flow meter was calibrated for Ar_2 gas. The corresponding regression line and equation is shown.

D NaF-AlF_3 Quantities

The following shows a calculation example to determine the quantities of NaF and AlF_3 needed to create a cryolitic melt with a cryolite ratio of 2.2 of 150 g.

An excess of AlF_3 of 12.7 wt% gives a cryolitic ratio of 2.2 on mole basis. This means that the molar ratio of NaF/AlF_3 = 2.2.

$M_{AlF_3} = 83.98$ g/mol

$M_{NaF} = 41.99$ g/mol

$$\frac{n_{NaF}}{n_{AlF_3}} = 2.2004 \tag{D.1}$$

Mole fraction:

NaF = 0.6875

AlF_3 = 0.3125

$$M_{AlF_3} = 83.98 \cdot 0.3125 = 26.24 g/mol \tag{D.2}$$

$$M_{NaF} = 41.99 \cdot 0.6875 = 28.87 g/mol \tag{D.3}$$

In one mole the sum of the amounts of AlF_3 and NaF becomes:

28.87 + 26.24 = 55.11 g

Weight percent of NaF and AlF_3 then becomes:

NaF: 0.5239

AlF_3: 0.4761

To create 150 g melt:

NaF: 78.59 g

AlF_3: 71.42 g

E Calculation Example: Using Riemann Sums for Calculating Total HF Formation

Equation E.1 shows the calculation of the quantity of HF when using the Riemann sum principle [40]. All columns in a chosen time interval are then added together. As a procedure the total quantity of HF was calculated for the 30 minutes following each alumina addition. Exceptions to that procedure were made when there were HF concentrations that reached the baseline given before the 30 minutes were reached. The Riemann sum calculation was terminated if the HF concentration measured reached the baseline given. This was done to avoid negative quantities of HF.

$$m_{HF} = \frac{((y(1)_{HF,ppm} - baseline_{ppm}) + (y(2)_{HF,ppm} - baseline_{ppm})) \cdot V_{gasflow} \cdot \Delta t \cdot M_{HF}}{2 \cdot 10^6 \cdot V_m} \tag{E.1}$$

In this equation m_{HF} equals the amount of HF in g, $V_{gasflow}$ and V_m is the volume flow of gas into the furnace (NL/s) and the volume of 1 mole ideal gas at 1 atm and 0°C (NL/mol) respectively. Δt equals the time difference between each measurement on the x axis in seconds. M_{HF} is the molar mass of HF (g/mol). Table 24 shows a summary of the parameters used. y(1) and y(2) represents two HF concentration values next to each other, taking the average value of the two (hence the division by two in the denominator).

Note that there is given two gas flows in Table 24. $V_{gasflow}$ is the gas flow usually used during all experiments. $V_{gasflow2}$ is the gas flow used when doubling the gas flow in front of addition 7 in Experiment 2. The gas flow was then increased from 98.79NmL/min ($1.65 \cdot 10^{-3}$NL/s) to 197.59NmL/min ($1.81 \cdot 10^{-3}$NL/s).

Table 24: Parameters used when calculating the Riemann sum of the HF formation.

Parameter	Quantity	Unit
$V_{gasflow}$	$1.65 \cdot 10^{-3}$	NL/s
$V_{gasflow2}$	$1.81 \cdot 10^{-3}$	NL/s
V_m	22.4	NL/mol
Δt	11	s
M_{HF}	20	g/mol

F Loss on Ignition

F.1 Calculation Example: LOI

Equation F.1 shows how to calculate the LOI value from room temperature to 160°C (200°C). Equation F.2 shows how to calculate the LOI value from 160°C (200°C) to 350°C. Equation F.3 shows how to calculate the LOI calue from 350-1000°C. [44]

$$LOI(RT-160^{\circ}C) = \frac{(m_{RT} - m_{160^{\circ}C}) \cdot 100\%}{m_{sample}} \tag{F.1}$$

$$LOI(160^{\circ}C-350^{\circ}C) = \frac{(m_{160^{\circ}C} - m_{350^{\circ}C}) \cdot 100\%}{m_{sample}} \tag{F.2}$$

$$LOI(350^{\circ}C-1000^{\circ}C) = \frac{(m_{350^{\circ}C} - m_{1000^{\circ}C}) \cdot 100\%}{m_{sample}} \tag{F.3}$$

m_{sample}, m_{RT}, $m_{160^{\circ}C}$, $m_{350^{\circ}C}$, $m_{1000^{\circ}C}$ represents the mass of the sample initially before any heating, mass at room temperature, mass at 160°C, mass at 350°C and mass at 1000°C, respectively.

F.2 Results from testing Loss on Ignition on Primary Alumina

Table 25 shows the results when doing LOI testing on the various primary alumina samples with drying at 160°C. This table creates the basis of the results reported in Table 4.

Table 26 shows the results of the LOI measurements on samples of alumina A that had been kept in a desiccator filled with water for three days in room temperature. Samples with a high amount of physisorbed water were created this way. The LOI testing was performed on samples that had been taken straight out of the desiccator without being stored on normal ambient conditions. This way the samples kept the properties that was created in of the humid environment. Table 26 creates the basis of the results presented in Table 5.

Table 25: Results from the LOI measurements performed on the primary alumina qualities, with drying at 160°C. *One of the crucibles with a sample containing bulk alumina A tipped over and some of the powder was spilled before the sample was weighed at 1000°C.

Quality	Mass [g]	LOI(RT-160°C) %	LOI(160-350°C) %	LOI(350-1000°C) %
A, hydrate	2.9325	0.18	28.90	5.71
A, hydrate	2.9021	0.20	28.88	5.73
A, calcined	3.0271	0.54	0.15	0.01
A, calcined	3.1640	0.46	0.15	0.14
A, bulk	3.0542	1.12	0.44	*
A, bulk	3.0258	1.17	0.44	0.64
A, +150μm	2.9840	1.07	0.61	0.96
A, +150μm	2.8967	1.05	0.57	0.90
A, -45μm	2.8543	1.49	0.62	0.74
A, -45μm	2.9929	1.45	0.57	0.84
B, bulk	3.0542	1.49	0.71	1.19
B, bulk	3.0335	1.53	0.66	0.97
B, +150μm	3.1166	1.77	1.04	1.13
B, +150μm	2.9859	1.80	1.18	1.03
B, -45μm	2.9403	1.50	1.76	1.31
B, -45μm	3.0187	1.44	1.76	1.26
C, bulk	3.0169	1.58	1.08	0.91
C, bulk	3.0356	1.59	1.05	0.85

Table 26: Results from the LOI measurements performed on the bulk fraction of alumina A stored in a desiccator filled with water for three days at room temperature.

Quality	Mass [g]	LOI(RT-160°C) %	LOI(160-350°C) %	LOI(350-1000°C) %
Moist A, bulk	3.0143	13.57	0.69	0.70
Moist A, bulk	3.0064	13.81	0.55	0.90

F.3 Results from testing Loss on Ignition on Secondary Alumina

Table 27 shows the results when performing LOI testing on secondary alumina. This table creates the basis of the results given in Table 6

Table 27: Results from the LOI measurements performed on the secondary alumina qualities, with drying at 160°C. *One of the crucibles with a sample containing bulk alumina B tipped over and some of the powder was spilled before the sample was weighed at 350°C.

Quality	Mass [g]	LOI(RT-160°C) %	LOI(160-350°C) %	LOI(350-1000°C) %
A, bulk	3.0130	2.17	0.90	2.00
A, bulk	3.0539	2.18	0.86	1.86
A, +150μm	3.0122	1.89	0.88	1.63
A, +150μm	3.0157	1.86	0.90	1.58
A, -45μm	3.0019	1.48	0.83	5.00
A, -45μm	3.0079	1.50	0.91	5.02
B, bulk	3.0214	2.24	*	2.45
B, bulk	3.0073	2.21	1.33	2.17
B, +150μm	3.0038	1.80	1.07	2.10
B, +150μm	3.0022	1.86	1.04	2.25
B, -45μm	3.0033	1.36	1.79	5.65
B, -45μm	3.0001	1.39	1.75	5.73
C, bulk	3.0013	2.00	1.22	2.09
C, bulk	3.0000	1.97	1.30	2.47

G Rietveld Refinement Details

Figure G.1 shows the attempt to run Rietveld analysis on the calcined sample of alumina A. The Topas software was used for the Rietveld refinement. Tables 28, 30 and 29 shows the atomic coordinates and space groups for the θ, κ and corundum phases. The corundum phase has a space group of R-3c, the κ-alumina phase has a space group of Pna21 and the θ-alumina has a space group of I2/m. [34, 35, 36] The PDF-4+ 2010 database available at NTNU was used to find the atomic coordinates and space groups.

In Figure G.1 the blue line is the diffractogram found when running XRD analysis. The red line is the curve fitting made by the Topas software. The curve fitting is obviously poor, and this is due to the mixture of amorphous and crystalline phases. After several attempts to curve fit the XRD diffractogram, the Rietveld analysis was given up.

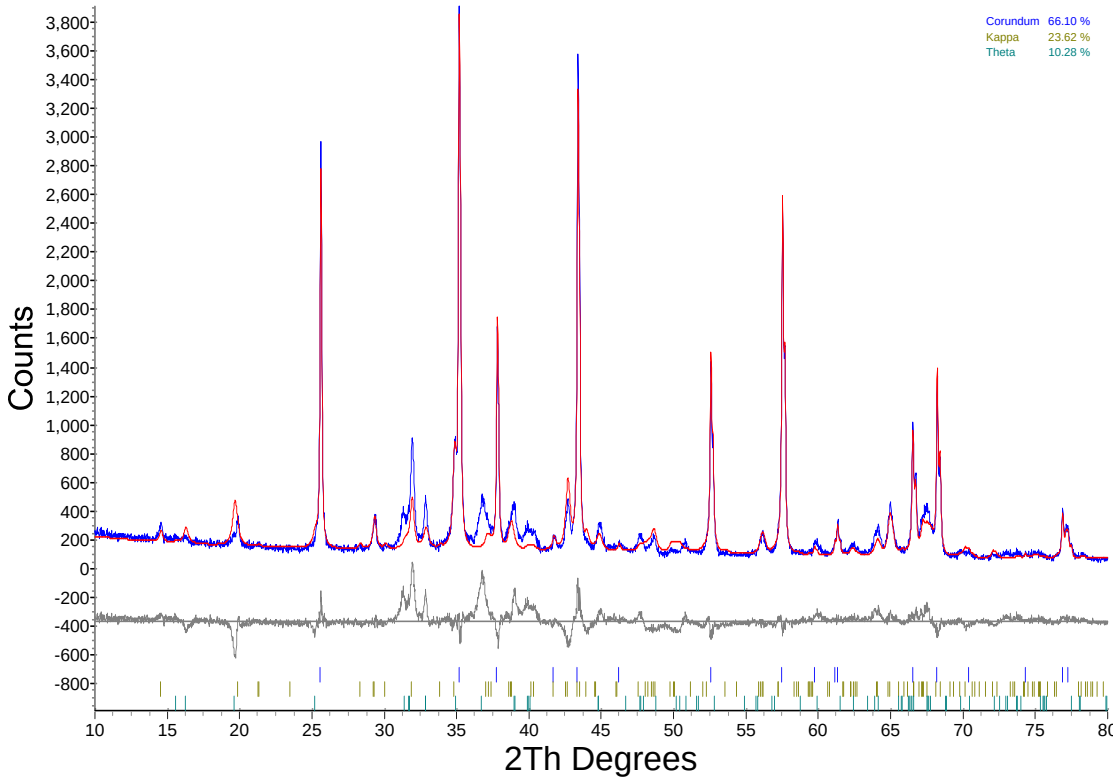

Figure G.1: The attempt to run Rietveld analysis of the alumina A calcined diffractogram.

Table 28: The atomic coordinates and occupancies for corundum (α-alumina) [34].

Atom	x	y	z	Occ.
Al	0.00000	0.00000	0.35227	1
O	0.30672	0.00000	0.25000	1

Table 29: The atomic coordinates and occupancies for θ-alumina [36].

Atom	x	y	z	Occ.
O1	0.82720	0.00000	0.42730	1
O2	0.49500	0.00000	0.25260	0.93
O3	0.16110	0.00000	0.09840	0.8
Al1	0.65095	0.00000	0.31650	0.9
Al2	0.91660	0.00000	0.20730	0.92

Table 30: The atomic coordinates and occupancies for κ-alumina [35].

Atom	x	y	z	Occ.
Al1	0.67870	0.84160	0.00000	1
Al2	0.18460	0.34320	0.78690	1
Al3	0.81150	0.64890	0.69720	1
Al4	0.66770	0.46960	0.99930	1
O1	0.32900	0.83130	0.89270	1
O2	0.02480	0.49020	0.62920	1
O3	0.47170	0.66470	0.63810	1
O4	0.51450	0.67280	0.12120	1
O5	0.86080	0.33010	0.86620	1
O6	0.33600	0.49920	0.90000	1

H Calculation Example: Using H_2O Quantities Found During TGA and LOI Characterisation for Calculating Total HF Formation

Equations H.1 - H.4 shows how to calculate the quantity of HF from H_2O quantities found during TGA and LOI characterisation. The TGA values used are given in Table 7. The LOI values used are given in Tables 4 and 5.

$$m_{H_2O} = m_{Al_2O_3} \cdot wt\%_{H_2O} \tag{H.1}$$

$$n_{H_2O} = \frac{m_{H_2O}}{M_{H_2O}} \tag{H.2}$$

$$n_{HF} = 2 \cdot n_{H_2O} \tag{H.3}$$

$$m_{HF} = M_{HF} \cdot n_{HF} \tag{H.4}$$

Table 31 shows a summary of the parameters used in Equations H.1 - H.4.

Table 31: Parameters used in Equations H.1 - H.4.

Symbol	Quantity	Explanation	Unit
m	Calculated	Mass	g
wt%	LOI and TGA values	Weight percent	%
n	Calculated	Amount of substance	mol
M_{HF}	20	Molar mass of HF	g/mol
M_{H_2O}	18	Molar mass of H_2O	g/mol

I Modelling of Gas Flows by Use of CSTR

CSTR modelling can be used to estimate the evacuation of gas from a crucible. Equation I.1 shows the principles for CSTR modelling [45].

$$C_{HF}(t) = C_{HF}(0)\exp((t - t_0)\cdot(-\frac{\dot{v}}{V})) \tag{I.1}$$

Tables 32 gives an explanation of the symbols in Equation I.1.

Table 32: Explanation of symbols in Equation I.1.

Symbol	Explanation	Unit
C_{HF}(t)	Conc. of HF at time t	ppm
C_{HF}(0)	Conc. of HF initially	ppm
t	Time	min
t_0	Initial time	min
$\dot{v}$	Volume flow of gas into reactor	NmL/min
V	Volume of crucible	mL

Table 33 shows the parameters used during the calculation of CSTR. $\dot{v}$ normal flow was used for the three calculations of normal flow, high and low peaks. The volume of the crucible equals the volume of the nickel crucible minus the volume of the Pt-crucible with the cryolite melt inside. The calculation was run was 30 minutes.

Table 33: Parameters used for CSTR modelling.

Symbol	Value	Unit
C_{HF}(0) normal flow	7890	ppm
C_{HF}(0) double flow	9131	ppm
C_{HF}(0) high peak	16963	ppm
C_{HF}(0) low peak	5254	ppm
t_0	0	min
$\dot{v}$ normal flow	98.79	NmL/min
$\dot{v}$ double flow	197.60	NmL/min
V	190	mL